

ENCLOSURE 5

TENNESSEE VALLEY AUTHORITY (TVA)
SEQUOYAH NUCLEAR PLANT (SQN)

Non-Proprietary

Final Report
Metallurgical Examination Results for
Tube Pull During SQN Unit 2 Cycle 14 Refueling Outage

Westinghouse Non-Proprietary Class 3

SG-CDME-07-21-NP
Revision 0

September 2007

Examination of a Steam Generator Tube Removed from Sequoyah Unit 2

Prepared for the
Tennessee Valley Authority



LEGAL NOTICE

This report was prepared as an account of work performed by Westinghouse Electric Company LLC. Neither Westinghouse Electric Company LLC, nor any person acting on its behalf:

- A. Makes any warranty or representation, express or implied including the warranties of fitness for a particular purpose or merchantability, with respect to the accuracy, completeness, or usefulness of the information contained in this report, or that the use of any information, apparatus, method, or process disclosed in this report may not infringe privately owned rights; or
- B. Assumes any liabilities with respect to the use of, or for damages resulting from the use of, any information, apparatus, method, or process disclosed in this report.

SG-CDME-07-21-NP
Revision 0

Prepared for the Tennessee Valley Authority

Examination of a Steam Generator Tube Removed from Sequoyah Unit 2

Author's Name Thomas P. Magee	Signature / Date <u>TPM (*)</u>	For Pages All
Verifier's Name Justin W. Cook	Signature / Date <u>JWC (*)</u>	For Pages All
Manager Name Earl P. Morgan	Signature / Date <u>EPM (*)</u>	For Pages All

** Electronically Approved Records Are Authenticated in the Electronic Document Management System*

This report has been prepared by Westinghouse Electric Company LLC and bears a Westinghouse Electric Company copyright notice. You are permitted to copy and redistribute all or portions of the report; however all copies made by you must include the copyright notice in all instances.

Westinghouse Electric Company LLC
P.O. Box 355
Pittsburgh, PA 15230-0355

© 2007 Westinghouse Electric Company LLC
All Rights Reserved

 TABLE OF CONTENTS

Table of Contents	ii
List of Tables	iv
List of Figures	v
1.0 Introduction	1-1
2.0 Removed Tube Characteristics.....	2-1
2.1 Objective	2-1
2.2 Tube Pull Operation	2-1
2.3 NRC Teleconference	2-2
3.0 Receipt Inspection	3-1
3.1 Visual Observations	3-1
3.1.1 Tubesheet Region and TTS	3-1
3.1.2 TSP#1	3-2
3.1.3 TSP#2	3-3
3.1.4 Freespan	3-3
3.2 OD Measurement Profiles	3-4
3.3 Deposit pH	3-4
4.0 Eddy Current Test Inspection.....	4-1
4.1 Introduction	4-1
4.2 Results	4-1
5.0 Destructive Examination Preparation.....	5-1
5.1 Leak Screening.....	5-1
5.2 Heat Tinting	5-1
5.2.1 Procedure.....	5-1
5.2.2 Results.....	5-2
5.3 Support Plate Region Expansion.....	5-3
5.3.1 Procedure.....	5-3
5.3.2 Post-Expansion Observations.....	5-3
5.4 Sectioning.....	5-4
6.0 Fractography.....	6-1
6.1 Procedure.....	6-1
6.2 Crack Surface Characterization.....	6-1
6.3 EDS Analysis of Crack Surfaces.....	6-2
6.4 EDS Analysis of OD Surfaces and Deposits.....	6-3
6.5 Depth Profiles and Ligament Sizing	6-3
7.0 Metallography	7-1
7.1 Procedure.....	7-1
7.2 Transverse Metallography.....	7-1
7.3 Radial Metallography.....	7-1
8.0 Material Characterization.....	8-1
8.1 Tensile Test.....	8-1
8.1.1 Procedure.....	8-1
8.1.2 Results.....	8-1
8.2 Bulk Chemistry	8-1

8.2.1	Procedure.....	8-1
8.2.2	Results.....	8-2
8.3	Microstructure Analysis.....	8-2
8.3.1	Procedure.....	8-2
8.3.2	Results.....	8-2
8.4	Microhardness Testing.....	8-3
8.4.1	Procedure.....	8-3
8.4.2	Results.....	8-3
8.5	Sensitization Assessment.....	8-3
8.5.1	Procedure.....	8-3
8.5.2	Results.....	8-4
9.0	Analytical Determination of Leak Rate and Burst Strength.....	9-1
9.1	Introduction.....	9-1
9.2	Destructive Exam (DE) Depth Profiles.....	9-1
9.3	Corrections to DE Depth Profiles for Uncorroded Ligaments.....	9-1
9.4	Burst Pressure Analysis Results.....	9-3
9.5	SLB Leak Rate Analysis Results.....	9-3
9.6	Use of Pulled Tube Data for Probability of Leak Correlation.....	9-4
9.7	Comparison of NDE Predictions from Field Data with DE Profiles and Post-Pull NDE Results.....	9-5
9.8	Conclusions.....	9-6
10.0	Discussion / Conclusions.....	10-1
11.0	References.....	11-1
	Appendix A - Crack Depth Profile Data.....	A-1

LIST OF TABLES

Table 1-1: Support Plate Elevations.....	1-3
Table 2-1: Pulled Tube R22C70 Section Lengths and Characteristics.....	2-3
Table 4-1: Field and Laboratory Eddy Current Inspection Results for R22C70.....	4-3
Table 5-1: Destructive Examination Samples.....	5-5
Table 6-1: Summary of EDS Analyses Performed on TSP#1 180° Crack Surfaces.....	6-4
Table 6-2: Summary of EDS Analyses Performed on TSP#1 110° Crack Surfaces.....	6-4
Table 6-3: Summary of EDS Analyses Performed on TSP#2 180° Crack Surfaces.....	6-4
Table 6-4: Summary of EDS Analyses Performed on TSP#1 OD Surfaces.....	6-5
Table 6-5: Opened Crack Characteristics.....	6-6
Table 6-6: Ligament Sizing Results.....	6-7
Table 7-1: Radial Metallography Grind/Polish Depths.....	7-3
Table 8-1: R22C70 (Pulled Tube) Tensile Test Results.....	8-5
Table 8-2: Chemical Composition of R22C70.....	8-5
Table 8-3: Microhardness Test Summary.....	8-5
Table 9-1: R22C70 Uncorroded Ligament Measurements.....	9-7
Table 9-2: R22C70 Calculated Burst Pressures from TSP#1 and TSP#2 180° Crack Destructive Exam Profiles.....	9-8

LIST OF FIGURES

Figure 3-1: As-Received Views of TTS Region	3-5
Figure 3-2: As-Received Views of TSP#1 Region	3-7
Figure 3-3: As-Received Close-Up Views of Cracks Near 180° Orientation of TSP#1	3-9
Figure 3-4: As-Received Close-Up Views of Other Cracks of TSP#1	3-10
Figure 3-5: As-Received Views of TSP#2 Region	3-11
Figure 3-6: As-Received Close-Up Views of Miscellaneous Features of TSP#2.....	3-13
Figure 3-7: Cross-Section of Tube Showing the Degree of Ovalization	3-14
Figure 3-8: Maximum and Minimum Diameter Profile Along Entire Length of the Tube	3-15
Figure 3-9: TSP#1 Laser Micrometer Profilometry Results	3-16
Figure 3-10: TSP#2 Laser Micrometer Profilometry Results	3-17
Figure 5-1: Heat Tinting.....	5-6
Figure 5-2: Post-Expansion Views of TSP#1 Region.....	5-7
Figure 5-3: Post-Expansion Views of TSP#2 Region.....	5-9
Figure 5-4: Post-Expansion Observations of TSP#1.....	5-11
Figure 5-5: Post-Expansion Observations of TSP#2.....	5-12
Figure 5-6: Piece 4B Sectioning.....	5-13
Figure 5-7: Piece 5 Sectioning Diagram	5-15
Figure 5-8: Piece 6 Sectioning	5-16
Figure 6-1: Overall Views of TSP#1 180° Crack (Sample 4C1).....	6-8
Figure 6-2: Overall Views of TSP#1 110° Crack (Sample 4C5).....	6-9
Figure 6-3: Overall Views of TSP#2 180° Crack (Sample 6B1).....	6-10
Figure 6-4: Example of Corrosion Surface (from Sample 4C1).....	6-11
Figure 6-5: Example of EDS Analysis of Crack Surface (Dark Anomaly on Sample 4C1).....	6-12
Figure 6-6: Example of EDS Analysis of OD Surface (Sample 4C1).....	6-13
Figure 6-7: Corrosion Depth Profile and Ligament Size for TSP#1 180° Crack.....	6-14
Figure 6-8: Corrosion Depth Profile and Ligament Size for TSP#1 110° Crack.....	6-15
Figure 6-9: Corrosion Depth Profile and Ligament Size for TSP#2 180° Crack.....	6-16
Figure 7-1: Typical Axial Crack (Sample 4C4 at ~315° Location).....	7-4
Figure 7-2: Circumferential Feature in Sample 6B2.....	7-5
Figure 8-1: Stress-Strain Curve for R22C70 (Pulled Tube).....	8-6
Figure 8-2: Microstructure of Freespan Region of R22C70 After a Nital Etch.....	8-7
Figure 8-3: Carbide Distribution of Freespan Region of R22C70 After a Methanol- Bromine Etch.....	8-8
Figure 9-1: Uncorroded Ligament Corrected Depths for the TSP#1 180° Crack.....	9-9
Figure 9-2: Uncorroded Ligament Corrected Depths for the TSP#2 180° Crack.....	9-10
Figure 9-3: Uncorroded Ligament Corrected Depths for the TSP#1 110° Crack.....	9-11
Figure 9-4: Addendum 6 Burst Pressure vs. Volts for 7/8" OD Alloy 600 SG Tubes	9-12
Figure 9-5: SLB Leak Rate (CRACKFLO) Versus Throughwall Axial Crack Length.....	9-13
Figure 9-6: ANL Ligament Tearing Pressures vs. Crack Depth	9-14
Figure 9-7: SLB Leak Rate (2405 psi) vs. Bobbin Amplitude	9-15
Figure 9-8: Comparison of DE and NDE Results with Pre-Pull and Post-Pull Depth and Volts for the TSP#1 180° Crack.....	9-16
Figure 9-9: Comparison of NDE and Ligament Corrected DE for the TSP#1 180° Crack	9-17
Figure 9-10: Comparison of NDE and Ligament Corrected DE for the TSP#2 180° Crack	9-18

Figure 9-11: Comparison of Field NDE and DE Depths for the TSP#1 110° Crack..... 9-19
Figure 9-12: +Point Volts for Field, Lab and Field Adjusted for Crack Separation..... 9-20

1.0 INTRODUCTION

Sequoyah Unit 2 (Sequoyah-2) is owned and operated by the Tennessee Valley Authority (TVA). Sequoyah-2 is a four loop Westinghouse designed pressurized water reactor sited on the banks of the Chickamauga Reservoir. The plant, which has a nominal rating of 1150 net MWe, commenced commercial operation in 1982 and has accumulated 17.5 EFPY of operation after 14 refueling cycles. The steam generators are of the Model 51 type manufactured by the Westinghouse Electric Corporation. Each steam generator contains 3388 heat transfer tubes. The mill annealed NiCrFe Alloy 600 steam generator tubes are nominally 0.875 inch in outer diameter and have a nominal wall thickness of 50 mils. The tubes are mounted in a low alloy steel tubesheet that is approximately 21.7 inches thick (including cladding). The tube-to-tubesheet crevices were closed using the WEXTEx process, in which tubes were explosively expanded. The tubes pass through seven carbon steel tube support plates (TSPs) that are 0.75 inch thick each, through drilled holes that have a nominal diameter of 0.891 inch. Table 1-1 provides a summary of the as-built elevations of the supports.

The secondary side environment of the steam generators has always used an all-volatile treatment (AVT) water chemistry. To reduce the number of tubes that needed to be plugged due to the presence of detectable axial outside diameter stress corrosion cracking (ODSCC), Sequoyah-2 initiated an alternative repair criteria (ARC) program.

At the end of the cycle 14 refueling outage (December 2006), TVA selected one steam generator tube from Sequoyah Unit 2 for removal and laboratory non-destructive and destructive examinations to support the ARC database. The tube selection and laboratory examination were in compliance with ARC requirements that were established in GL95-05 (Reference 2). The tube that was removed, R22C70, was from steam generator 4, and included two support plate intersections.

The tube was cut below the third support, pulled from the generator and delivered to Westinghouse's Science and Technology Department (STD) facility for non-destructive and destructive examinations. The emphasis of the laboratory activities was to perform tube integrity testing and to characterize the depth and type of defects that caused the ECT indications. The examinations included:

- Verification of Sample Identification - For all tubes, all segments were measured for length and visually surveyed for landmark features (e.g., TSP intersections) for comparison with tube removal records.
- Visual characterization of the pulled tubes. The purpose of this was to identify and characterize any tube degradation, characterize the appearance of any secondary side deposits, and identify any damage from the tube pulling operation.
- Eddy current characterization, including bobbin exam, +Point exam, and UT. This information served to precisely locate defects for the metallography and to determine any differences from the pre-pull inspection.
- The OD profile of tube segments in areas of interest (TTS and TSPs).
- Characterization of surface deposits, including pH, appearance and approximate elemental composition.

-
- SEM characterization of mechanically opened cracks. Develop length versus depth profile with sufficient data points that a linear interpolation between data points yields the crack profile and average depth. Uncorroded ligaments were sized in terms of length, area and angular orientation.
 - Metallographic examination of the cracks.
 - Determination of leak rate and burst pressure.
 - Non-degraded tubing from a free-span area was tensile tested to ASTM standards to determine the yield strength, ultimate tensile strength, percent elongation, and reduction in area.
 - Characterization of the tubing material by microhardness testing and sensitization testing.

Westinghouse has completed all of the above examinations on the tube removed from Sequoyah-2. This report documents the examinations performed and the results from the examinations.

All examinations and testing presented in this report were treated as safety-related and are in accordance with the Westinghouse Quality Assurance program (Reference 3), which satisfies the requirements of 10CFR50 Appendix B. This examination was initiated by the Reference 4 work authorization (Westinghouse SAP network number 117731).

Table 1-1: Support Plate Elevations
(Reference 1)

	Distance Above Tube Mouth (inches)	Distance Above TTS (inches)
Tube Mouth	0	
Primary Side of Clad	0.22	
Primary Side of Tubesheet	0.37	
Top of Tubesheet (TTS)	21.40	0
Centerline of TSP#1	71.525	50.125
Centerline of TSP#2	122.025	100.625
Centerline of TSP#3	172.525	151.125

2.0 REMOVED TUBE CHARACTERISTICS

2.1 Objective

The ARC database (Reference 5) required pulled tube data from an indication with a bobbin voltage between 3 and 6 volts. Tube R22C70 from SG 4 was chosen for laboratory examination because it had the larger of two bobbin indications, between 3 and 6 volts, discovered during the cycle 14 refueling outage eddy current inspection. Distorted signal indications (DSIs) were reported by bobbin probe at the 01H and 02H support plate intersections (4.74-volts and 0.66-volt, respectively). These intersections were tested with a plus-point (+Point) probe. MAI (multiple axial indication) calls were reported at both intersections, without an indication of denting.

2.2 Tube Pull Operation

Westinghouse removed sections from the hot leg side of R22C70 from Sequoyah-2 steam generator 4 during the EOC-14 refueling outage. [

] a,c,e

A maximum force of 4080 lbs was the originally reported maximum force required to pull the tube out of the generator, however this was later shown to have been incorrect; the actual pull force may have been significantly higher. Subsequent tensile testing demonstrated that the force required to pull the tube out of the generator exceeded the yield strength of the material.

The tube was cut into seven sections as it was pulled through the tubesheet (the terms “section” and “piece” are used interchangeably throughout this report). Most cuts were made []^{a,c,e} at an angle that was about 45° to the axis of the tube. The tube was “nicked” []^{a,c,e} at the top of each tube section on the side of the tube opposite the divider plate. The tube was cut in convenient lengths to preserve the “areas of interest”, and put into hard clear plastic tubes. Each section was identified with the tube section number on the clear plastic packaging.

Table 2-1 lists the sections, their lengths and their location. Reference 6 demonstrated that the length of the pieces measured in the lab closely matched the measurements made on the pieces after removal from the steam generator. Based on the labeling that was placed on the individual bag that held each tube and the match between lengths in Reference 6 and those measured in the lab, it was verified that the correct pieces were received and were labeled correctly.

After initial inspection, the ends of the tube sections were deburred to facilitate eddy current inspections. Select sections of tube were subsequently cut into smaller specimens for ECT examination. The identification and traceability of specimens was maintained in accordance with the Reference 7 procedure. The designation of each cut specimen includes the number of the

original piece. For instance, specimen 2B was cut from piece 2, and specimen 2B1 was cut from piece 2B, etc. An orientation system was arbitrarily chosen to aid in the description of the tube specimens. The 0° orientation of each specimen was related to a tube pull grind mark at the bottom of the tube piece (the tube sections were marked on the side facing the periphery), and 90° is clockwise of 0° when looking in the upward (primary flow) direction. Unless otherwise stated, this orientation system is used throughout this report.

2.3 NRC Teleconference

It is common for the tube pulling operation to cause scrapes and some gouging of the pulled tube. However, observations in the laboratory of the as-received condition of the sections from R22C70 suggested that an excessive amount of force may have been required to remove the tube from the generator. There were two significant observations:

- Post-pull laboratory bobbin coil voltages for both TSP regions were about a factor of ten higher than the pre-pull in-generator bobbin coil voltages (a factor of two is typical).
- A simple, informal, leak test was conducted on the TSP#1 region. One end of the section containing TSP#1 was plugged with a rubber stopper. The section was held vertical and filled with DI water. With about 16 inches of water head as pressure, leakage was observed from the TSP#1 region at a rate of approximately 1 drop every 10 seconds. There were no reports of significant tube leakage during operation of the steam generators.

It was judged that certain characteristics of tube R22C70 were no longer representative of its in-generator condition. Most importantly, it was judged that the cracks for both TSP regions were significantly unrepresentative of their condition when the in-generator bobbin coil data was acquired; the ARC database (Reference 5) relating leak rates and burst pressures to bobbin voltages would be adversely affected.

In response to the concerns about the condition of the tube, a teleconference was conducted between TVA, Westinghouse and the NRC on February 13, 2007 to discuss how to proceed. The NRC agreed to accept an analytical determination of the leak rate and burst pressure in place of the laboratory leak and burst test requirements of the ARC (Reference 2, attachment 1, paragraph 4c). The NRC agreed that a substitute tube pull would not be necessary if it could be demonstrated that leak rates and burst pressures from these two TSP regions were reasonable in comparison to the existing database.

As a consequence of the teleconference, the scope of work was altered. Original plans to leak and burst test the TSP regions were replaced with:

- Actions/examinations to assess extent of tube-pull tearing.
- Hydraulic/pneumatic expansion of TSP regions
- SEM/EDS of mechanically opened cracks
- Engineering evaluation to analytically derive leak rate and burst pressure of TSP regions
- Radial metallography to investigate the observed circ openings

The results of the altered scope of work are documented in this report.

Table 2-1: Pulled Tube R22C70 Section Lengths and Characteristics

Piece	Lab Measured Length (inches)	Remarks
1	9-7/8	
2	23-1/2	Includes TTS region
3	20	
4	23-1/2	Includes TSP#1 Region
5	24	
6	30-3/4	Includes TSP#2 Region
7	35	

3.0 RECEIPT INSPECTION

3.1 Visual Observations

After receipt at the laboratory, sections of the tube from Sequoyah-2 were visually inspected to document and to identify areas of corrosion, deposits, etc. for more detailed analyses. This examination was conducted with the unaided eye and with a variable magnification stereomicroscope. Observations about tube conditions were recorded and are discussed below. The conditions of regions of interest (TTS and TSP regions) were documented using low magnification digital photographs.

3.1.1 Tubesheet Region and TTS

Sections 1 and 2 contained the regions of tube that were located within the tubesheet. Section 1 included the spear that was used to pull the tube from the SG, firmly installed in the lower end of the section. Section 2 included the TTS, located 10¼ inches above the bottom of section 2. Section 2 had an orientation mark indicating which side of the tube faced away from the divider plate; section 1 did not.

Figure 3-1 presents a series of photographs of the TTS region, taken at eight locations around the circumference of the tube. There was a narrow band with a slight build-up of deposits, which corresponded with the location of the TTS. With the exception of the TTS, there were no deposits remaining on the tube.

No cracks, pits or any other forms of corrosion were observed near the TTS or anywhere else on section 1 and section 2.

Above the TTS there were numerous scratches and several deep gouges. In region where there weren't any scratches, the circumferential belt polishing marks (from the tube manufacturing process) were plainly visible. Below the TTS were numerous deep scratches that were most likely a result of the tube pull operation.

The tubesheet region was severely scraped, although scraping in the tubesheet region is typical for pulled tubes. The tubesheet region also included several deep gouges. The deep gouges had a rough surface and consisted of smeared and raised material from the base metal of the tube. The deep gouges continued above the TTS, but there was less of the shallow scrapes that were present below the TTS. Where there was no scrapes or gouges, circumferential belt polish marks (from the tube manufacturing process) were visible. It was estimated that about 75% of the surface of the tube was either scraped or gouged below the TTS; above the TTS it was about 40%.

[

] ^{a,c,e} The tube ovalization continued, approximately to the same degree and orientation, up the length of the rest of the tube sections. However, neither section 1 or 2 were bent or bowed along the length of the tube.

3.1.2 TSP#1

Section 4 contained the region of the tube that intersected the first hot leg tube support plate. The TSP#1 region was centered 17-¼ inches above the bottom of section 4. The section was severely scraped and contained several deep gouges. It was estimated that about 40% of the surface was either scraped or gouged. The entire length of the section was visibly ovalized; pushed in at the 0° and the 180° orientations. Section 4 was not bowed or bent along its length.

Figure 3-2 presents photographs of the TSP#1 region around the circumference of the tube. Due to numerous scrapes and several deep gouges, there was little deposit left on the outer surface of the tube. There were some deposits remaining in the support plate region; a ¾ inch long area with patches of grayish deposits. Specks of copper were visible by stereomicroscope in much of the remaining deposit. Belt polish marks were visible in the areas of TSP#1 that had not been scraped and not covered by deposits.

Cracks were plainly visible at the 180° orientation. Cracks are typically not visible in the as-received condition of a pulled tube, even with the aid of a stereomicroscope; the tube pulling operation had induced stresses that opened these cracks such that they were made visible. Figure 3-3 shows several views of the cracks near the 180° orientation. A deep gouge ran directly through these cracks, obscuring some of the cracks with smeared metal, and tearing other openings/cracks.

There was a short circumferentially oriented crack segment that had opened wide in this region. It is connected to a short axially oriented crack segment that had opened wide as well. These short segments were part of a small patch of other connected short circumferential and axial crack segments that hadn't opened quite as wide, suggesting the presence of a small patch of IGA or cellular corrosion. This patch apparently has been partially obscured by the nearby deep gouge. Slightly below this patch were several axial-only cracks that hadn't opened quite as wide. The axial direction of the tube pulling forces would have opened the circumferentially oriented cracks and the forces that ovalized the tube cross section would tend to open axial cracks, so an assessment of the depth of axial vs. circumferential oriented crack segments cannot be made from a simple view of the OD surface.

Other axial cracks were visible at various locations around the circumference of the TSP#1 region. These are shown in Figure 3-4. Figure 3-4 shows axial cracks that were seen at the 110°, 150° and 315° orientations. These did not open as wide as those near the 180° orientation. Other cracks were seen by high magnification stereomicroscope at the 70° and 340° orientations, but had not opened sufficiently to be viewed by photo documentation. These other cracks consisted of short, unconnected axial segments, with no circumferential element. Other cracks may have obscured by the scratches and gouges.

3.1.3 TSP#2

Section 6 contained the region of the tube that intersected the second hot leg tube support plate. The TSP#2 region was centered 20 inches above the bottom of section 6. The section was severely scraped and contained several deep gouges. OD gripper marks, made by the tool used to pull the tube out of the steam generator, were visible at various locations around the circumference of the tube, just below the TSP#2 region (the uppermost gripper mark was actually in the TSP#2 region). It was estimated that about 40% of the surface was either scraped or gouged. The entire length of the section was visibly ovalized; pushed in at the 0° and the 180° orientations. Section 6 was slightly bowed along its length.

Figure 3-5 presents photographs of the TSP#2 region around the circumference of the tube. Due to numerous scrapes and several deep gouges, there was nearly no deposit left on the outer surface of the tube. There were some very thin amounts of gray colored deposits remaining in the support plate region. Nevertheless, sufficient deposits remained to discern the precise location of the TSP#2 intersection. Belt polish marks were visible through the deposits in the areas of TSP#2 that had not been scraped.

Cracks were visible with a stereomicroscope at the 40°, 90°, 180° and 315° orientations. These are shown in Figure 3-6. A deep gouge ran directly through the 180° crack area, obscuring some of the cracks with smeared metal, and tearing open a very short circumferential opening within the gouge. There was no evidence of circumferentially oriented cracks outside of the gouge. None of the cracks had opened as wide as those in the TSP#1 region, but the fact that they were visible at all in the as-received condition is consistent with the ovalization that was observed.

3.1.4 Freespan

A brief examination of the freespan sections of the pulled tube was performed. Tube pull gripper marks were visible 12 inches above the bottom of section 3 and just below TSP#2 on section 6. Only section 6 showed any sign of bowing along the tube length. Other observations are similar to those made for sections 2, 4 and 6, namely that the sections were heavily gouged and scraped, there was no deposits remaining on the freespan sections and that the cross-section was visibly ovalized.

To demonstrate the degree of ovality, an end piece was cut from a freespan section, mounted in epoxy to show the cross-section, ground and rough polished so as to show the general shape of the tube. The result is shown in Figure 3-7. The figure includes a perfect circle (shown in red) that was drawn on top of the cross-section to approximate what the nominal shape of the ID wall should look like. It shows that the degree of ovalization is roughly equal to the width of the tube wall. The measured minimum inner diameter (measured from another location along the length of the tube using a set of mandrels with different diameters) was 0.697 inch, compared to the nominal value of 0.775 inch.

From Figure 3-7, it was estimated that the deepest gouge was about 10% throughwall (%TW). The deepest gouges were generally found at the 0° and 180° orientations, but deep gouges were found at other locations around the circumference of the tube.

3.2 OD Measurement Profiles

The maximum and minimum outer diameter (OD) of the tube sections was measured at selected locations along the length of the tube. Assuming that the width of the cut that was made between sections was []^{a,c,e}, the outer diameter profile shown in Figure 3-8 can be constructed. The length is constructed from the distance to the bottom of section 1 and does not include the [

] ^{a,c,e} The locations of the minimum and maximum OD measurements are indicated by the symbols within each line. The minimum and maximum OD is compared with the nominal OD (shown by the dashed line). [

] ^{a,c,e}

It was found that above 12", the minimum diameter was always at 0° and the maximum at 90°. Below 12" the location of the maximum and minimum varied [

] ^{a,c,e}

The location of TSP#2 was 123-5/8 inches above the bottom of section 1. [

] ^{a,c,e} and comparing with the values in Table 1-1, show that the tube was elongated by about 1.85 inches, or about 1.5%. This indicates that the forces required to remove the tube from the tubesheet exceeded the yield strength of the material.

A laser micrometer was used to obtain a detailed profile of the support plate regions. The results are shown in Figure 3-9 and Figure 3-10 for TSP#1 and TSP#2, respectively. Usually these results can be used to ascertain whether or not the support plate region had been dented, however due to the significant ovalization and raised metal from the gouges on the tube; these results are of limited use. It cannot be determined if the support plate regions were dented or not.

3.3 Deposit pH

The purpose of this test was to determine if the crevice chemistry was highly acidic or highly caustic.

[

] ^{a,c,e} did not indicate an abnormal pH.

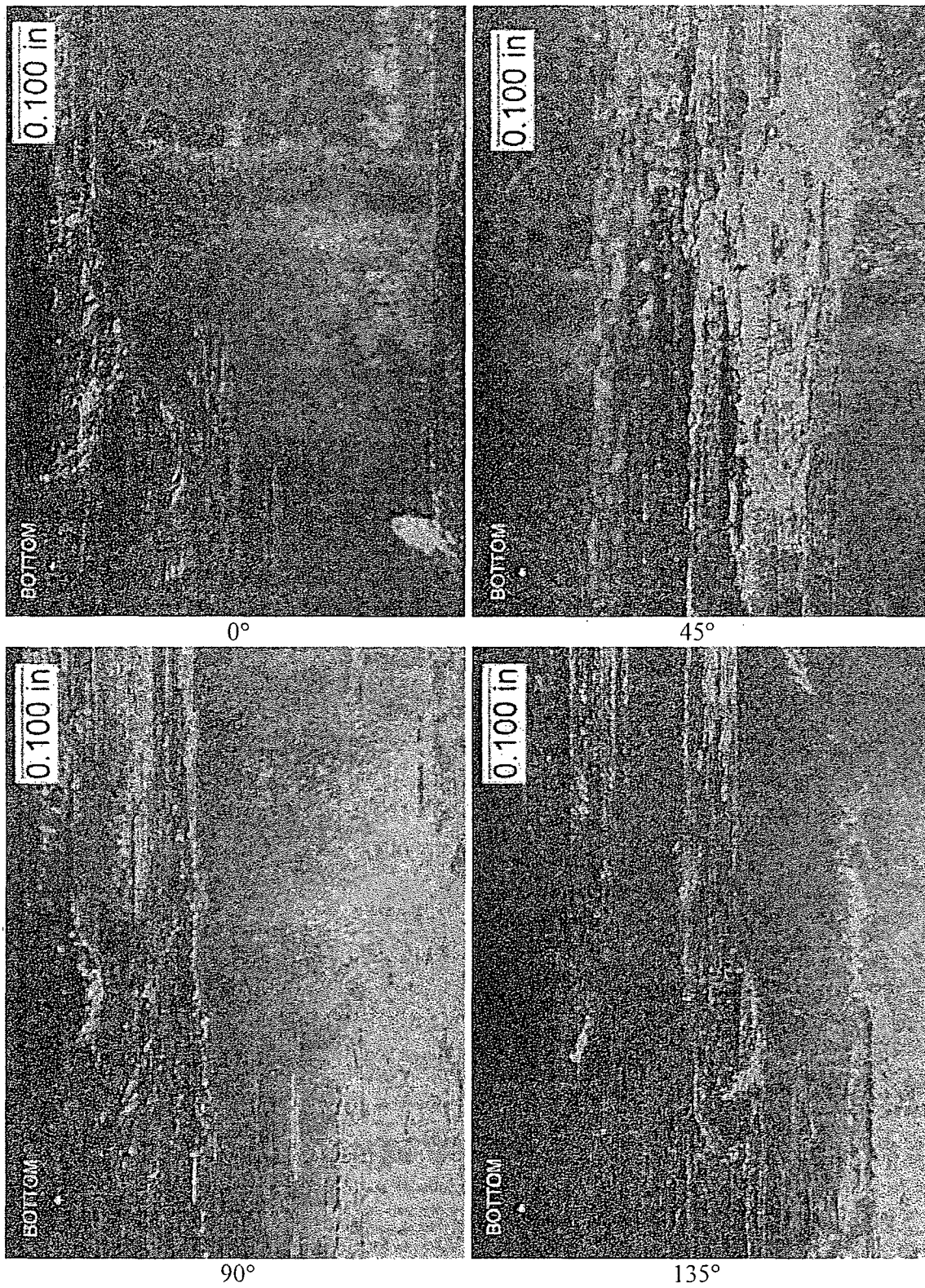


Figure 3-1: As-Received Views of TTS Region

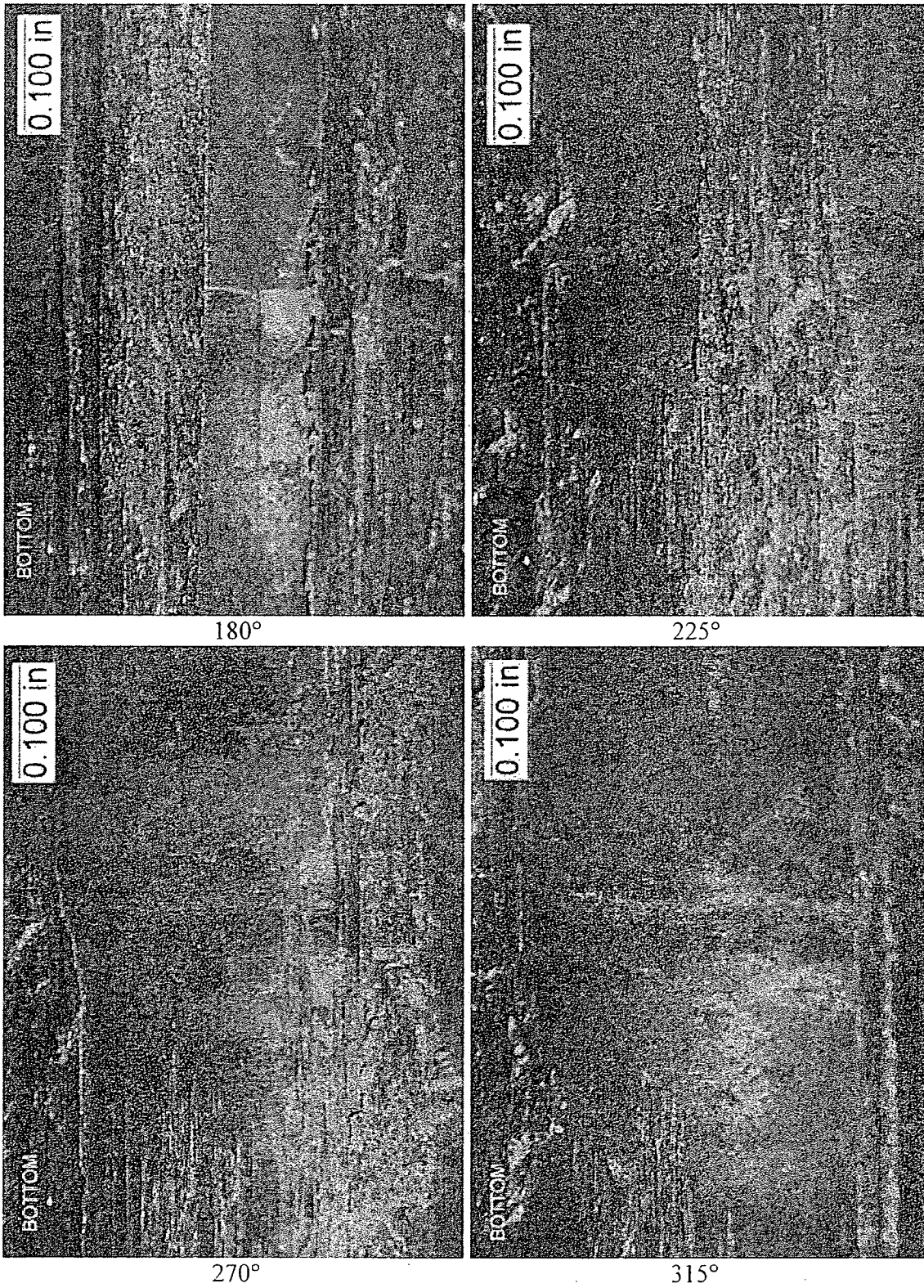


Figure 3-1: As-Received Views of TTS Region (continued)

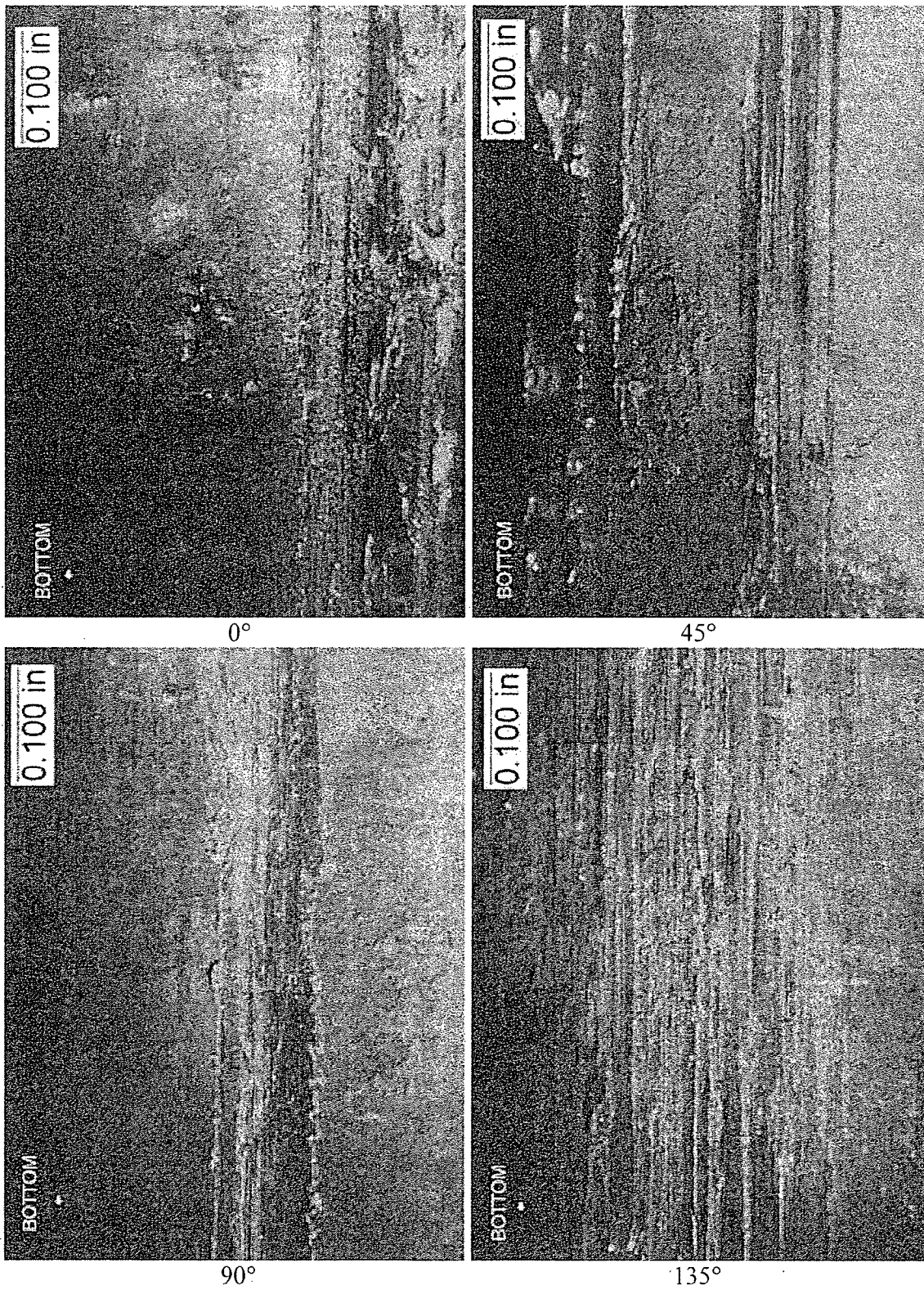


Figure 3-2: As-Received Views of TSP#1 Region

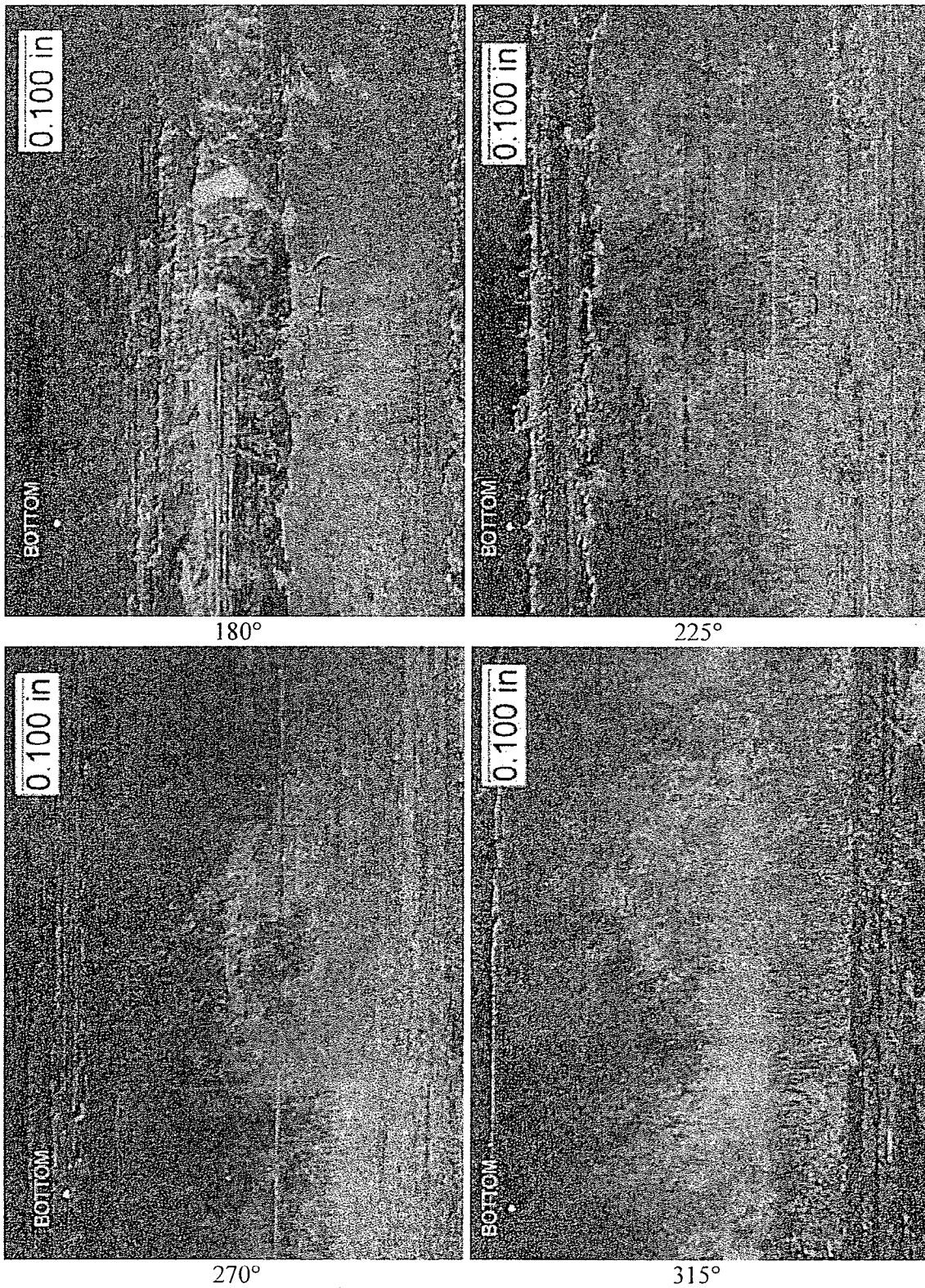


Figure 3-2: As-Received Views of TSP#1 Region (continued)

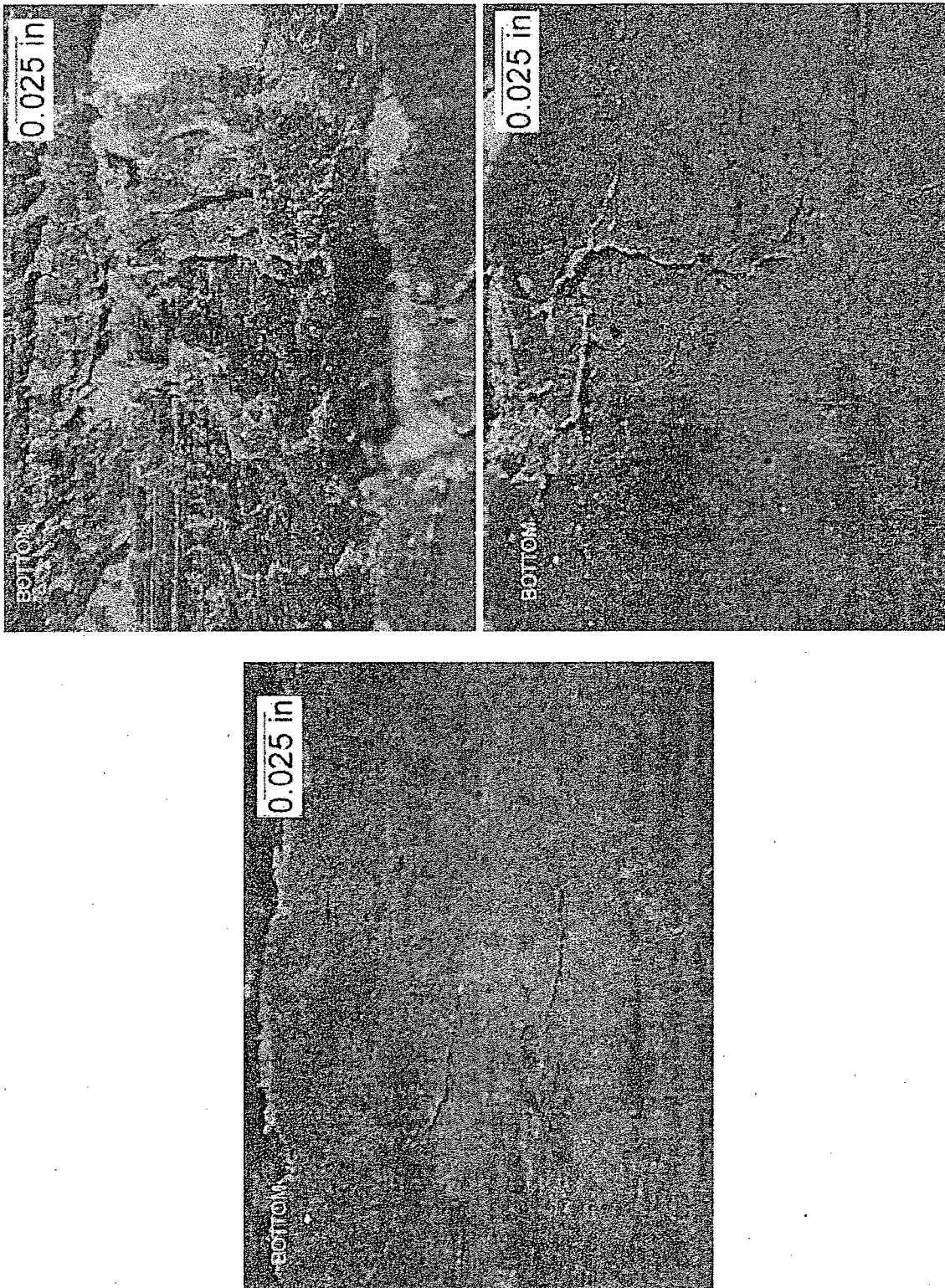


Figure 3-3: As-Received Close-Up Views of Cracks Near 180° Orientation of TSP#1

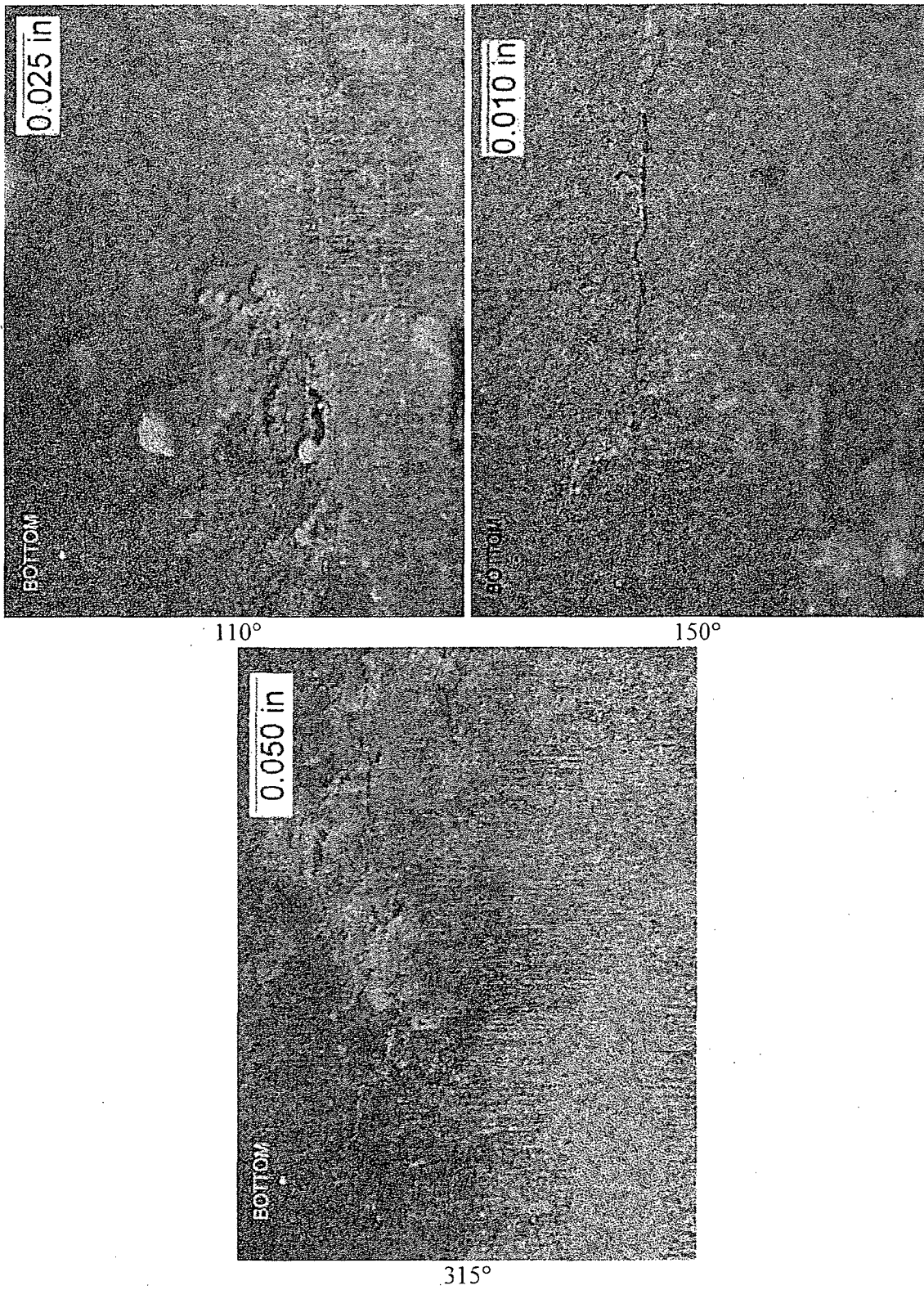


Figure 3-4: As-Received Close-Up Views of Other Cracks of TSP#1

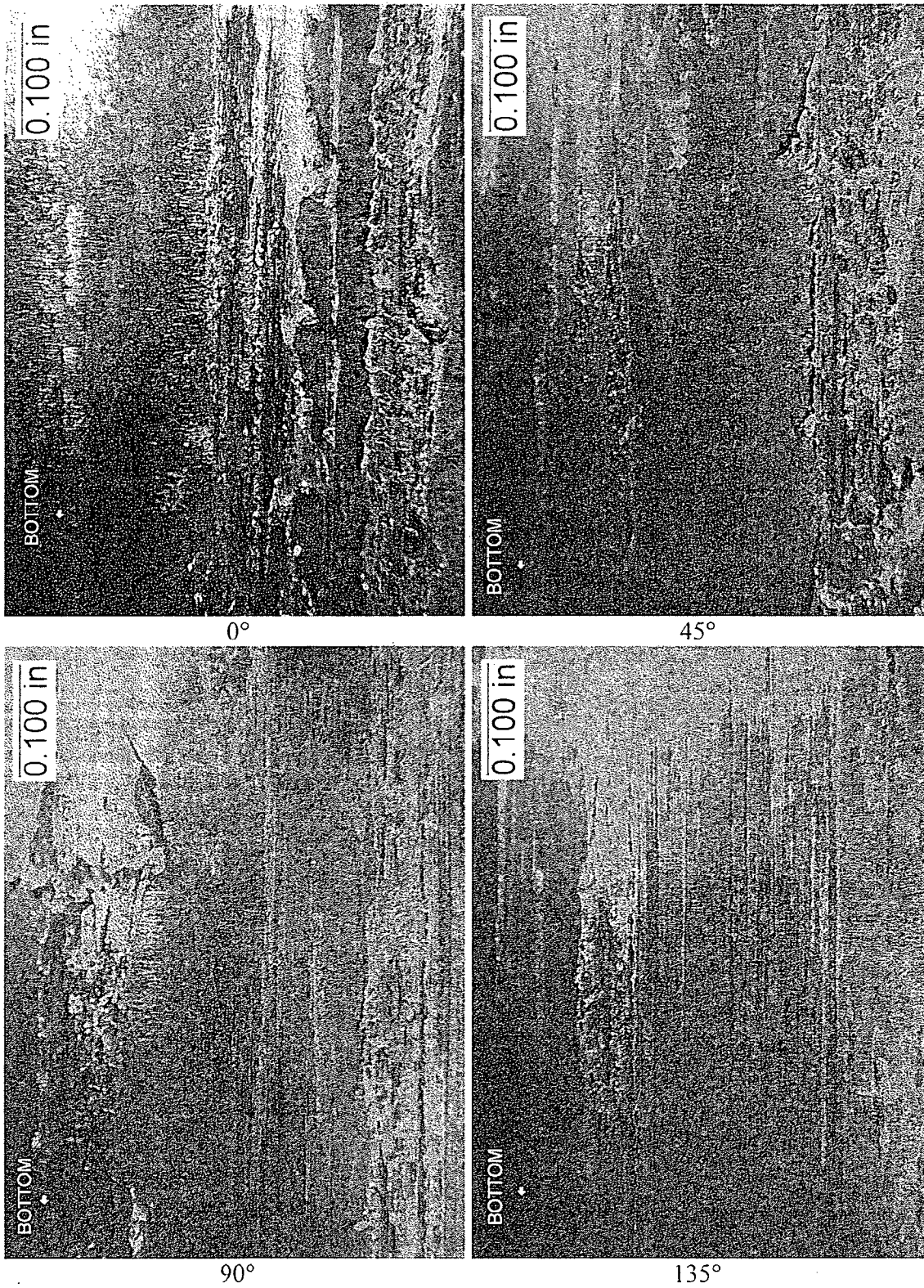


Figure 3-5: As-Received Views of TSP#2 Region

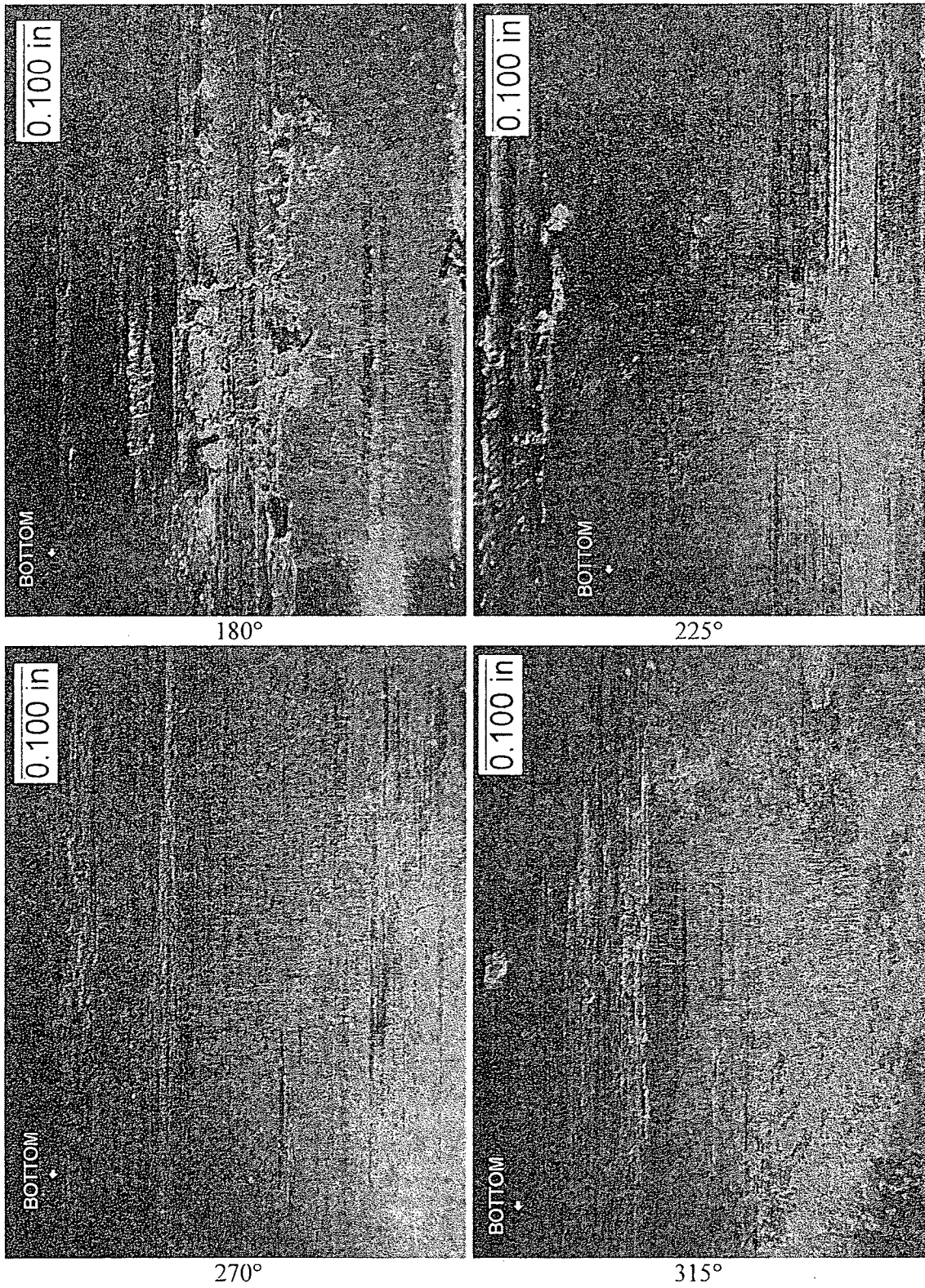


Figure 3-5: As-Received Views of TSP#2 Region (Continued)

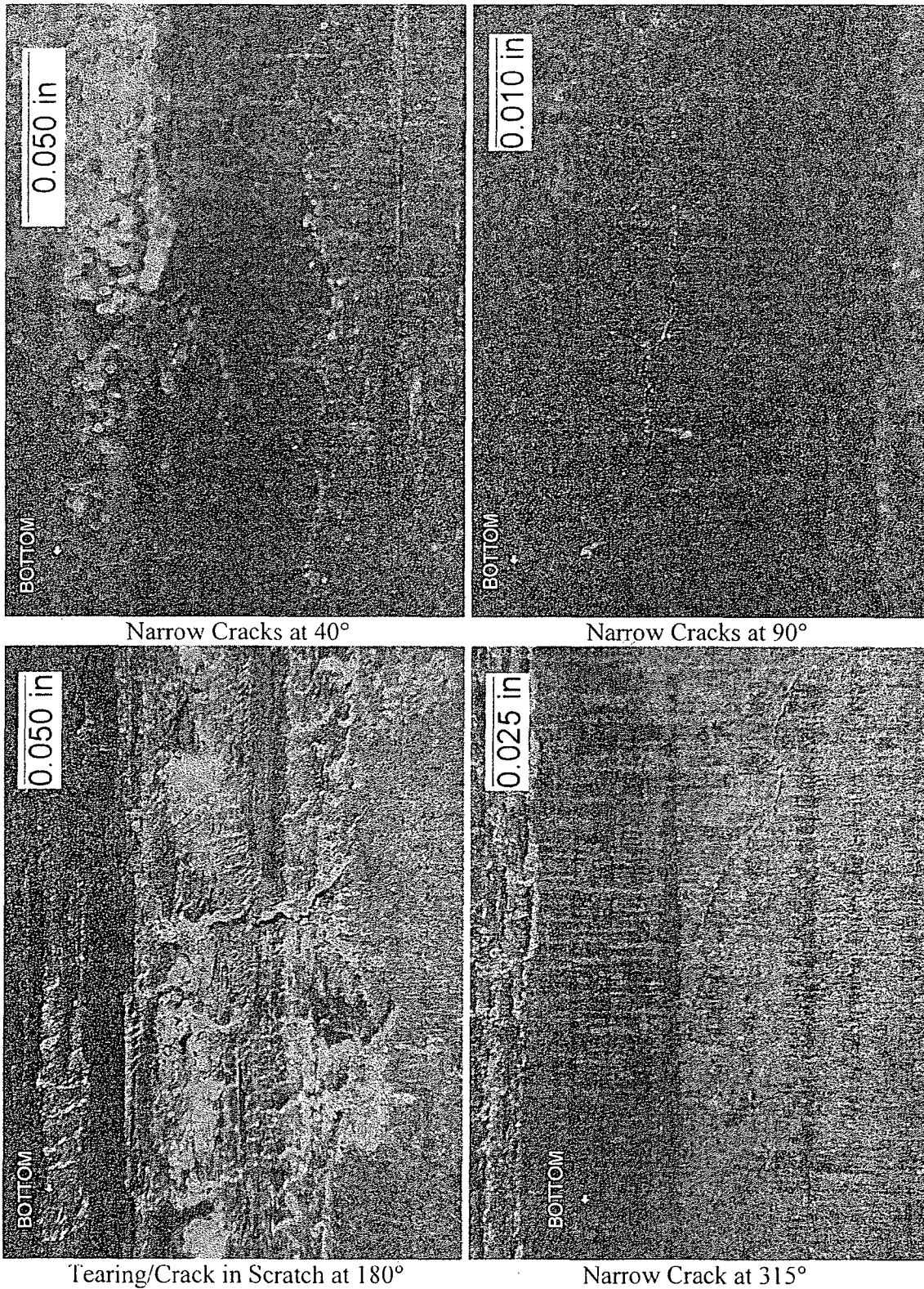


Figure 3-6: As-Received Close-Up Views of Miscellaneous Features of TSP#2



Figure 3-7: Cross-Section of Tube Showing the Degree of Ovalization

The red line is a perfect circle that approximates the nominal shape of the ID wall of the tube.



Figure 3-8: Maximum and Minimum Diameter Profile Along Entire Length of the Tube



Figure 3-9: TSP#1 Laser Micrometer Profilometry Results

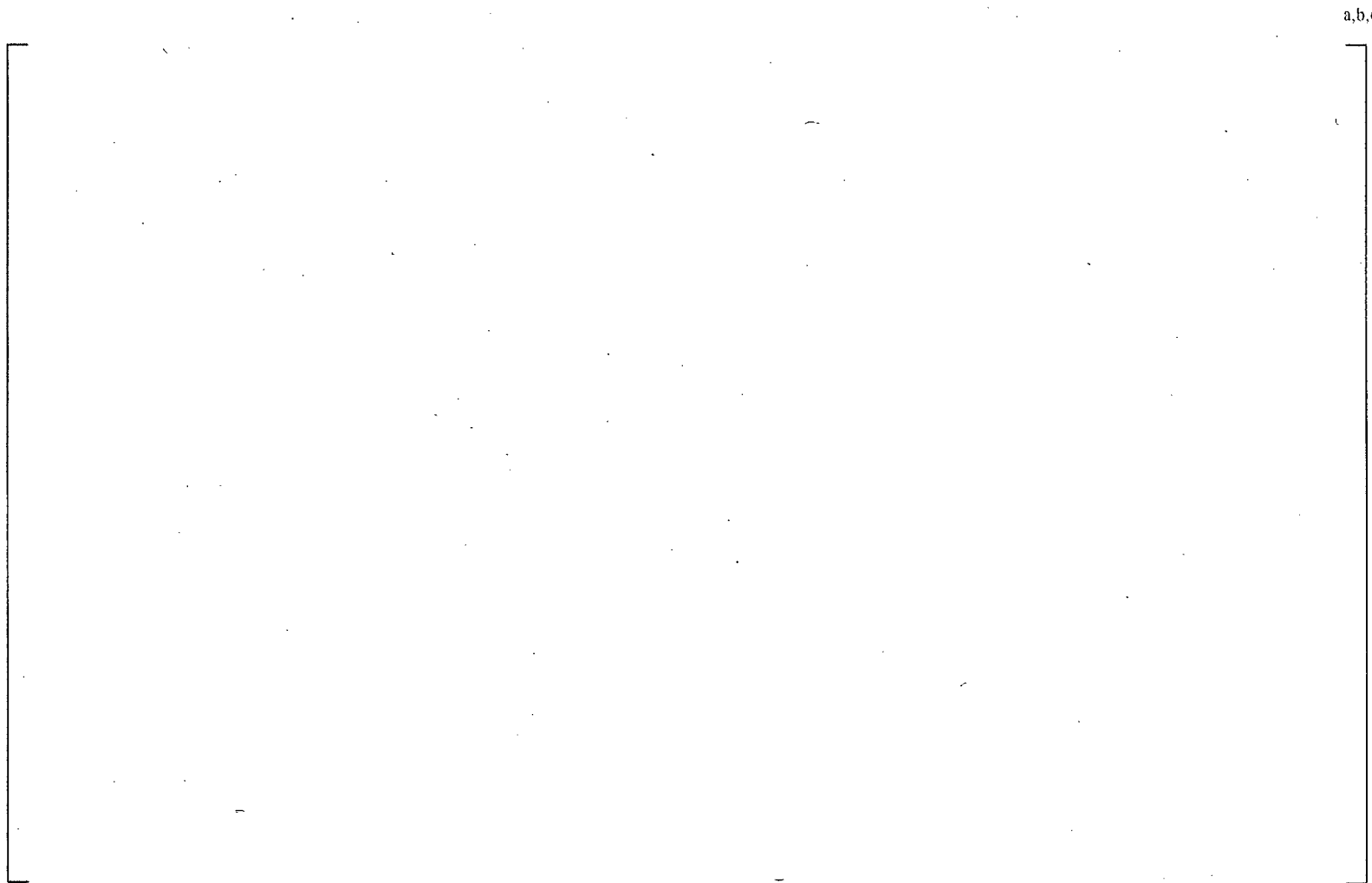


Figure 3-10: TSP#2 Laser Micrometer Profilometry Results

4.0 EDDY CURRENT TEST INSPECTION

4.1 Introduction

The tube examination included elements of non-destructive inspection to help guide the destructive inspection. The field eddy current test (ECT) data were re-evaluated to provide more detailed characterization of the indications than is normally provided in the field inspection reports such as the relative orientations of indications and depth estimate/profiles of the individual indication. Also, as part of the laboratory examination, the tube sections are normally eddy current inspected in a manner consistent with the field inspection. However, that was not possible during this examination. Tube distortion associated with the tube removal process ovalized the tube sufficiently such that the 0.72 inch diameter probes typically used to perform the inspection would not fit inside the tube. Consequently for the bobbin coil examination a 0.680 inch diameter probe was used. For the rotating coil examination, a 0.680 inch diameter, single +Point coil probe was used. [

] a.c.c

The +Point inspection data obtained during the tube examination provides information such as the azimuthal location and extent of the indications, that is used to locate the indications within the tube segment. For this examination these measurements are qualitative at best. [

] a.c.c

After the as-received observations were completed, the end of the tube sections were squared-off and deburred to facilitate eddy current inspections.

4.2 Results

Table 4-1 presents a summary of field and laboratory eddy current data obtained on the pulled tubes for the TSP crevice regions of interest. The data are presented in a manner to allow for one-to-one comparison of the field and laboratory results. Bobbin coil calls were made using 400/100 kHz MIX data from the differential mode. Since the laboratory inspections used the 0.680 inch diameter probe, its ability to center was not expected to be optimal. Consequently, each tube piece was tested four times with the tube pieces rotated 90 degrees between each inspection. Rotating probe calls were made from the +Point coil using 300 kHz differential mode data. In addition, the analysis of the laboratory data used the 400kHz +Point data channel calibrated for depth measurement using the CEOG amplitude method to supplement estimates of the degradation extent.

Table 4-1 shows that the re-evaluation of the bobbin data showed results that were similar to the original field evaluation. The re-evaluation of the TSP#1 +Point data confirmed the presence of one large amplitude indication, and the additional low-amplitude indications. The re-evaluation of the TSP#2 +Point data also identified additional low-amplitude indications.

[]^{a,c,e} During this examination, however, the tube distortions were such as to make data interpretation difficult. The laboratory ECT data for TSP#1 showed indication responses that were significantly larger in amplitude than the field data. The large change in the amplitude response is consistent with the opening of ligaments within the degraded regions by the tube removal process. The +Point responses had characteristics of circumferential involvement suggesting the opening of cellular corrosion by the axial stresses of the tube removal near the end of the indication. Further, where there were discernable indications in the original field inspection, the laboratory exam showed a more blended together response suggesting that ligaments within the degraded region had been opened during tube removal. Measurement of the indication responses and orientation were complicated by tube distortions associated with the tube removal.

The laboratory bobbin coil ECT data identified an indication at the location of TSP#2 and showed a significant increase in its amplitude compared with the field response consistent with the observations for TSP#1. Further, the indication was comprised of a signal associated with tube deformation and also that of the degradation response. In the +Point examination, analysis of the results identified at least four regions of the tube circumference that are areas of possible degradation. Only one of these regions was undistorted by artifacts of the removal such that measurements were believed to reflect the degradation response. This measurement was included in Table 4-1.

Table 4-1: Field and Laboratory Eddy Current Inspection Results for R22C70

Location	Field				Lab	
	Bobbin (0.720 in.) 400/100 kHz (Mix)		Field +Point (3-Coil) 300kHz		Lab Bobbin (0.680 in.) 400/100 kHz (Mix)	Lab +Point Single coil 0.680 in. U-bend probe
	Field	Lab Re-evaluation	Field	Lab Re-evaluation		
TSP#1	4.74V DSI	4.82V 94%	MAI (6) Largest 1.98V	MAI Largest 1.92V (95%)	48.9V @ 0° 36.9V @ 90° 36.3V @ 180° 51.9V @ 270°	Azimuthally Orientated between 160° and 190° 300 kHz 9.9V (99% by phase) 400kHz 10.26V (92% by amplitude)
TSP#2	0.66V DSI	0.77V <20%	MAI (2) Largest 0.24V	0.25V 20% 0.12V 10%	7.11V @ 0° 8.39V @ 90° 10.5V @ 180° 10.2V @ 270°	Azimuthally Orientated 284° 300 kHz 0.81V (<20% by phase) 400kHz 0.71V (56% by amplitude)

5.0 DESTRUCTIVE EXAMINATION PREPARATION

The large increase in the eddy current voltages, shown in Table 4-1, raised a concern that the tube pull operation had significantly altered the characteristics of the crack. There was a concern that a representative leak rate test could not be conducted. Prior to the NRC teleconference discussed in Section 2.3 of this report, helium and water leak screening was conducted.

After the completion of the non-destructive examinations, and prior to cutting the samples for the performance of the destructive examinations, the two support plate regions required special preparation. Heat tinting was used in an attempt to make a distinction between tube-pull induced and laboratory induced ligament tearing. This was followed by hydraulic expansion of the support plate regions to open all OD cracks for visual identification and destructive examination planning.

5.1 Leak Screening

To determine if a leak path had developed through the tube wall, each TSP region was screened for leakage using []^{a,c,e} helium. For each section []^{a,c,e}

The TSP#1 region leaked with less than 10 psi helium pressure. TSP#2 did not leak with as much as 20 psi of helium.

To determine if the TSP#1 region was capable of holding water, a simple room temperature water leak screening test was conducted. []^{a,c,e}

With 16 inches of head, drops of water were observed to leak from the center of TSP#1 at the 180° orientation. A leak rate of 1 drop every 10 seconds was observed.

Since there were no reports of significant tube leakage during operation of the steam generators, it was concluded that the crack integrity characteristics had been significantly altered by the tube pulling operation.

5.2 Heat Tinting

5.2.1 Procedure

To access the cracks for laboratory examination, the cracks need to be mechanically opened. The cracks within nickel alloy steam generator tubes have almost entirely been intergranular; their morphology is easily distinguished by its "rock candy" appearance, as seen by optical microscope or scanning electron microscope (SEM). The laboratory mechanical opening splits apart the intergranular crack faces and tears uncorroded material. The tearing leaves a surface that is characterized as ductile dimpling, which is

easily distinguished from the rock candy surface caused by the corrosion. A corrosion crack depth profile can be obtained by SEM examination.

The process of removing the tube from the steam generator will cause mechanical tearing if sufficiently high stress is applied. The morphology of any in-generator tearing during the tube pulling operation is indistinguishable from the tearing that is produced in the laboratory to open the crack.

In the case of tube R22C70, it was desirable to determine the amount of tearing caused by the tube pulling operation. [

] a,c,e

5.2.2 Results

[

] a,c,e

After the cracks of TSP#1 and TSP#2 were opened for examination, their surfaces were documented by high magnification color photography and backscattered electron SEM. Selected areas were further scrutinized by SEM elemental dot map imaging.

None of these techniques provided any conclusive evidence that tube-pull tearing had occurred. However, there was a significant amount of evidence that indicated that ligaments had torn during the tube pull. Section 4.2 of this report discussed how the eddy current testing showed that the large change in the amplitude response is consistent with the opening of ligaments within the degraded regions by the tube removal process. It was determined that the low pressure, room temperature water leak rate observed in Section 5.1 of this report was only possible if ligaments had torn.. Section 9.2 provides further discussion of the tube pull ligament tearing.

[]^{a,c,e} It is not known why a discernable tint was not found on the torn ligaments of R22C70.

5.3 Support Plate Region Expansion

5.3.1 Procedure

The support plate regions were diametrically expanded to open all OD initiated corrosion for visual identification of crack locations. [

] ^{a,c,e}

5.3.2 Post-Expansion Observations

Following expansion, each TSP region was photographed, examined with a stereomicroscope and observations recorded.

Figure 5-2 and Figure 5-3 present views around the circumference of TSP#1 and TSP#2, respectively. Figure 5-4 and Figure 5-5 present diagrams summarizing observations made on TSP#1 and TSP#2, respectively, after expansion.

The expansion caused the tighter cracks to open allowing for better identification by stereomicroscope. There were no new areas of cracks around the circumference of the tube than what had been observed in the as-received condition, however most of the cracks were found to be longer than what had been observed previously.

The 110° crack of TSP#1 opened considerably and was found to have a length of 0.4 inches. The 180° crack of TSP#1 was about 0.56 inch long, less than the width of the TSP region and did not extend past the upper or lower bound of the TSP region. The 180° crack of TSP#2 extended to the bottom of the TSP region, but did not extend past the upper or lower bound of the TSP region.

These three cracks were selected for detailed examination by SEM.

No significant patches of IGA or cellular corrosion were found. A very small patch was observed near the 180° crack of TSP#1, and this area was selected for examination by radial metallography. A short circumferential opening was observed in a gouge near the 180° crack of TSP#2, and this area was selected for examination by radial metallography as well.

5.4 Sectioning

Table 5-1 summarizes the number and description of the samples used for the destructive examination.

Figure 5-6 shows how the TSP#1 region was sectioned.

Figure 5-7 shows where freespan samples were taken from.

Figure 5-8 shows how the TSP#2 region was sectioned.

Table 5-1: Destructive Examination Samples

Report Section	Description	Number of Samples	Location
5.2	Examination of Opened Cracks - Color Photography	3	TSP#1, #2
6.2, 6.3	Examination of Opened Cracks - SEM Characterization	3	TSP#1, #2
6.4	SEM/EDS of Deposits	2	TSP#1
6.5	Examination of Opened Cracks - SEM Depth Profile	3	TSP#1, #2
7.1	Defect Metallography - Transverse Section	2	TSP#1, #2
7.3	Defect Metallography - Radial Section	2	TSP#1, #2
8.1	Tensile Test	1	Freespan
8.2	Bulk Chemistry	1	Freespan
8.3	Microstructure - Freespan	1	Freespan
8.4	Microhardness	2	TSP#1, #2
8.5	Sensitization Test (Modified Huey)	2	Freespan



Figure 5-1: Heat Tinting

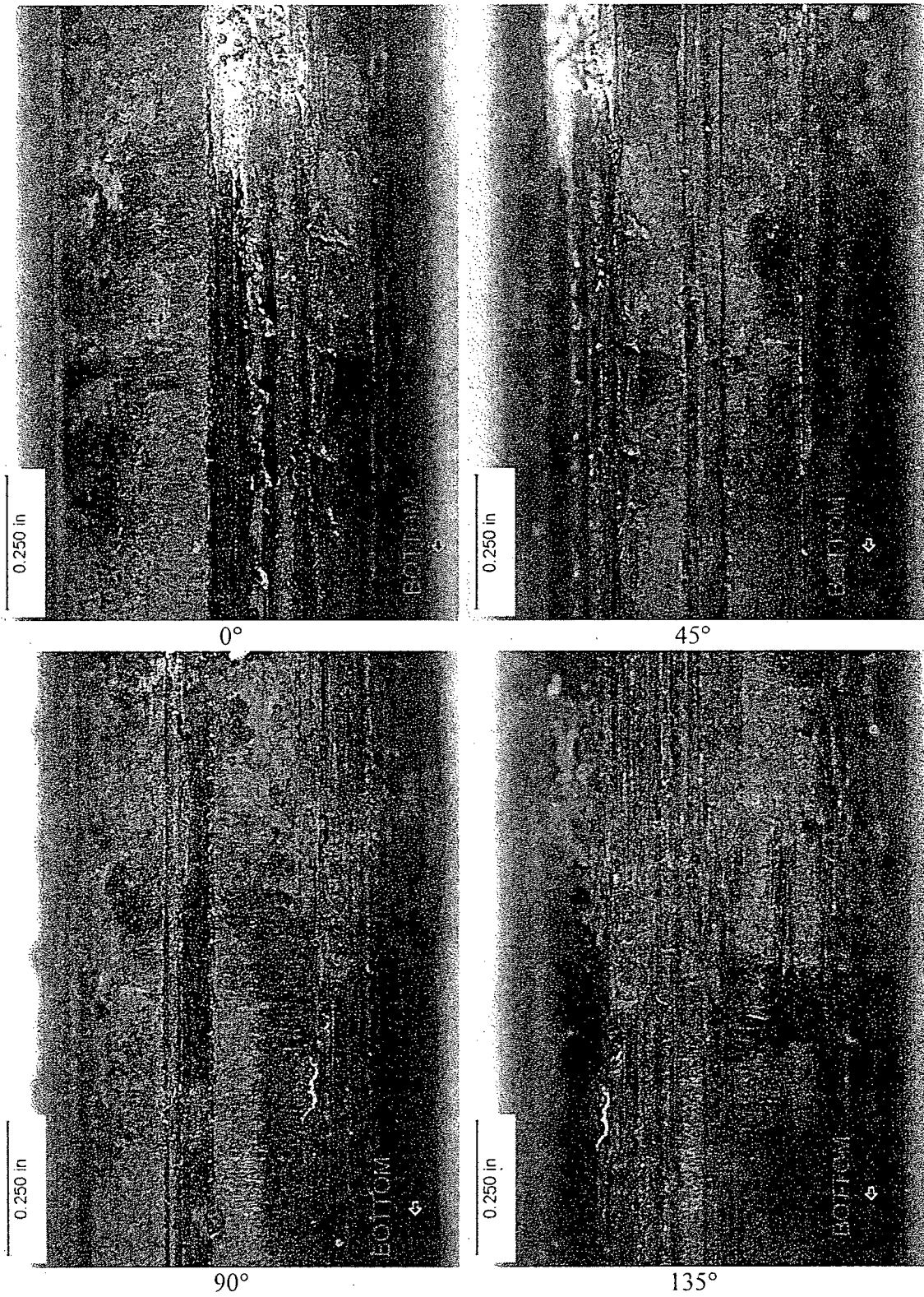


Figure 5-2: Post-Expansion Views of TSP#1 Region

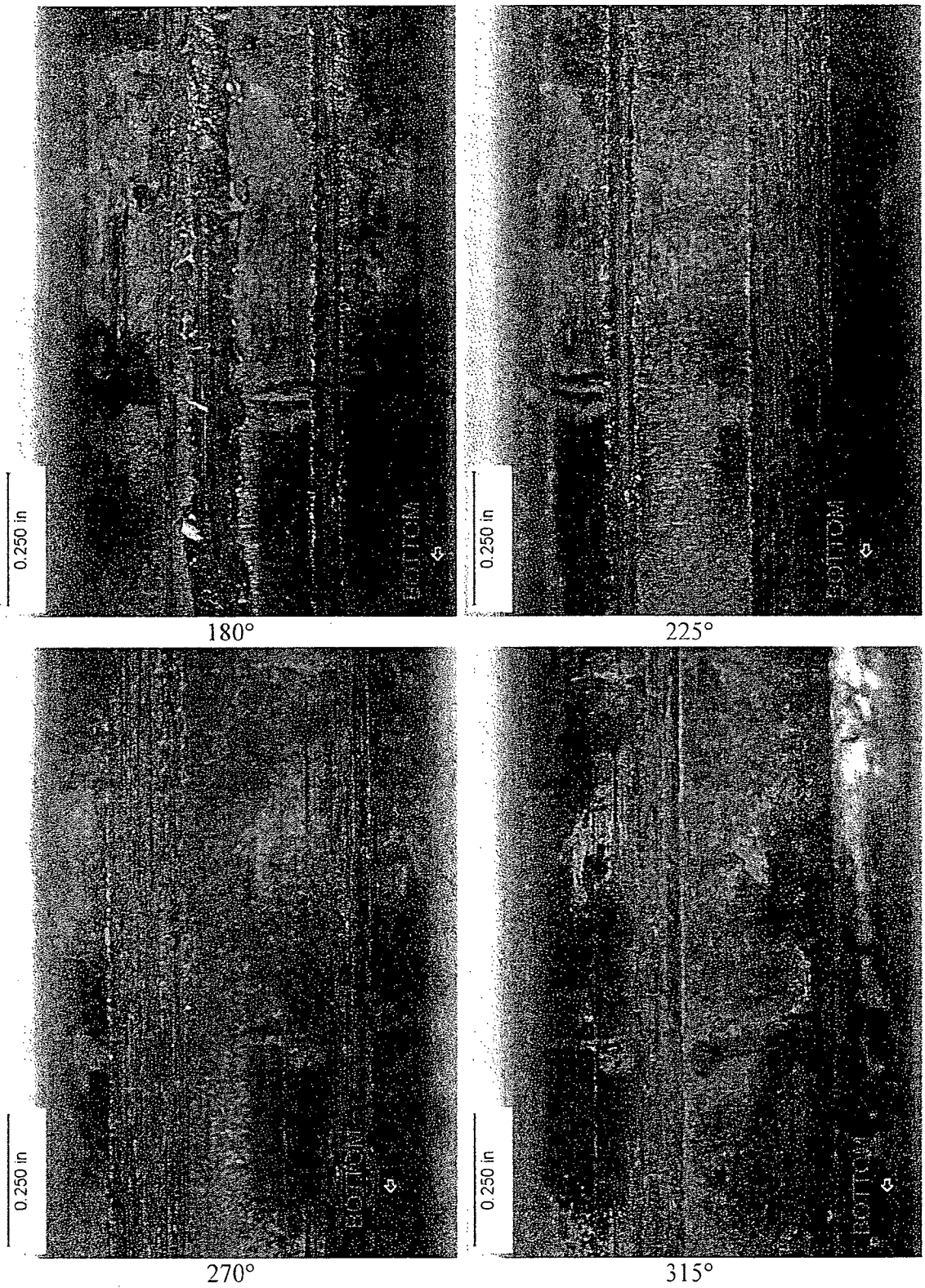


Figure 5-2: Post-Expansion Views of TSP#1 Region (Continued)

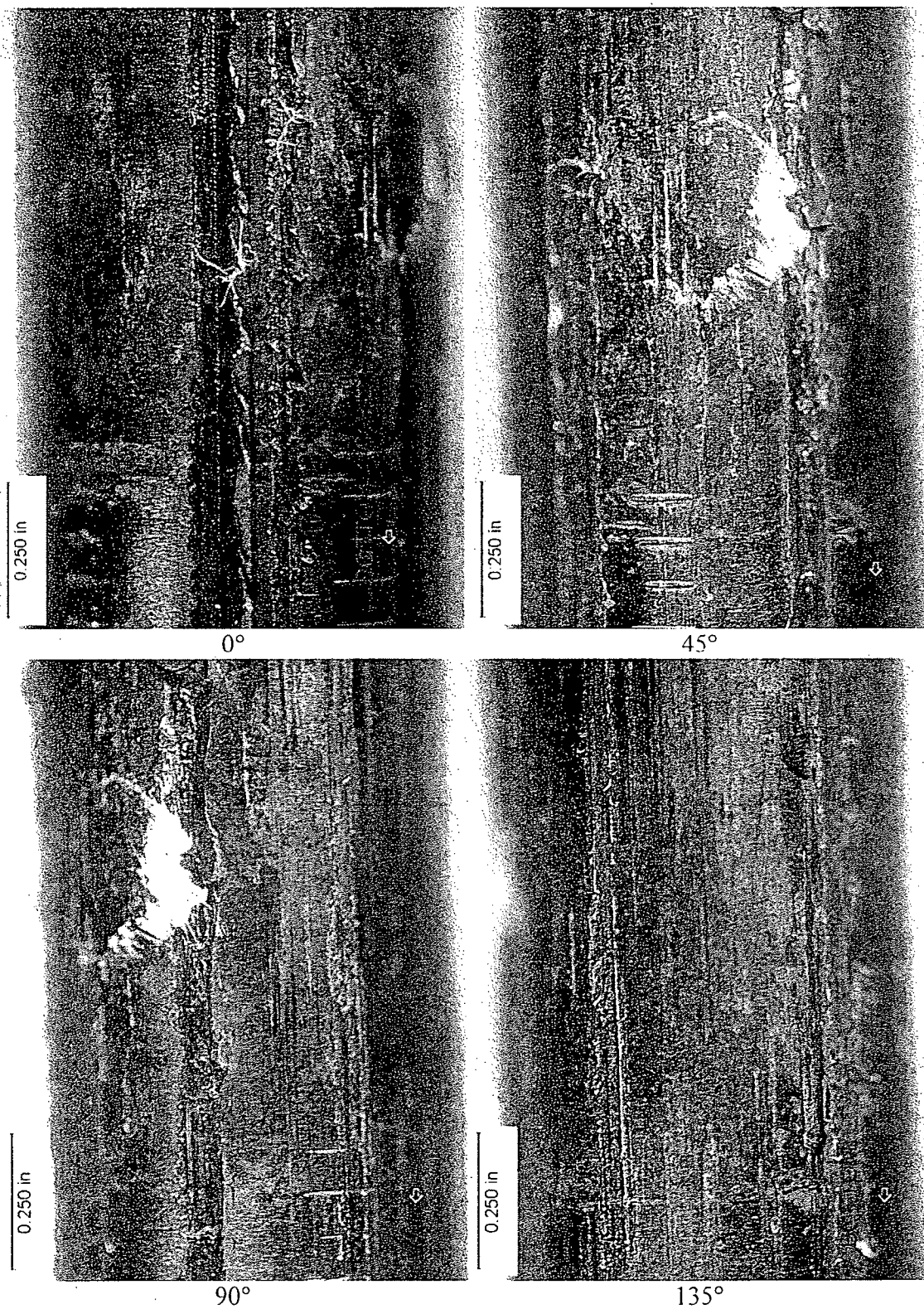


Figure 5-3: Post-Expansion Views of TSP#2 Region

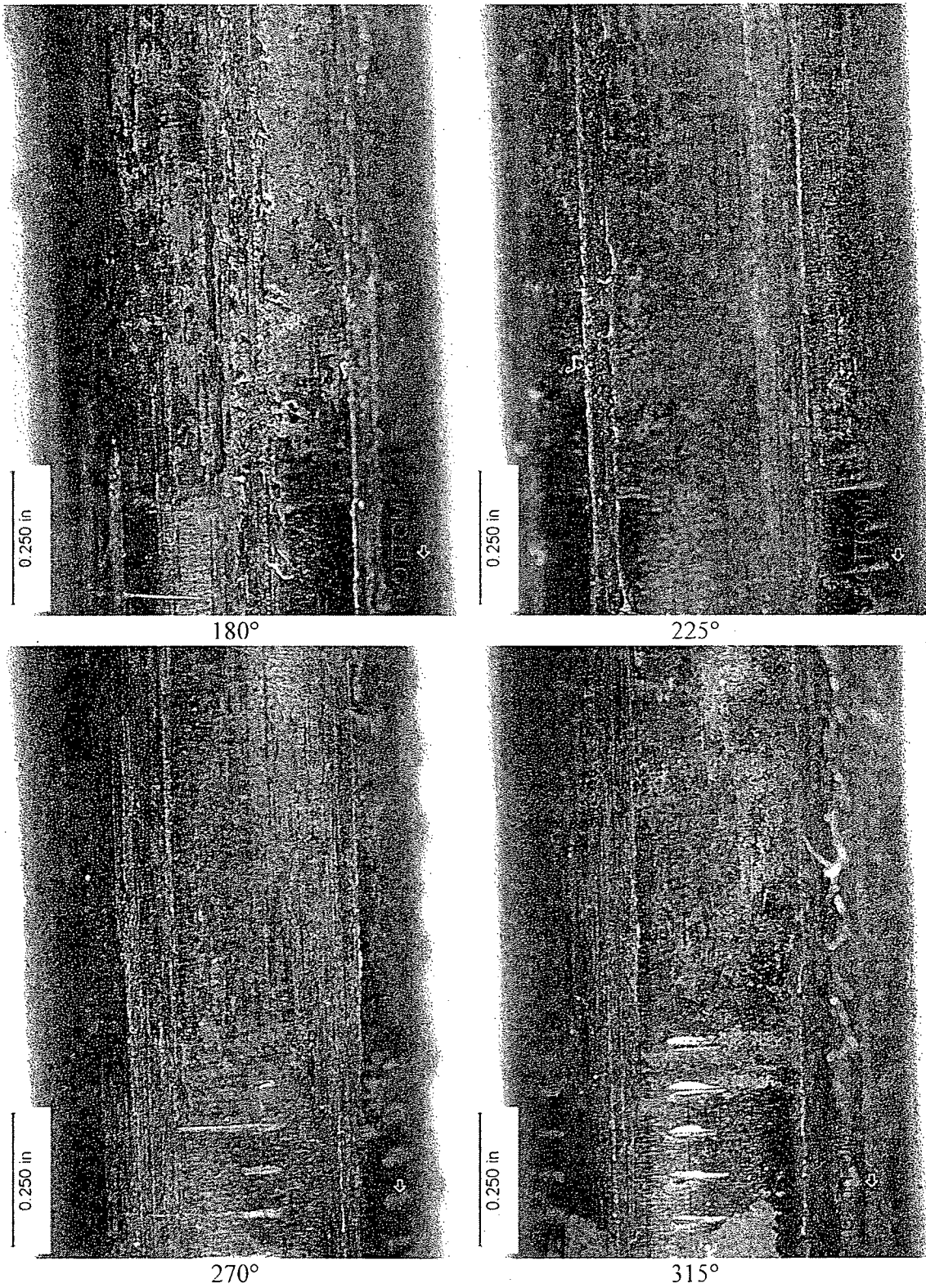


Figure 5-3: Post-Expansion Views of TSP#2 Region (Continued)

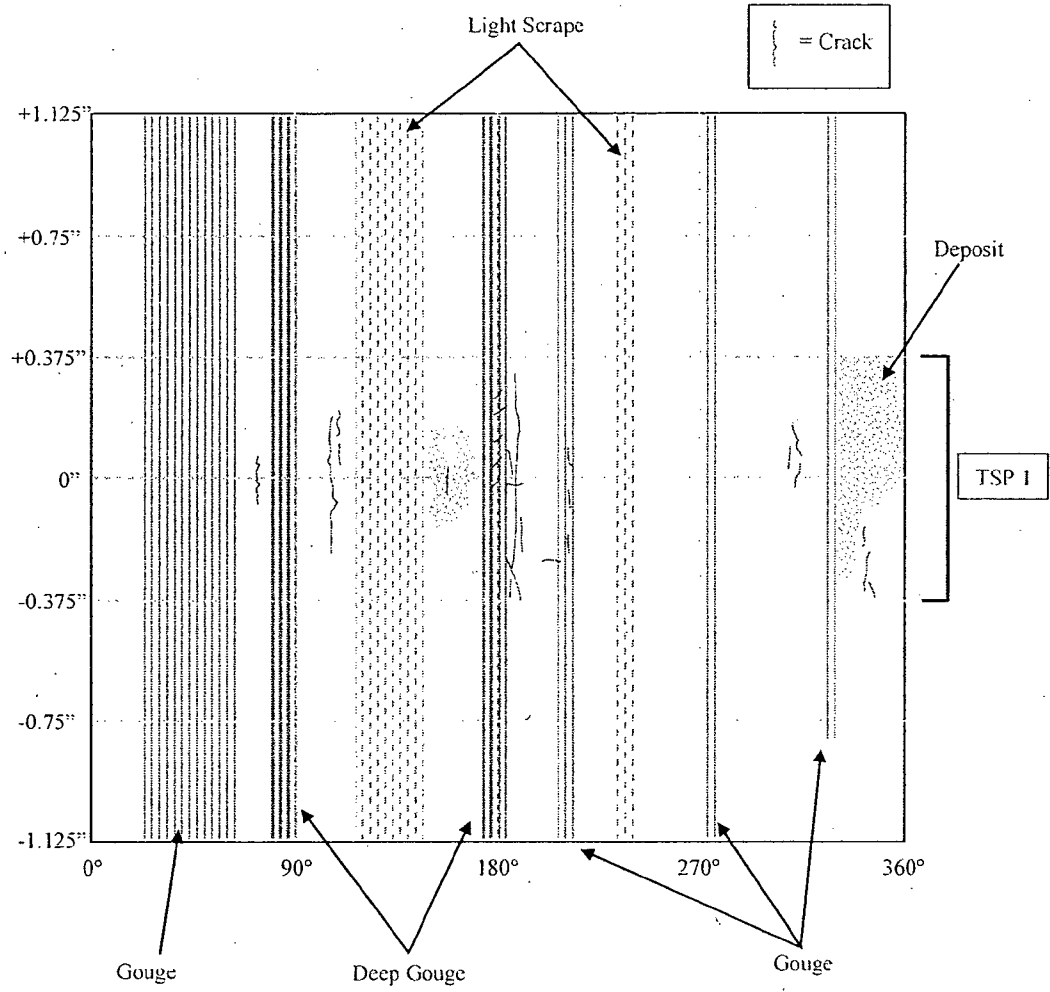


Figure 5-4: Post-Expansion Observations of TSP#1

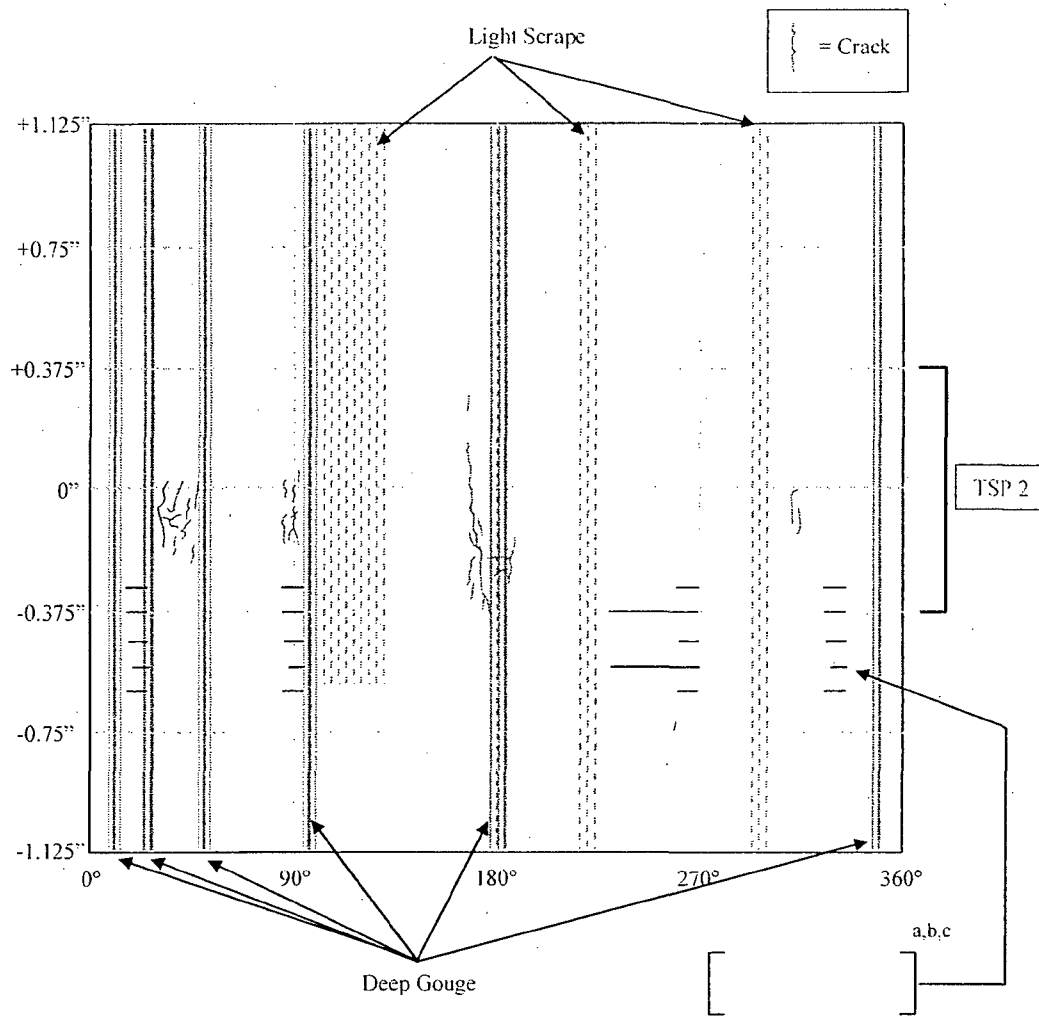


Figure 5-5: Post-Expansion Observations of TSP#2

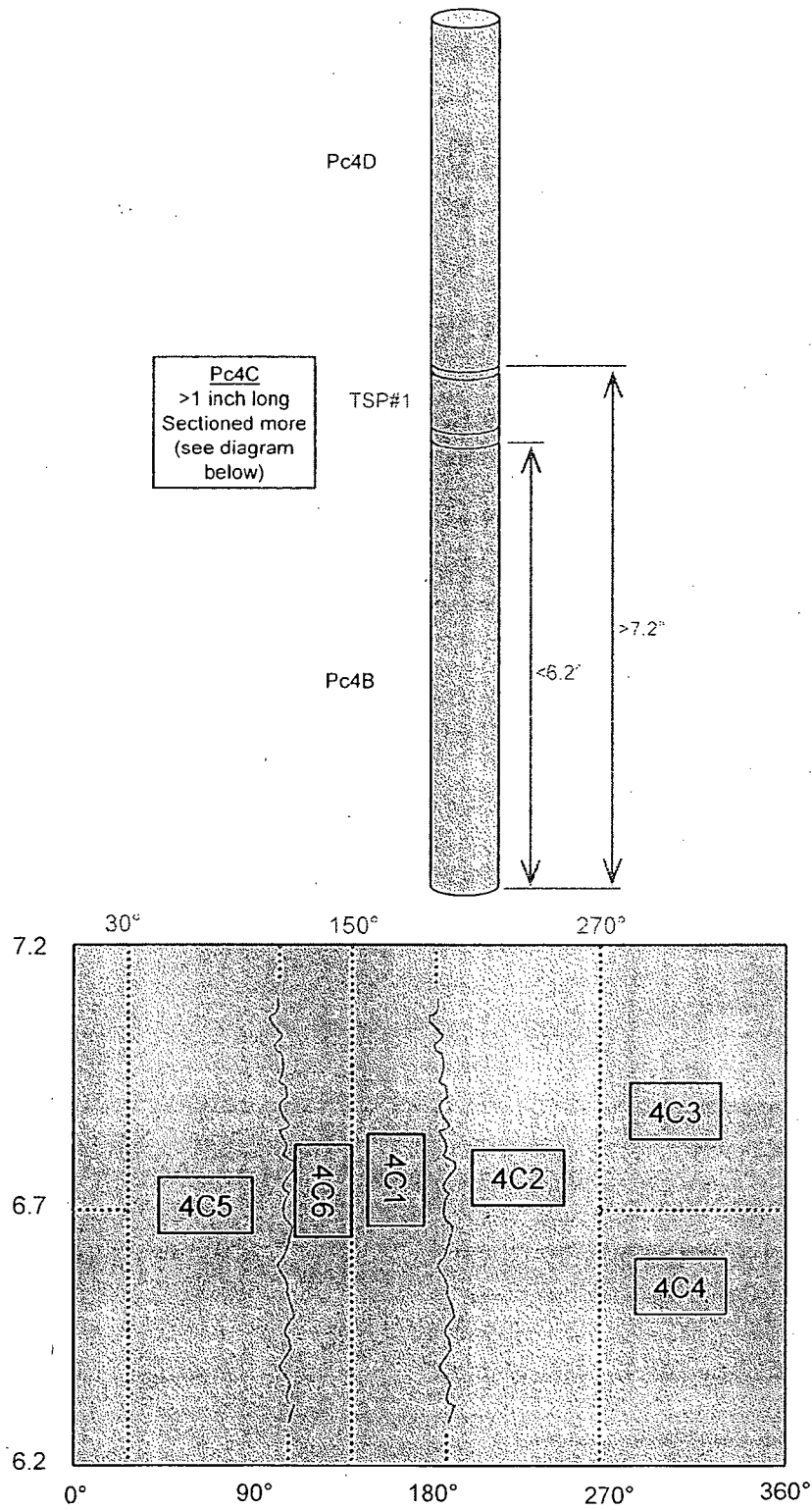


Figure 5-6: Piece 4B Sectioning

(see next page for sample usage)

Sample	Usage
4B	unused
4C1	Examination of Opened Cracks - Color Photography
	Examination of Opened Cracks - SEM Characterization
	Examination of Opened Cracks - SEM Depth Profile
	SEM/EDS of Deposits
4C2	Defect Metallography - Radial Section
4C3	unused
4C4	Defect Metallography - Transverse Section
	Microhardness
4C5	Examination of Opened Cracks - Color Photography
	Examination of Opened Cracks - SEM Characterization
	Examination of Opened Cracks - SEM Depth Profile
	SEM/EDS of Deposits
4C6	unused
4D	unused

Figure 5-6: Piece 4B Sectioning (continued)

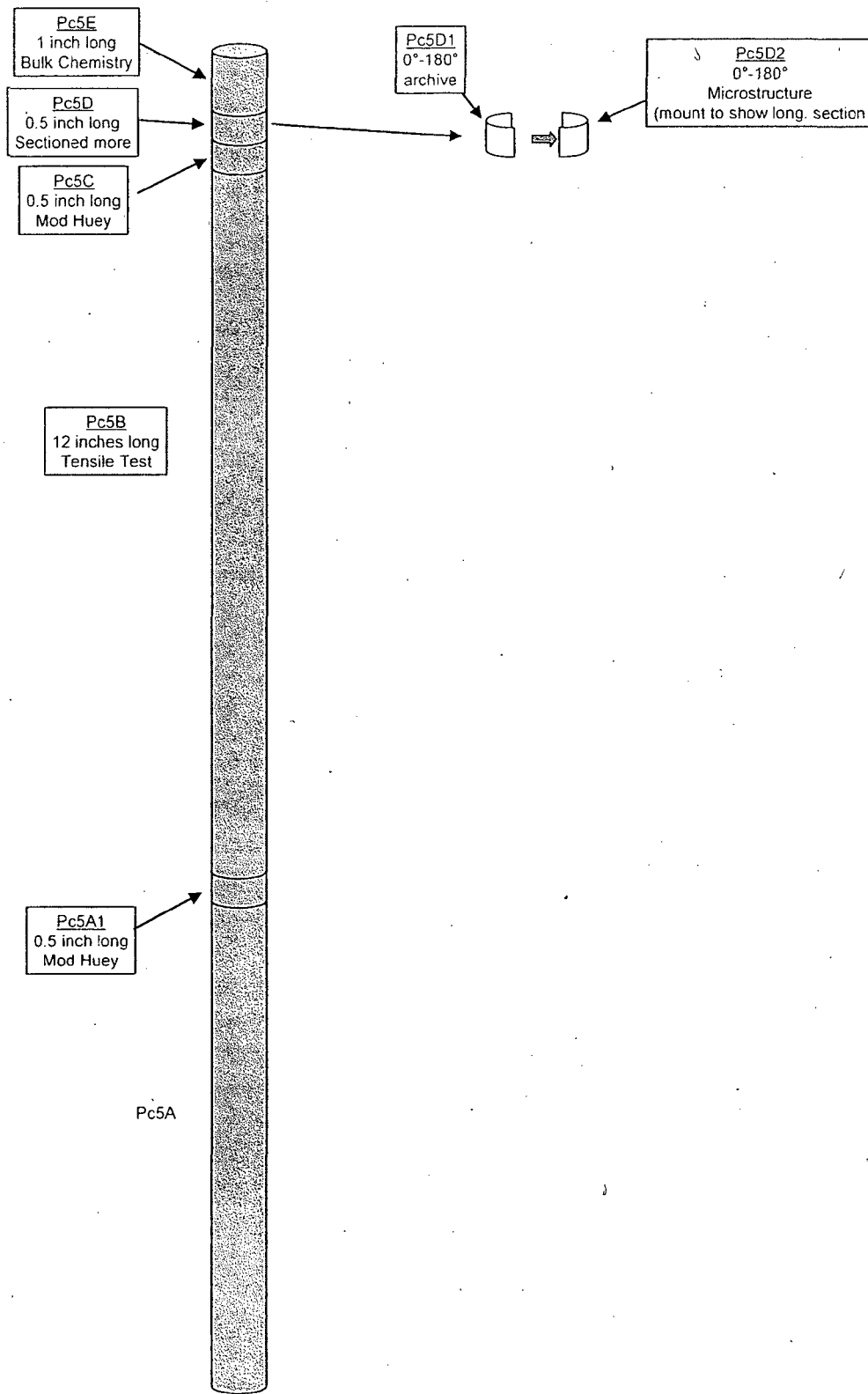
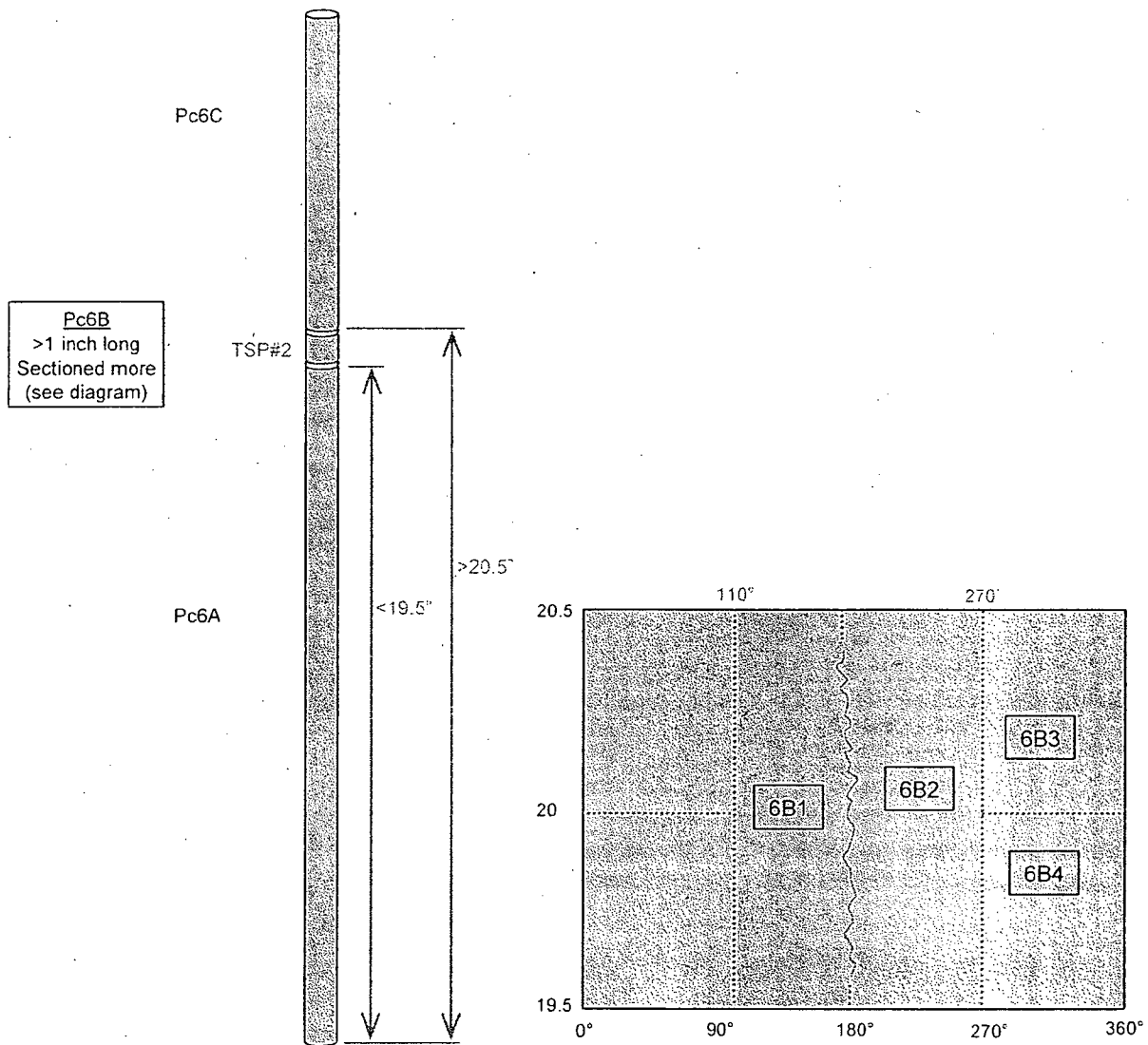


Figure 5-7: Piece 5 Sectioning Diagram



Sample	Usage
6A	unused
6B1	Examination of Opened Cracks - Color Photography
	Examination of Opened Cracks - SEM Characterization
	Examination of Opened Cracks - SEM Depth Profile
6B2	Defect Metallography - Radial Section
6B3	unused
6B4	Defect Metallography - Transverse Section
	Microhardness
6C	unused

Figure 5-8: Piece 6 Sectioning

6.0 FRACTOGRAPHY

Samples 4C1, 4C5 (from TSP#1, see Figure 5-6) and 6B1 (from TSP#2, see Figure 5-8) were examined in detail by scanning electron microscopy (SEM) and Energy Dispersive X-ray Spectroscopy (EDS) in conjunction with the SEM. The SEM/EDS examination included depth profiling, ligament sizing, opened crack fractography, and a semi-quantitative elemental analysis of the crack surface and OD deposits.

6.1 Procedure

Each sample examined by SEM/EDS was blown with a jet of dry oil-free air to minimize non-conductive particulates from the fracture surfaces that would otherwise collect an electrical charge (and thus hinder the view) during the SEM examination. Observations made during the SEM examination were documented photographically. Operation of the SEM/EDS followed the manufacturer's instruction. ASTM has not published procedures for fractography examinations. However, surfaces examined by SEM in accordance with accepted scientific principles and EPRI guidelines can be compared with fractographs presented in various fractography textbooks, such as "Metals Handbook, Volume 12, Fractography", 9th Edition, American Society of Metals, 1985. EDS spectra were analyzed using a standardless semi-quantitative algorithm.

SEM fractographs were taken of the entire fracture surface of each burst opening that had corrosion at approximately 75X. These fractographs were taken with secondary electron and back-scattered electron SEM. These fractographs were then aligned end to end to complete a photomontage of each crack surface. The depth of the corrosion was measured at selected intervals, providing a set of depth vs. axial location measurements. The depths were converted to percent throughwall (%TW) values by dividing by the depth measurement at a completely throughwall location.

Uncorroded ligaments were sized in terms of length, area and axial location. Ligaments were characterized as "in-plane" (the face of the ligament running parallel with the crack face) or "out-of-plane" (running perpendicular to the crack face), depending on which direction most of the ligament area was oriented.

Fractographs were taken of selected locations at magnifications up to 2000X to characterize the surface of the crack. The elemental composition of selected areas on the crack and OD surface were analyzed by EDS.

Figure 6-1, Figure 6-2 and Figure 6-3 show a low magnification view of the crack samples, showing the cracks with different contrasts and viewing angles. The figures are each a montage of SEM fractographs taken at a higher magnification. The photomontages shown in these figures provided the starting point for the SEM examination as well as the data from which the depth profile and ligament size measurements were made.

6.2 Crack Surface Characterization

Figure 6-4 presents an example of the crack surface at a higher magnification view. The fractograph shows that the corrosion was intergranular, as was shown by the rock candy

topography. All of the corrosion on all three opened cracks was intergranular; there was no evidence of transgranular cracking. Shallow (short) circumferentially oriented cracks that were perpendicular to this axial crack were observed. The non-corroded portion of the opening shows that final failure was by ductile tearing, as is shown by the dimpled surface. The interface between the ductile tearing and the intergranular corrosion represents the crack tip; depth measurements for depth profiling were made perpendicular to the OD surface, from the OD surface to the crack tip.

6.3 EDS Analysis of Crack Surfaces

EDS analyses were performed on selected areas of each crack. Figure 6-5 presents an example of one of the areas that an EDS analysis was performed. The fractograph in the upper left shows the general area that was examined. The fractograph in the upper right shows the area on which the EDS analysis was performed. The spectrum is the result of the EDS analysis.

Figure 6-5 represents the only unusual artifact that was examined by EDS. A dark deposit or oxide patch was present in the middle of the crack.

Several areas on each of the three cracks were examined by EDS. In addition to crack surfaces, the ductile region was examined by EDS so as to obtain spectra of the base metal and to confirm that sample handling did not introduce elements to the crack surface. Table 6-1, Table 6-2 and Table 6-3 provide summaries of the crack surface EDS results for samples 4C1 (180° crack of TSP#1), 4C5 (110° crack of TSP#1) and 6B1 (180° crack of TSP#2), respectively.

Ratios of Ni:Cr are very consistent in all of the areas examined and are close to the values of Ni:Cr that are found within the base metal. This suggests that conditions within the crevice were not excessively acidic or caustic.

The dark anomaly shown in Figure 6-5 was found to have a large amount of iron, as well as enhanced amounts of carbon and a significant amount of copper. It appears to have a composition similar to that of the deposits on the outer surface of the tube. This was the only area where copper was found on the crack surface.

Areas of the crack near the outer surface were found to have a spotty coating of a heavy oxide. These areas had enhanced amounts of oxygen as well as other elements that were not detectable in the base metal, such as magnesium, phosphorus, calcium, sulfur and lead. It can be difficult to differentiate between lead and sulfur with EDS, thus for sample 4C5 one of the analyses were performed for an extended period of time to allow for the confirmation of the presence of lead. The presence of lead was confirmed.

These results do not provide data that can be used to assess the cause of the cracking in the TSP regions; however they do suggest that both lead and copper were present in the crevice region during cracking. Both of these elements are known to increase susceptibility to IGSCC (or in the case of lead, transgranular SCC as well) in low temperature mill annealed Alloy 600.

6.4 EDS Analysis of OD Surfaces and Deposits

EDS analyses were performed on selected areas of the OD surface near the TSP#1 region cracks. Figure 6-6 presents an example of one of the areas that an EDS analysis was performed, an area of light deposits near the 180° crack. The fractograph in the upper left shows the general area that was examined, an area between a deep gouge and the crack. The fractograph in the upper right shows the area on which the EDS analysis was performed. The area shows the belt polish marks on the tube surface (the fine horizontal lines). The spectrum is the result of the EDS analysis of the area within the square.

EDS analyses were also performed on a region of thicker deposits near the 110° crack and on copper color particles embedded in the deposit. The summary of all the OD deposit EDS analyses are provided in Table 6-4.

The deposits are composed primarily of iron and oxygen, as is typical. The deposits also contain elements not found in the underlying base metal, such as magnesium, phosphorus, calcium, zinc, sulfur and lead. Copper was found primarily in discrete copper-rich particles on the surface, but was present in smaller concentrations in other parts of the deposit.

These results do not provide data that can be used to assess the cause of the cracking in the TSP regions; however they do suggest that both lead and copper were present in the crevice region during cracking. Both of these elements are known to increase susceptibility to IGSCC (or in the case of lead, transgranular SCC as well) in low temperature mill annealed Alloy 600.

6.5 Depth Profiles and Ligament Sizing

Appendix A presents the crack depth and ligament size data. Figure 6-7, Figure 6-8 and Figure 6-9 present the crack depth profiles and uncorroded ligament sizing results for samples 4C1 (180° crack of TSP#1), 4C5 (110° crack of TSP#1) and 6B1 (180° crack of TSP#2), respectively. Table 6-5 summarizes some of the key characteristics of each of the three cracks.

The TSP#1 180° crack had two throughwall corrosion cracks, one was 59.9 mils long and the other was 30.8 mils long. The two throughwall cracks were separated by an in-plane ligament that was 42.3 mils long and has an average width of 4.3 mils.

Table 6-6 summarizes the ligament sizing results.

Table 6-1: Summary of EDS Analyses Performed on TSP#1 180° Crack Surfaces

Sample	Location	Spectrum ID	Composition (Atomic Percent)												
			C	O	Mg	Al	Si	P	Ca	Ti	Cr	Mn	Fe	Ni	Cu
4C1	TW region, near OD, overall	11-eds-1	2.925	24.875	0.225	0.335	3.098			0.257	10.585	0.409	6.079	51.212	
	TW region, near OD, heavy oxide	11-eds-2	3.283	24.791	0.307	0.318	2.881		0.150	0.242	10.566	0.228	5.968	51.267	
	TW region, near OD, light oxide	11-eds-3	3.002	8.650	0.214	0.512	0.848			0.190	13.851	0.220	7.068	65.445	
	TW region, crack center, overall	11-eds-4	2.402	21.613	0.153	0.271	1.747			0.204	11.676	0.262	6.303	55.369	
	Dark anomaly near crack center	11-eds-5	12.599	17.965	2.807	1.829	3.506	0.243	1.702	0.357	1.584	1.900	45.909	8.468	1.131
	Crack end, near crack tip	17-eds-1	2.613	19.888		0.191	0.546			0.176	12.448	0.309	6.435	57.395	
	Ductile tear region (base metal)	17-eds-2	3.204	4.033		0.516	0.702			0.754	15.035	0.284	7.686	67.787	

Table 6-2: Summary of EDS Analyses Performed on TSP#1 110° Crack Surfaces

Sample	Location	Spectrum ID	Composition (Atomic Percent)												
			C	O	Mg	Al	Si	S	Ca	Ti	Cr	Mn	Fe	Ni	Pb
4C5	Near OD, heavy oxide	9-eds-1	2.163	44.553		0.101	2.632	0.101	0.306		10.218	0.114	6.233	32.114	1.464
		long acquire time	15.788	37.766		0.282	4.072	0.125	0.254	0.099	7.234	0.178	4.902	28.673	0.626
	Near OD, light oxide	9-eds-2	4.833	14.911		0.450	0.752				12.955	0.207	6.206	59.685	
	Near OD, overall	9-eds-3	3.056	29.173		0.133	4.107			0.204	10.475	0.245	5.571	47.037	
	Crack center, overall	9-eds-4	6.732	27.522		0.153	3.364	0.021	0.140		10.065	0.274	5.258	45.550	0.920
	Crack tip, overall	9-eds-5	4.692	14.183		0.246	0.492			0.198	12.995	0.365	6.682	60.147	
	Ductile tear region (base metal)	9-eds-6	2.426	2.967		0.388	0.652			1.075	15.238	0.185	7.559	69.511	

Table 6-3: Summary of EDS Analyses Performed on TSP#2 180° Crack Surfaces

Sample	Location	Spectrum ID	Composition (Atomic Percent)													
			C	O	Mg	Al	Si	P	S	Ca	Ti	Cr	Mn	Fe	Ni	Pb
6B1	Near OD, heavy oxide	13-eds-1	3.176	48.066	0.233	0.373	6.371	0.166	0.045	0.450	0.097	5.414	0.159	6.258	28.509	0.685
	Near OD, light oxide	13-eds-2	3.670	5.484	0.258	0.690	0.838			0.081	0.175	14.104	0.256	7.706	66.739	
	Near OD, overall	13-eds-3	3.090	28.772	0.390	0.748	3.536	0.294	0.016	0.525	0.184	9.579	0.254	7.756	43.905	0.952
	Crack tip, overall	13-eds-4	3.861	10.631	0.193	0.370	0.627			0.046	0.198	13.640	0.347	6.955	63.132	
	Ductile tear region near tip	13-eds-5	3.053	3.186		0.573	0.756				0.299	15.215	0.217	7.581	69.120	
	Ductile tear region (base metal)	13-eds-6	4.357	2.520		0.672	0.553				0.236	14.736	0.207	7.560	69.160	
	Crack end, near crack tip	15-eds-1	3.095	9.896		0.701	0.398		0.039	0.031	0.216	13.630	0.494	6.773	63.872	0.856

Table 6-4: Summary of EDS Analyses Performed on TSP#1 OD Surfaces

Sample	Location	Spectrum ID	Composition (Atomic Percent)															
			C	O	Mg	Al	Si	P	S	Ca	Ti	Cr	Mn	Fe	Ni	Cu	Zn	Pb
4C1	Light OD Deposit	29-eds-1	11.162	45.761	4.930	3.143	5.106	0.858	0.074	1.361	0.120	1.805	0.914	19.432	4.377	0.390	0.207	0.361
	Bare Tube	29-eds-2	2.951	44.674	0.352	0.791	1.387	0.418	0.088	0.600	0.412	17.653	2.080	10.859	13.236	1.677	0.797	2.024
	Ductile Tear (Base Metal)	29-eds-3	7.556	7.534		0.821	1.176			0.136	0.250	13.691	0.167	7.014	61.656			
4C5	Heavy OD Deposit Area 1	14-eds-1	7.427	30.407	1.318	4.416	2.236	1.570	0.113	4.169	0.317	0.401	2.211	39.740	2.457	2.213		1.006
	Semi-Bare Metal Area 1	14-eds-2	13.284	36.413	1.187	2.086	3.015	0.212		0.781	0.269	12.701	0.669	8.313	17.649	0.730	0.332	2.360
	Copper Particle Area 2	14-eds-3	4.437	26.288	0.102	0.122	0.648			0.254		0.360	0.417	4.511	0.485	62.376		
	Semi-Bare Metal Area 2	14-eds-4	4.017	37.942	0.291	0.614	1.073	0.116		0.441	0.295	15.635	0.761	9.095	26.203	0.971		2.545

Table 6-5: Opened Crack Characteristics

TSP	Location	Sample	Maximum Depth (%TW)	Average Depth (%TW)	Length (inch)	Number of Uncorroded Ligaments
1	180°	4C1	100	78	0.559	10
1	110°	4C5	91.4	69	0.395	4
2	180°	6B1	70.8	44	0.720	18

Table 6-6: Ligament Sizing Results

TSP	Location	Sample	Ligament #	Distance Above Crack Bottom (mils)	Orientation	Area (mils ²)	Ligament Depth (%TW)
1	180°	4C1	28	444	Out-of-Plane	341	100
			24	410	Out-of-Plane	114	32
			27	397	Out-of-Plane	179	64
			23b	320	Out-of-Plane	121	41
			23a	298	Out-of-Plane	71	41
			22	235	Out-of-Plane	672	69
			26	220	Out-of-Plane	513	88
			25	177	In-Plane	121	34
			20	157	Out-of-Plane	243	62
1	110°	4C5	18	74	In-Plane	134	19
			11	297	Out-of-Plane	246	46
			13	170	Out-of-Plane	294	83
			12	113	Out-of-Plane	630	62
2	180°	6B1	10	53	Out-of-Plane	149	69
			23	698	In-Plane	461	32
			22	662	In-Plane	201	21
			21B	646	Out-of-Plane	72	23
			30	637	Out-of-Plane	87	19
			21A	624	Out-of-Plane	77	18
			29	599	In-Plane	250	23
			20	523	Out-of-Plane	393	48
			28	497	Out-of-Plane	260	42
			27c	466	Out-of-Plane	309	58
			27b	453	Out-of-Plane	349	46
			27a	444	Out-of-Plane	90	41
			19	395	Out-of-Plane	178	73
			18	325	In-Plane	291	71
			17	280	Out-of-Plane	40	21
			26	249	In-Plane	277	64
16	130	Out-of-Plane	144	57			
25	34	Out-of-Plane	103	30			
24	20	Out-of-Plane	51	44			



Figure 6-1: Overall Views of TSP#1 180° Crack (Sample 4C1)

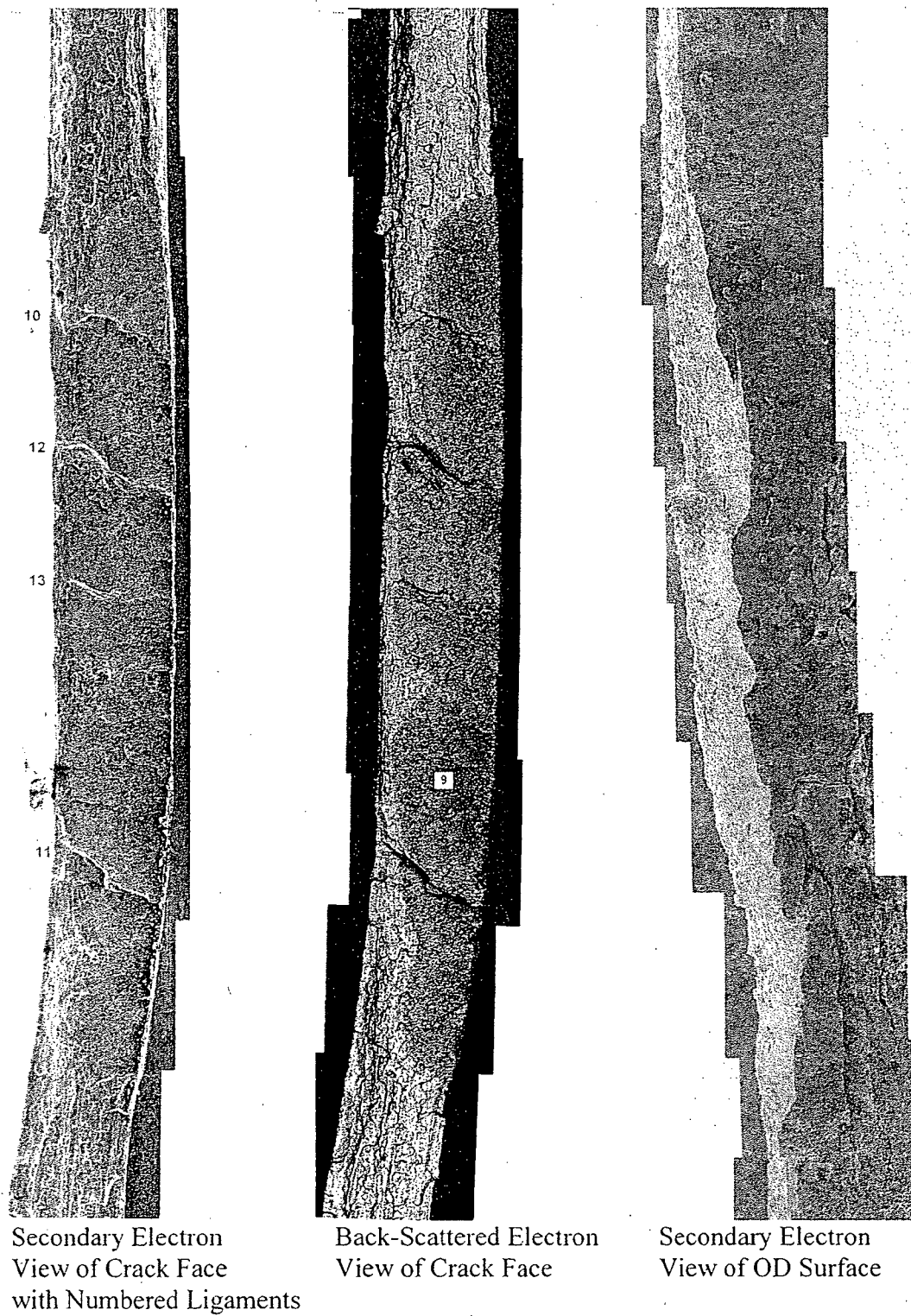


Figure 6-2: Overall Views of TSP#1 110° Crack (Sample 4C5)



Figure 6-3: Overall Views of TSP#2 180° Crack (Sample 6B1)

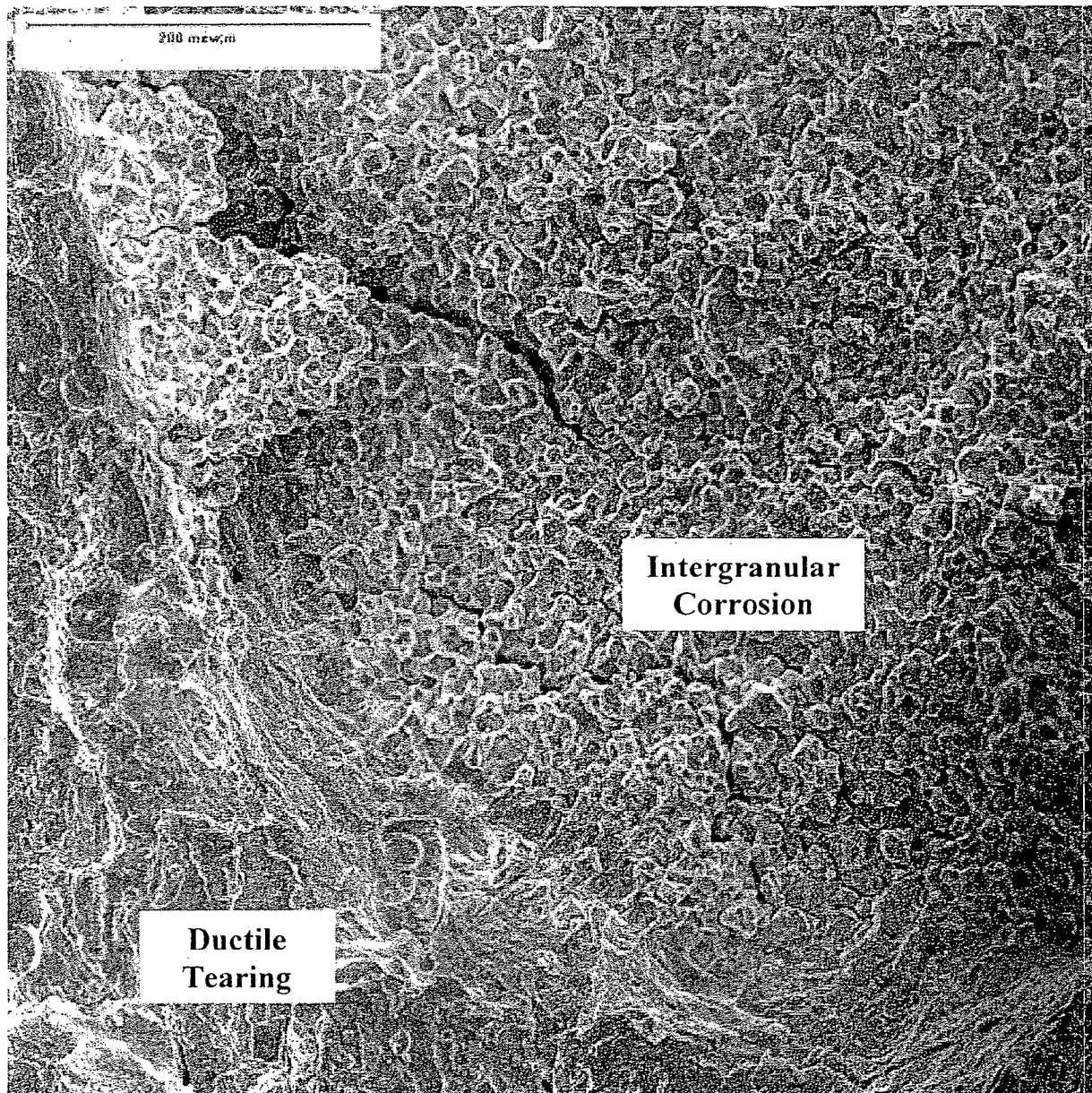


Figure 6-4: Example of Corrosion Surface (from Sample 4C1)

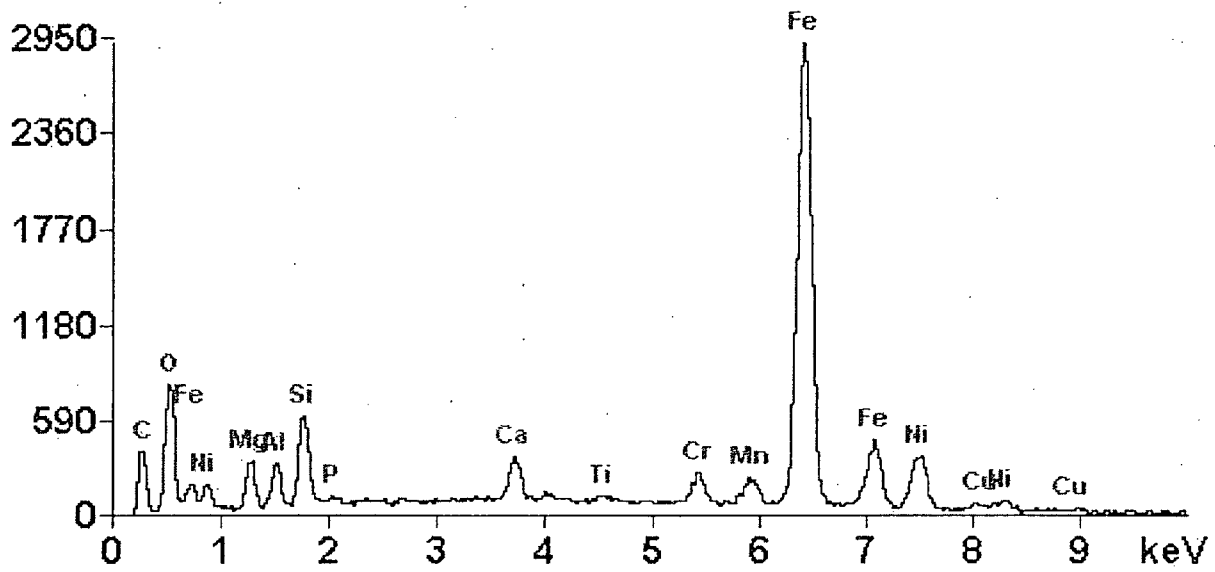
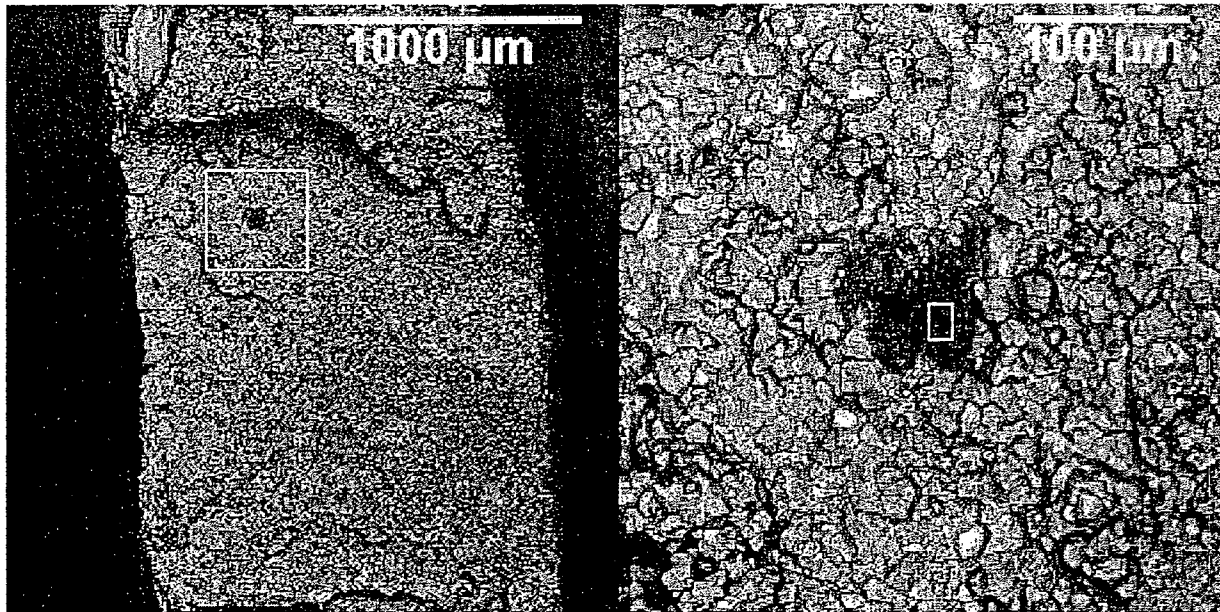


Figure 6-5: Example of EDS Analysis of Crack Surface (Dark Anomaly on Sample 4C1)

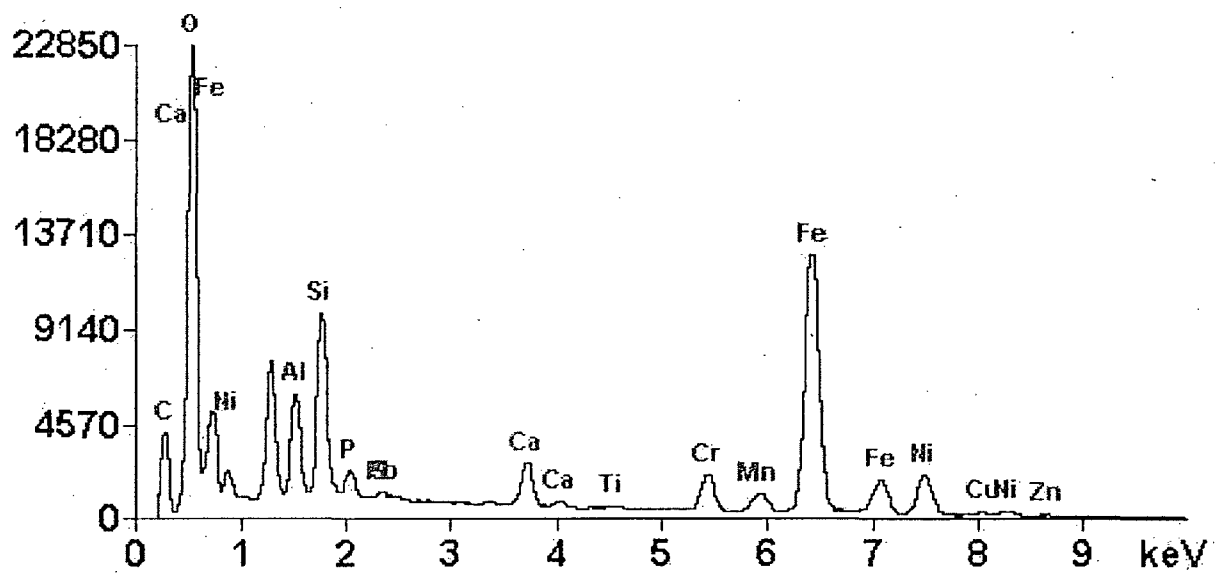
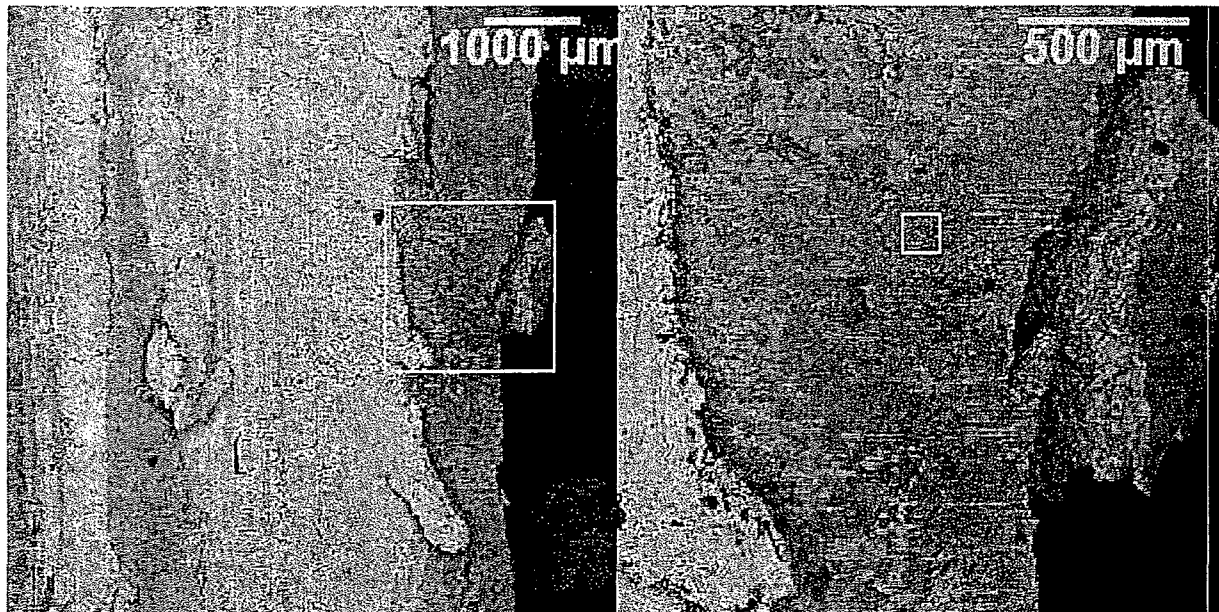


Figure 6-6: Example of EDS Analysis of OD Surface (Sample 4C1)

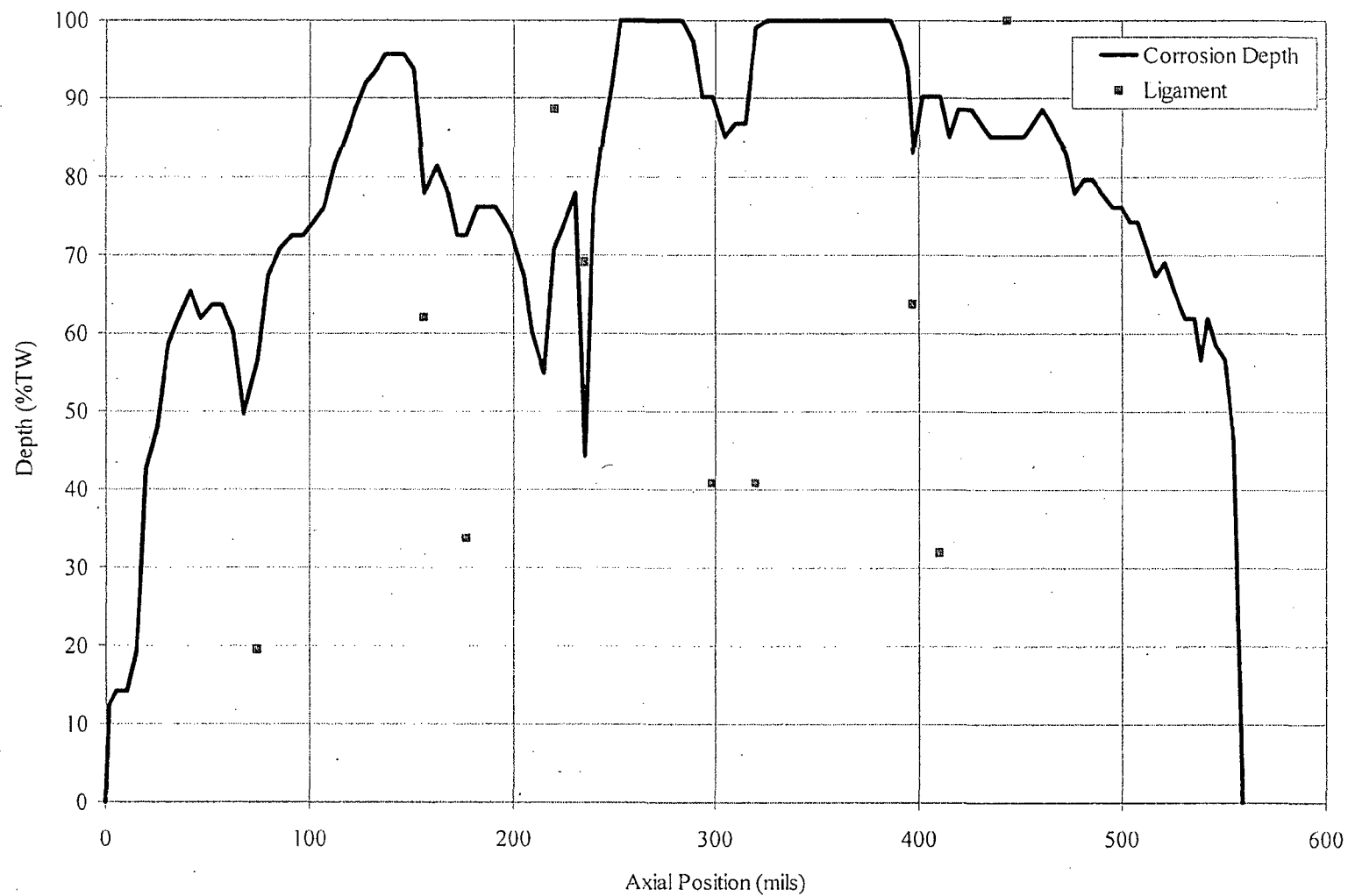


Figure 6-7: Corrosion Depth Profile and Ligament Size for TSP#1 180° Crack

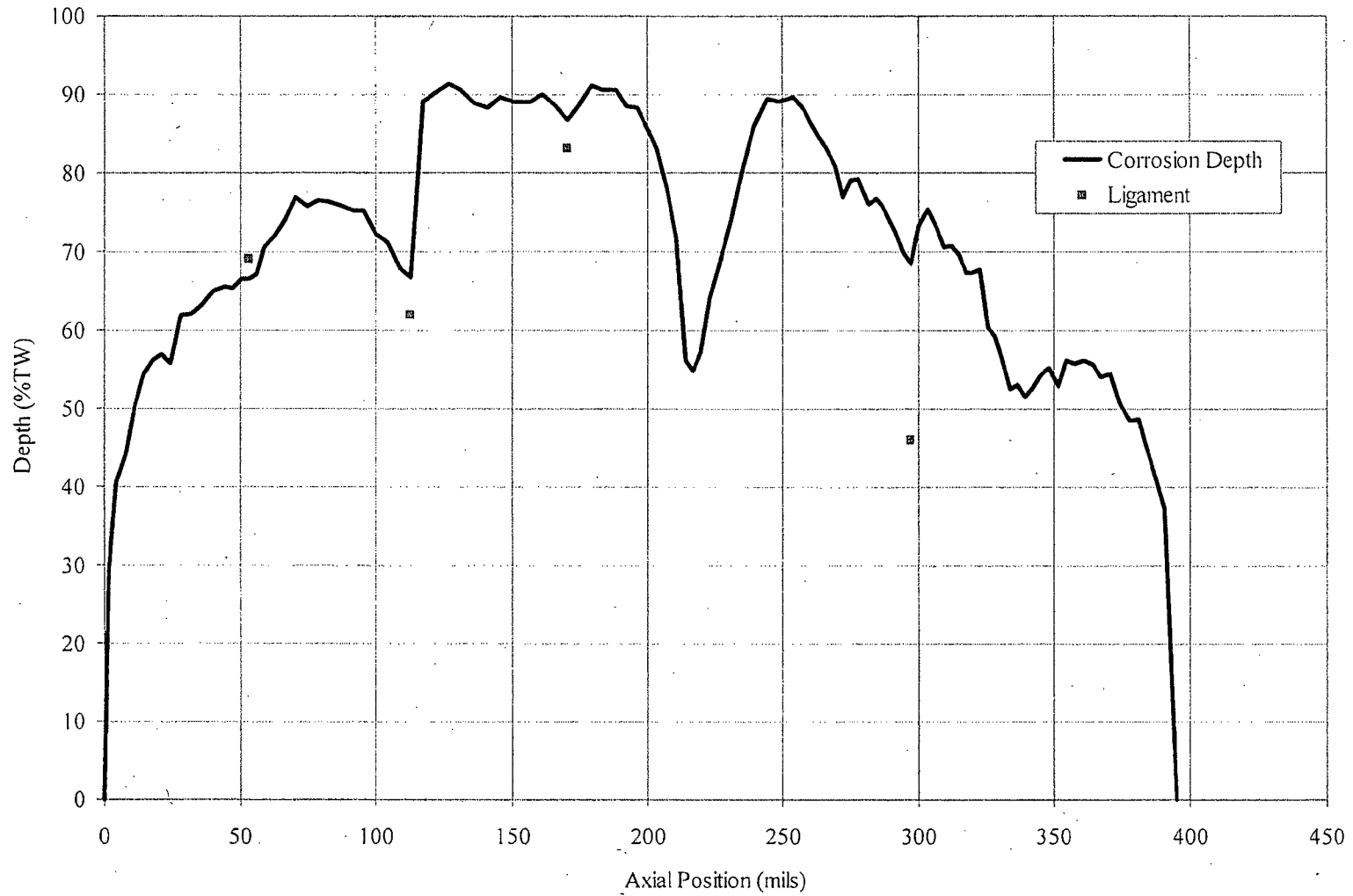


Figure 6-8: Corrosion Depth Profile and Ligament Size for TSP#1 110° Crack

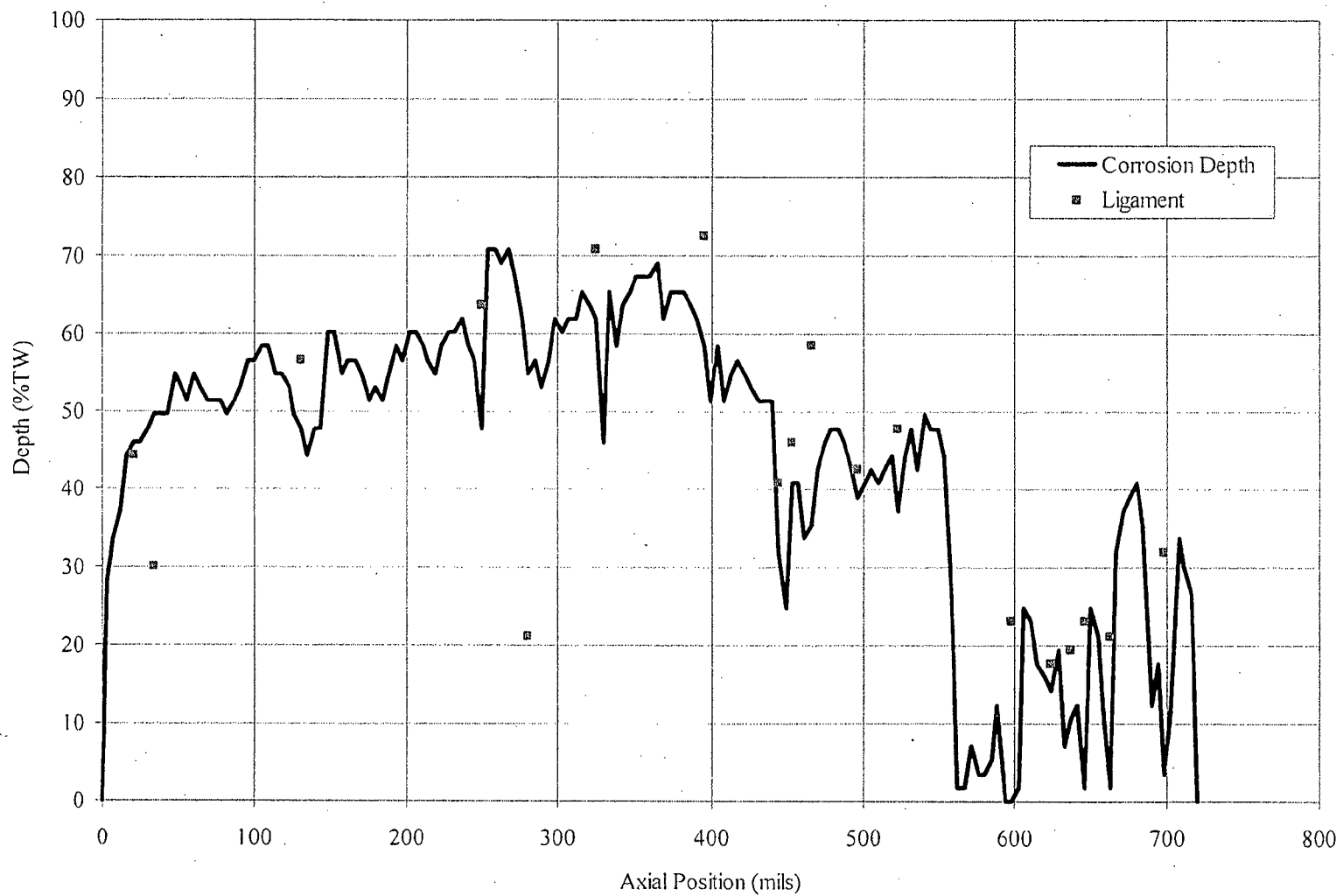


Figure 6-9: Corrosion Depth Profile and Ligament Size for TSP#2 180° Crack

7.0 METALLOGRAPHY

7.1 Procedure

Samples 4C4 and 6B4, from TSP#1 and TSP#2, respectively (see Figure 5-6 and Figure 5-8), were mounted to show a transverse section for examination of axial cracks by metallography.

Samples 4C2 and 6B2, from TSP#1 and TSP#2 (see Figure 5-6 and Figure 5-8), respectively, were flattened and their OD surfaces examined by radial metallography. Sequential grinding, polishing and photography into the OD surface provided a view of the orientation of cracks, progressing radially into the tube wall.

[

] a.c.e

7.2 Transverse Metallography

Figure 7-1 shows a typical axial crack that was revealed by transverse metallography. The one shown in Figure 7-1 was taken from TSP#1 at approximately the 315° location (sample 4C4). The cracks in this location were composed of short, unlinked cracks. The crack shown in the figure was one of the deeper cracks examined by transverse metallography, 47%TW.

All of the cracks examined were intergranular; no transgranular cracking was identified. There was some shallow (1-2 grain deep) intergranular attack observed, but the deeper cracks were all intergranular stress corrosion cracks (IGSCC).

7.3 Radial Metallography

One section was removed from the TSP#1 region and one from the TSP#2 region. Both samples were taken from the right side of the deepest crack for each TSP region. It was in these areas that circumferentially oriented cracks had been observed visually. [

] a.c.e

An overall photo and a series of higher magnification photomicrographs were used to document the corrosion pattern.

[

] ^{a,c,c} Nevertheless, the radial metallography provided valid results that demonstrated that circumferential cracking was not significant.

[

] ^{a,c,c} Table 7-1 identifies the approximate throughwall depth of each grind/polish step.

The circumferential cracking that was visually observed on the TSP#1 sample was shallow and was ground away on the first grind, leaving short axial cracks. Grinding continued through the sample so that areas that did not flatten well could be examined. No significant circumferential cracks were observed in the TSP#1 region.

The same was true with the TSP#2 sample; however a significant circumferential feature was noted within a deep groove on the surface. Several grinds were necessary to reach the feature in the groove. At the 23 mil level, the feature became evident (Figure 7-2). A closer view of the feature showed that its crack faces were smooth and the grains on the crack faces were elongated, indicating the circumferential feature was a tear in the groove and not a circumferentially oriented crack.

Table 7-1: Radial Metallography Grind/Polish Depths

Level	TSP1	TSP2
	Sample 4C2	Sample 6B2
1	5 mils	5 mils
2	9 mils	10 mils
3	13 mils	17 mils
4	18 mils	23 mils
5		30 mils

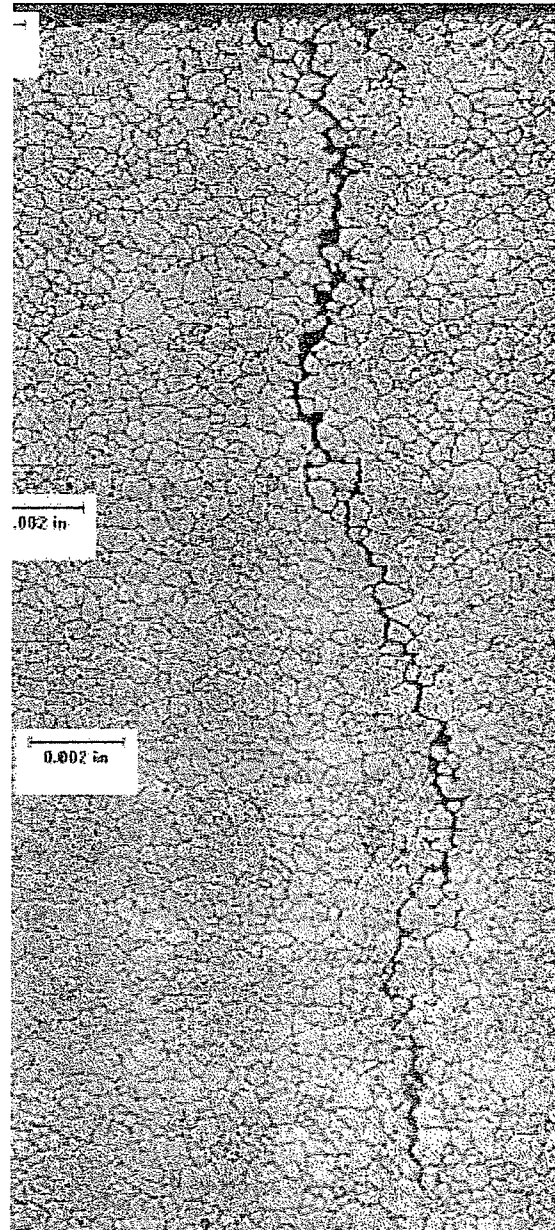


Figure 7-1: Typical Axial Crack (Sample 4C4 at $\sim 315^\circ$ Location)

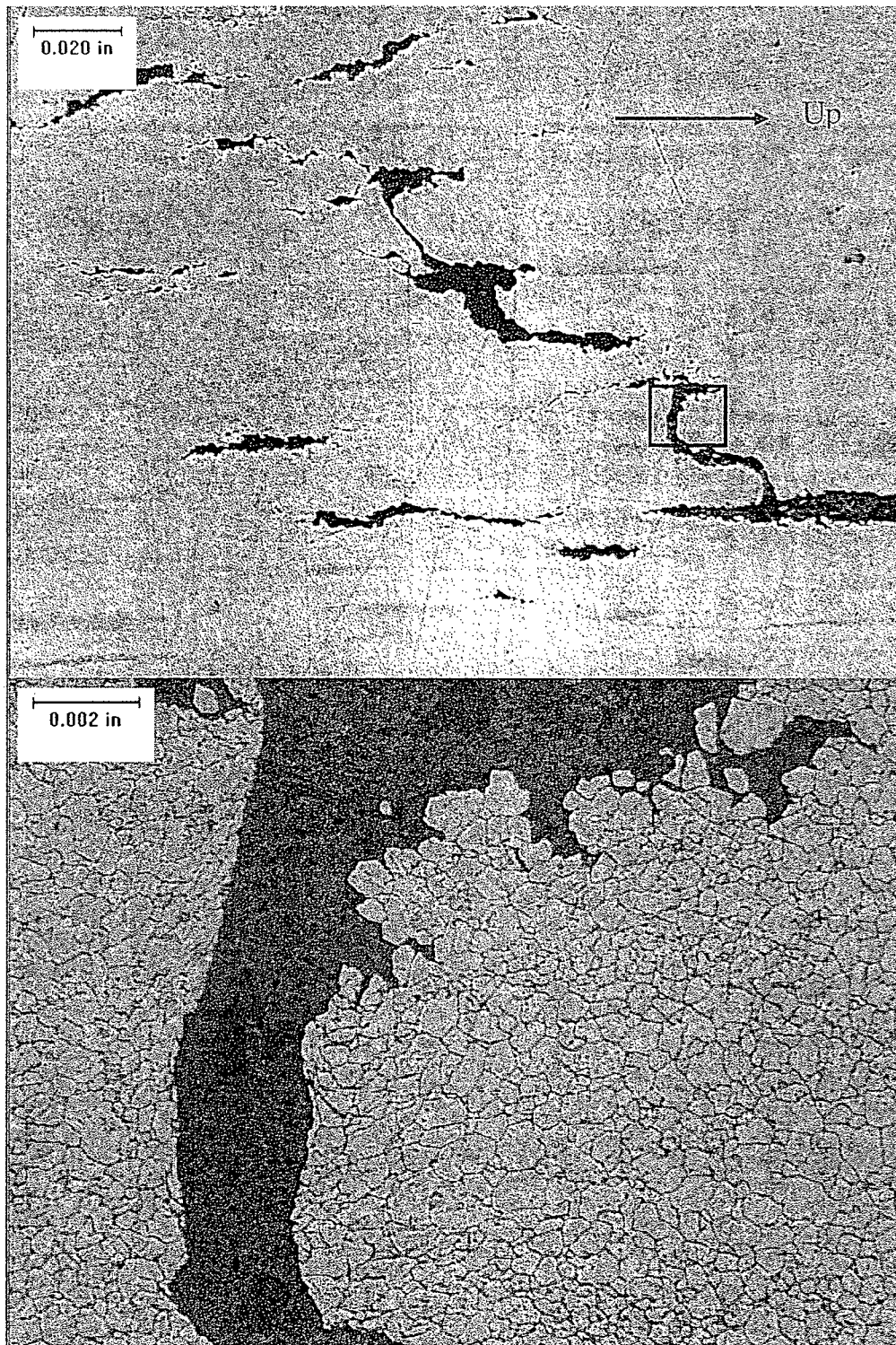


Figure 7-2: Circumferential Feature in Sample 6B2

8.0 MATERIAL CHARACTERIZATION

8.1 Tensile Test

8.1.1 Procedure

The tensile properties (i.e., yield strength, ultimate tensile strength, percent elongation) of R22C70 were determined by a room temperature tensile test of a full cross section tubular specimen approximately 12 inches in length that was removed from section 5B (see Figure 5-7). The full cross section tubular specimen was fitted with snug-fitting stainless steel plugs (mandrels) machined in accordance with ASTM Standard Method E8.

[

] a.c.c

The ovalization and the gouges in the tube did not allow for a direct determination of the cross-section of the specimen. The cross-sectional area was determined in another location on the tube. Equispaced measurements made around the circumference of the tube from the metallography specimen shown in Figure 3-7 indicated a variation in wall thickness (0.051 inch, 0.050 inch, 0.056 inch and 0.053 inch). These above-nominal wall thicknesses and the variation were also observed in the previous Sequoyah pulled tube examination (see Table 11-2 in Reference 9). For the determination of the mechanical properties of the tube, it was assumed that the wall thickness of the tube was the average of these measurements (0.053 inch) and that the tube had a nominal OD (0.875 inch), resulting in a cross-sectional area of 0.1369 in².

8.1.2 Results

Figure 8-1 provides the stress-strain curve from the tensile test. Table 8-1 provides the results of the room temperature tensile test. The high yield strength result (95.5 ksi) confirms that the tube pulling operation exceeded the nominal (pre-pull) yield strength of the material, typically about 55 ksi for this type of Alloy 600.

8.2 Bulk Chemistry

8.2.1 Procedure

The chemical composition of the base metal of the tube was determined by quantitative chemical analysis of a one inch section from a freespan location (see Figure 5-7). [

] a.c.c

8.2.2 Results

The results of the chemical analyses for R22C70 are provided in Table 8-2. The composition of the tube is within the limits set by specification SBI67-A02.

8.3 Microstructure Analysis

8.3.1 Procedure

The microstructure of the pulled tubing was examined to determine the grain size and the general distribution of the carbide precipitation. Sample 5D2 was examined from a freespan location between the TSP regions (see Figure 5-7). The sample was mounted to show a longitudinal view. It was etched in a 5% nital solution and examined by optical microscopy for grain size rating per the ASTM procedures. The nital etch was examined at the mid-wall location and at locations near the ID and OD walls. The sample was also examined for carbide precipitation by SEM following polishing and etching in a 2% bromine-methanol solution.

8.3.2 Results

Figure 8-2 shows an example of the microstructure after a nital etch. The sample was also examined for carbide precipitation by Scanning Electron Microscopy following etching in a 2% bromine-methanol solution. Figure 8-3 shows an example of the carbide distribution.

The microstructure is characterized as having a small grain size, generally in the range ASTM 9-11, which is typical of low temperature mill annealed tubing and is consistent with tubes previously pulled from Sequoyah-2. The microstructure exhibits some banding, also typical.

The carbide distribution is somewhat random, with a significant amount of intragranular carbides. There is nearly no intergranular precipitation and the carbides on the grain boundaries may be classified as discontinuous. The intragranular carbides are not randomly distributed within each grain; rather they tend to occur in a linear pattern, suggesting precipitation at grain boundaries prior to the final mill anneal. The carbide distribution of this tube is typical of low temperature mill annealed tubing.

The key factor in determining the microstructure of cold-drawn and annealed tubing is the final mill anneal temperature. If the final mill anneal temperature is too low, the cold-worked grains will recrystallize but the carbides present from prior thermal processing will not dissolve. This will inhibit grain growth, producing a fine grain structure, and also on cool down there will be relatively little carbon available to precipitate on the new grain boundaries. Typically, annealing temperatures of 1650°-1750°F will result in fine grain microstructure with predominantly intragranular carbides.

Material with an elevated resistance to stress corrosion cracking tends to have low strength, coarse grains, few intragranular carbides and a semi-continuous to continuous

network of intergranular carbides. The R22C70 mill annealed Alloy 600 microstructure is typical of the tubing that was supplied with Westinghouse steam generators when Sequoyah-2 was built.

8.4 Microhardness Testing

8.4.1 Procedure

Microhardness tests are used to provide information such as general hardness, verification of specific heat treatment, random hardness variations, and hardness gradients caused by localized cold work. Microhardness measurements were performed across each tube wall for samples from each TSP region (sample 4C4 from TSP#1 and 6B4 from TSP#2, see Figure 5-6 and Figure 5-8, respectively). The Vickers hardness measurements were performed in accordance with Westinghouse Procedure MR 9111 Rev 1. Vickers hardness is determined by dividing the applied kg-force load by the surface area of the indentation in square millimeters, computed from the mean of the measured diagonals of the indentation. A 500-g load was used for the measurements on a polished transverse cross-section.

8.4.2 Results

Table 8-3 summarizes the microhardness results. The OD surface had a considerably higher microhardness than the mid-wall locations on both samples. There is a trend of lower microhardnesses away from the OD surface for both samples. The lowest microhardness values (176 VPN) is a relatively high value for mill-annealed tubing. The relatively high microhardness values and variability across the tube wall are consistent with the stresses, ovalization and deep gouges encountered during the tube pulling operation.

8.5 Sensitization Assessment

8.5.1 Procedure

During the manufacture of the tube, carbon that has been dissolved during the final mill annealing operation, and has been retained in solid solution, precipitates to form (primarily) intergranular chromium carbides. Short-range diffusion of chromium to the boundaries to effect the precipitation of intergranular $M_{23}C_6$ can result in a Cr-depleted region adjacent to the grain boundaries. This condition is typically referred to as "sensitization", and is a condition that renders the material susceptible to intergranular attack in aggressive oxidizing chemical environments (but not generally in PWR primary water).

The extent of grain boundary carbide precipitation is controlled by alloy composition (in particular carbon and chromium), final mill annealing temperature, diffusivity of chromium, grain size, and the availability of dissolved carbon for precipitation at the grain boundaries.

Westinghouse, along with the industry in general, adopted a modified Huey test (ASTM A262 Practice C) as the principal tool for evaluation of grain boundary chromium depletion in Alloy 600. The test was modified to a single 48-hr exposure in boiling 25w% nitric acid. This modification was necessary to enhance the sensitivity of the test for detecting chromium depletion.

Two modified Huey tests were performed, both from freespan regions (see Figure 5-7).

8.5.2 Results

The results of the 25w% HNO₃ Modified Huey tests showed weight losses of 70.0 mg/dm²/day from sample 5A1 and 54.4 mg/dm²/day from sample 5C. Both results are less than that associated with a sensitized condition []^{a,c,e} Tube R22C70 was not sensitized.

Table 8-1: R22C70 (Pulled Tube) Tensile Test Results

Assumed Area Gage (in) ²	Tensile Load Yield 0.2% Offset (lbs)	Tensile Load Ultimate (lbs)	Plastic Displacement 4.26 in. Gage Length (in)	Tensile Yield Strength 0.2% Offset (ksi)	Ultimate Tensile Strength (ksi)	Tensile Elongation 4.26 in. Gage Length (%)
0.1369	13072	15075	0.887	95.5	110.1	20.8

Table 8-2: Chemical Composition of R22C70

Element	SB167-A02 N06600 Specification (wt%)	R22C70 Composition (wt%)
Co		0.05
Cr	14.0-17.0	15.84
Cu	0.5 max	0.16
Fe	6.0-10.0	8.06
Mg		0.0102
Mn	1.0 max	0.33
Mo		0.07
Nb		0.02
Ni	72.0 min	74.72
Pb		0.00087
Si	0.5 max	0.31
Ti		0.21
V		0.01
N		0.0141
C	0.15 max	0.034
S	0.015 max	<0.001
Al		0.16

Table 8-3: Microhardness Test Summary

Distance from OD (inch)	Vickers Hardness Value	
	TSP#1	TSP#2
	Sample 4C4	Sample 6B4
0.006	238	389
0.011	215	315
0.016	204	276
0.021	183	256
0.026	176	256

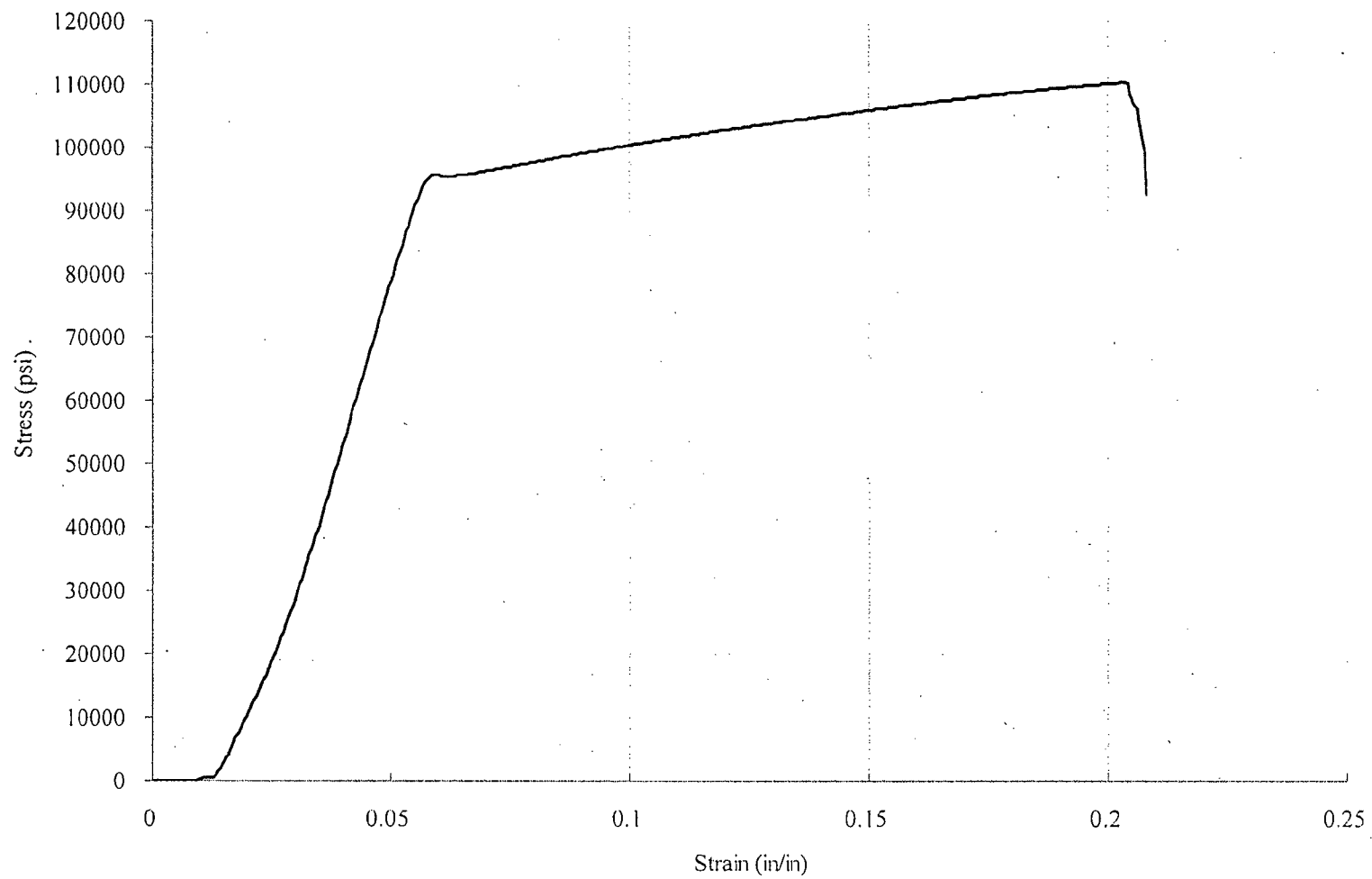


Figure 8-1: Stress-Strain Curve for R22C70 (Pulled Tube)

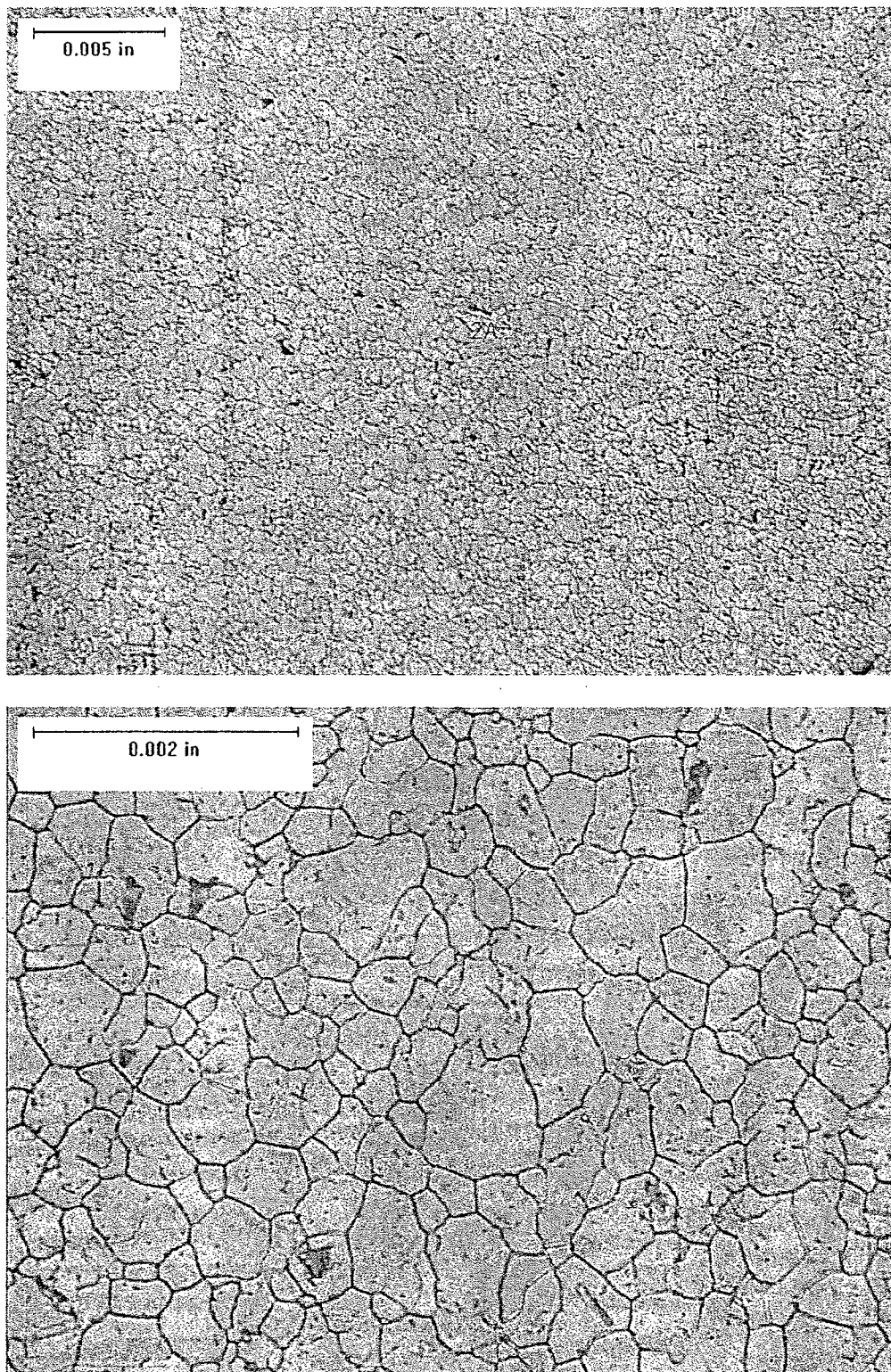


Figure 8-2: Microstructure of Freespan Region of R22C70 After a Nital Etch

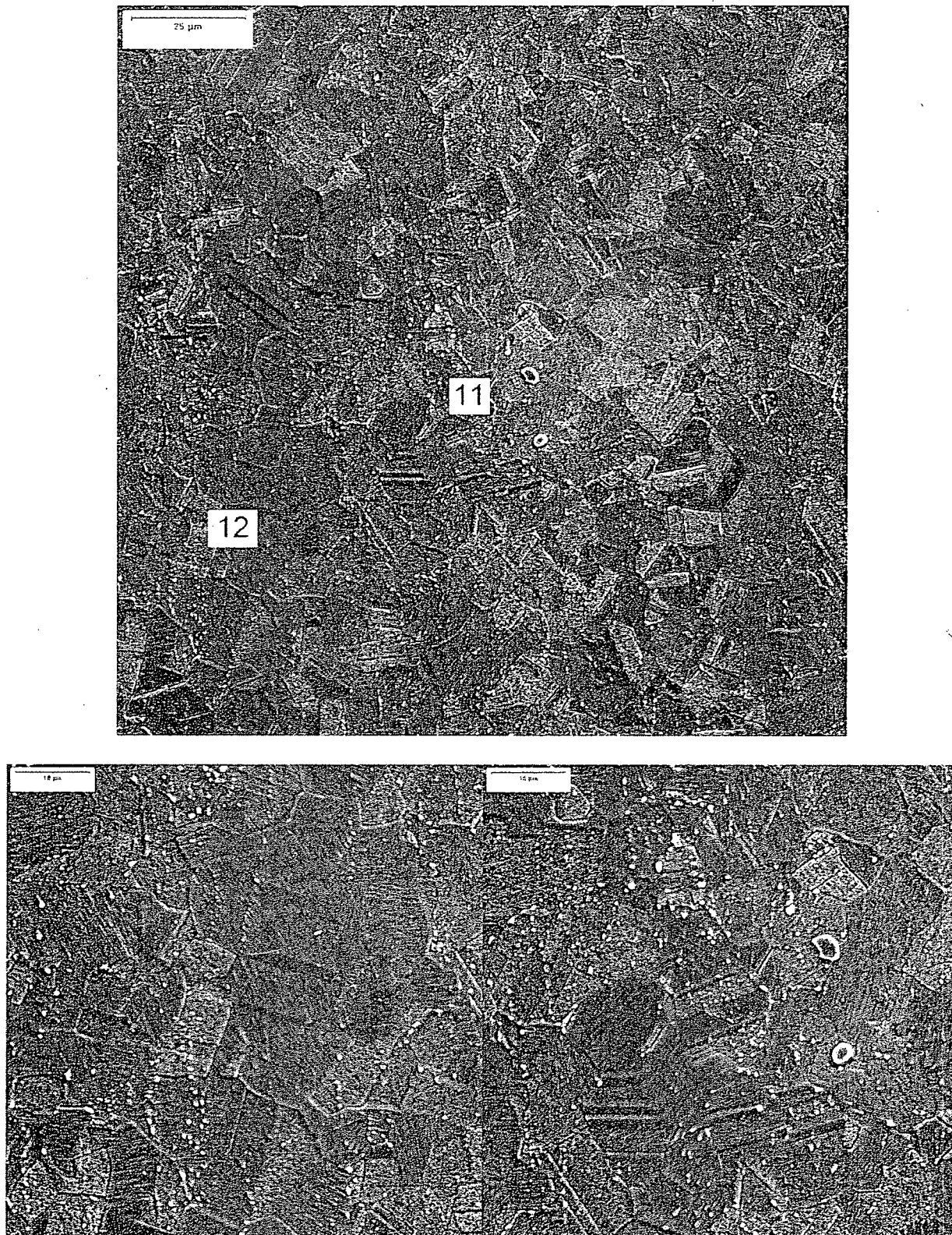


Figure 8-3: Carbide Distribution of Freespans Region of R22C70 After a Methanol-Bromine Etch

9.0 ANALYTICAL DETERMINATION OF LEAK RATE AND BURST STRENGTH

9.1 Introduction

Due to distortion of tube R22C70 from the tube pulling operations, the indications at TSP#1 and TSP#2 could not be burst and leak tested with any confidence that the test results would yield meaningful results. To assess whether the burst pressures and leak rates for these flaws would be consistent with the ODSCC ARC correlations, analyses were performed based on the destructive examination depth profiles from the pulled tube exam (Reference 11). This section of the report describes the results of these analyses.

9.2 Destructive Exam (DE) Depth Profiles

To aid separation of corrosion cracking from potential tearing of the crack face due to the tube pulling operations, the TSP#1 and TSP#2 specimens were []^{a,c,e} prior to other operations to open the crack, as described in Section 5.2 of this report. Following heat tinting, a []^{a,c,e} was used to expand both TSP regions of R22C70 in order to open the corrosion cracks, as described in Section 5.3 of this report. Due to the high tube pull axial forces increasing the flow stress for the tube and the use of a []^{a,c,e} the pressures attained for each TSP do not represent a lower bound of the burst pressure. The material properties measured at a location between the TSPs, as noted in Section 8.1 of this report, indicate a flow stress of 102.83 ksi. The flow stress reduction factor to a nominal value of 68.78 ksi would be 0.669. The uncertainties in correcting the pressures would have made any attempt to measure the burst pressures too uncertain for ARC applications.

Following expansion, each TSP region was examined under a microscope to select cracks for further examination. Two cracks from TSP#1 were opened for further examination, at the 110° and 180° orientations where the large crack is at the 180° location. One crack from TSP#2 was opened at the 180° orientation. Depth profiles and ligament analyses were performed, as noted in Section 6.5 of this report.

Figure 6-7, Figure 6-8 and Figure 6-9 show the measured depth profiles for the three cracks. The TSP#1 180° crack, which had a bobbin voltage of 4.74 volts and a maximum +Point voltage of 1.92 volts (see Table 4-1), has two 100% throughwall lengths of about 0.030 and 0.060 inch. Ligament tearing of the length between the two throughwall lengths would be required for the crack to have significant leakage. The TSP#1 110° crack had a maximum +Point voltage of 0.25 volt and the maximum depth of 91.4% is higher than expected for this low voltage indication. The TSP#2 180° crack had a bobbin voltage of 0.66 volt with a maximum +Point voltage of 0.25 volt and the maximum crack depth of 70.8% is consistent with this +Point voltage as shown in Section 9.7 of this report. Corrections to these crack profiles for uncorroded ligaments are discussed in Section 9.3 below.

9.3 Corrections to DE Depth Profiles for Uncorroded Ligaments

The location, area and length of the uncorroded ligaments were measured for each of the three cracks as part of the pulled tube exam. Table 9-1 shows the measured values (see Table 6-6) and

additional calculated parameters for the uncorroded ligaments. The TSP#1 180° crack has larger ligament areas than usually found for a deep crack. The burst effective average depth for this crack is reduced by about 7% by the ligaments, which is one of the largest ligament corrections found for an axial crack profile. The TSP#2 180° crack also has large ligament areas although this is fairly common for shallow cracks which have not yet developed sufficiently to corrode the ligaments between the microcracks forming the macrocrack. The TSP#1 110° crack has only a few remaining uncorroded ligaments.

The method used to calculate the corrections to the DE depth profiles for uncorroded ligaments can be described by the following steps.

[

] a.c.e

Figure 9-1, Figure 9-2 and Figure 9-3 compare the direct DE profiles with the ligament corrected depth profiles for the three cracks having DE depth profiles. The TSP#1 180° crack and TSP#2 180° crack show significant ligaments in the deepest part of the crack profile that can be expected to increase the burst pressure compared to the direct DE profile, which corresponds to a depth profile assuming all ligaments have been corroded away.

9.4 Burst Pressure Analysis Results

Burst pressures were calculated for TSP#1 180° crack and the TSP#2 180° crack following Section 5.1.4 (for part-throughwall axial cracks) in the EPRI flaw handbook, Reference 13. This is a “weak link” method that searches all possible sub-lengths of the crack profile for the lowest burst pressure based on the length and average depth of the crack segment. The length and average depth of the lowest burst pressure segment are called the burst effective length and burst effective average depth. Burst pressures were calculated for the ligament corrected depth profile and the direct DE profile to show the increase in burst pressure resulting from the uncorroded ligaments.

The best estimate burst pressures, based on the ligament corrected depth profiles, are 4.79 ksi for TSP#1 180° crack and 6.94 ksi for the TSP#2 180° crack as given in Table 9-2. The ligaments are seen to increase the burst pressures by 0.60 ksi for TSP#1 180° crack and 0.32 ksi for the TSP#2 180° crack. The burst effective average depth for TSP#1 180° crack is decreased by the ligaments from 85.9% to 78.2% and the ligaments result in an increase in the burst effective length from 0.430 inch to 0.446 inch.

The calculated burst pressures can be compared to the ODSCC ARC burst pressure correlation from the latest published Addendum 6 database report, Reference 5. As shown in Figure 9-4, the burst pressures lie about half-way between the nominal ARC correlation and the lower 95% prediction interval at lower tolerance limit material properties. The calculated burst pressures are thus consistent with the ODSCC ARC database.

9.5 SLB Leak Rate Analysis Results

SLB leak rate analyses were performed for the TSP#1 180° crack depth profiles of Figure 9-1. The analysis method applied the leak rate methodology for the axial PWSCC ARC of Reference 14. This method calculates leakage from the depth profile, accounts for potential ligament tearing up to the SLB pressure differential and uses leak rate analysis methods correlated and adjusted to measurements. Nominal leak rate calculations were performed. Since the profiles are destructive exam results, no uncertainties are applied to the depth profile. [

] ^{a,c,e} The methods apply the ANL ligament tearing model, as described in Reference 14, to calculate potential ligament tearing at SLB conditions. The leak rates were not significantly affected by including uncertainties in the ANL tearing model. The ligament tearing pressure is calculated for all potential sub-lengths of the crack profile to obtain the longest crack length that would tear at SLB conditions. For the R22C70 profile, [

] ^{a,c,e} This is the case when the methods are applied

the R22C70 TSP#1 180° crack. Leak rate analyses were performed for the SLB pressure differential of 2405 psi applicable to Sequoyah-2.

For significant leakage, the ligament between the two throughwall lengths in the crack profile of Figure 9-1 would have to tear. This ligament is about 0.03 to 0.04 inch long and has an average depth on the order of 90%. Figure 9-6 shows ligament tearing pressures as a function of average crack depth for the ligament. Assuming the ligament was the only crack, it is seen from Figure 9-6 that ligaments less than 0.1 inch would require >7 ksi pressure differential to tear the 90% deep ligament and ligament lengths >0.3 inch at 90% depth would be required for tearing at SLB conditions. With the ligament between two throughwall crack lengths, the tearing pressures could be lower than that of Figure 9-6. From Figure 9-6, a ligament length of ≥ 0.2 " is required to tear at 2405 psi SLB conditions for an average depth of about 97% and ≥ 0.3 " is required to tear for an average depth of about 93%. For crack lengths spanning the TW lengths of the Figure 9-1 depth profile with ligament corrections, a length of 0.144" has an average depth of 96% and a length of 0.178" has an average depth of 92%. Thus, the ligament would not be expected to tear at SLB conditions. For the depth profile of Figure 9-1 without ligament corrections, a length of 0.154" has an average depth of 97% and a length of 0.235" has an average depth of 93%. Thus, ligament tearing would not be expected for either depth profile of Figure 9-1. The expected SLB leak rate can be calculated from the CRACKFLO results of Figure 9-5. For the longest DE throughwall length of 0.06 inch, the CRACKFLO predicted leak rate would be about 10^{-5} gpm. For these low leak rates, the adjustment of the calculation to measurement increases the leak rate by about a factor of 10. Thus the nominal SLB leak rate would be expected to be on the order of 10^{-4} gpm. The analysis code would be expected to increase this leak rate due to predicted tearing at the edges of the crack.

Calculations applying the computer code methods of Reference 14 yield a leak rate of 0.00023 gpm (0.052 liter/hr) at the 2405 psi SLB condition for Sequoyah-2. Both the direct DE and ligament corrected profiles of Figure 9-1 yield the same leak rate. Consistency with the above 10^{-4} gpm estimate shows that the ligament between the two 100% TW lengths did not tear in the analysis.

Figure 9-7 compares the predicted SLB leak rate with the ODSCC ARC Addendum 6 leak rate correlation. The predicted leak rate of 0.052 liter/hr is consistent with the lowest leak rates in the ARC database and well below the median leak rate. The leak rate is consistent with the ARC database. If it is assumed that the calculated leak rate was a measurement, the effect of including the leak rate in the ARC correlation would be a modest increase in the slope of the correlation with slightly lower leak rates for indications below about 5 bobbin volts.

9.6 Use of Pulled Tube Data for Probability of Leak Correlation

Based on the DE depth profiles, the TSP#1 180° crack would show some SLB leakage based on the 100% TW length, as shown by the above analyses. The TSP#2 180° crack is too shallow to leak at SLB conditions. These two data points can be confidently included in the ARC correlation for probability of leakage as equivalent to leak rate measurements.

9.7 Comparison of NDE Predictions from Field Data with DE Profiles and Post-Pull NDE Results

Figure 9-8 shows the TSP#1 180° crack DE ligament corrected depth profile and the NDE profile predictions based on amplitude sizing for the field NDE data and the lab NDE data. The amplitude sizing correlation applied for the NDE analyses is a generic calibration curve that has been used at Westinghouse over the last three years and has shown good agreement with DE profiles. The post-pull lab data show about a factor of 5 increase in amplitude. The large increase in amplitude leads to post-pull depth predictions much deeper than predicted from the field NDE or found for the DE profile. Potential causes for the increased post-pull amplitudes are further discussed later in this section. NDE depth profiles are generally compared with DE running average (RA) profiles averaged over 0.1" segments. Figure 9-9 shows this comparison for the field NDE data with reasonably good agreement obtained between the NDE and DE profiles.

Figure 9-10 shows the TSP#2 180° crack DE ligament corrected depth profile together with the DE RA profile and the NDE profile predictions based on amplitude sizing for the field NDE data and the lab NDE data. The field NDE predictions are in very good agreement with the DE profile. Again, the post-pull amplitudes are about a factor of 4 higher than the field amplitudes and the depth profile predicted from these amplitudes is much deeper than the DE profile.

Figure 9-11 shows the TSP#1 110° crack DE ligament corrected depth profile together with the DE RA profile and the NDE profile predictions based on amplitude sizing for the field NDE data. Post-pull NDE data are not available for this flaw. In this case, the DE depths are significantly deeper (about 25% depth) than the NDE predictions. The DE depths are unusually high for a 0.25 max +Point amplitude, which is the same peak amplitude as the shallower TSP#2 180° crack. The difference between the NDE prediction and DE data is one of the largest found for the amplitude sizing correlation used for the NDE analyses.

As noted above, the post-pull lab NDE data show large increases in +Point amplitudes and predicted depths compared to the field NDE data. [

] ^{a,c} The tearing of the ligament with crack separation is consistent with the post-pull +Point peak amplitude increase from about 2 to 10 volts. It is very difficult to postulate any mechanism for the increase in amplitude that did not include tearing of the ligament. The post-pull voltage profile of Figure 9-8 shows amplitude increase by factors of 3 to 5 across the total length of the profile. Tearing of the ligament between the two TW segments is necessary to obtain the post-pull peak amplitude near 10 volts. The post-pull amplitude increases are consistent with tearing of the shallow ligament between the two TW segments, crack face separation and possibly some minor wall thickness tearing along the length of the crack.

An estimate of the effects of crack face separation can be made by comparing +Point amplitudes for EDM notches (typically 5-6 mil wide cuts) and for cracks. A correlation for the ratio of EDM notch volts to crack volts was made using EDM notch calibration standard voltage measurements and the crack amplitude sizing correlation used for the sizing analyses. For 100% TW, the crack amplitude was assumed to be about four volts for consistency with tearing of the ligament. [

] ^{a,c,e} The general agreement between the magnitudes of the adjusted field volts and the post-pull volts supports crack separation as a major contributor to the post-pull amplitude increases.

As part of the tube examination process, the cracks were [

] ^{a,c,e} was to assist identification of ligaments torn during the tube pulling operation from ligaments torn during the pressurization tests. However, this process did not identify tearing of wall thickness or out-of-plane ligaments that must have torn to obtain the increased post-pull amplitudes and the post-pull low pressure leak rate.

9.8 Conclusions

Based on the evaluations of this report, it can be concluded the predictions of the burst pressures and SLB leak rates from the DE depth profiles are consistent with the burst and leak rate correlations in the ODSCC ARC Database Addendum 6 (Reference 5). This is shown in Figure 9-4 and Figure 9-7. The TSP#1 180° crack leak rate analyses indicate that the wall thickness ligament between the two throughwall crack segments would not be expected to tear at SLB pressure differentials, which results in a low leak rate for the indication.

It is further concluded that the tube pulling operations led to tearing of uncorroded ligaments including the shallow wall thickness ligament between the TSP#1 180° crack throughwall crack segments and also resulted in crack face separation. This conclusion is supported by the large increases in post-pull +Point amplitudes compared to the pre-pull field data and by calculations of the crack opening area needed to obtain the measured low pressure leak rate. Given the changes to the cracks from the tube pull operations, post-pull measurements of burst pressures or SLB leak rates would not have yielded meaningful results.

Table 9-2: R22C70 Calculated Burst Pressures from TSP#1 and TSP#2 180° Crack Destructive Exam Profiles

Crack Location	DE Profile with Uncorroded Ligament Corrections			Measured DE Profile		
	Burst Pressure (ksi)	Burst Effective Average Depth (%TW)	Burst Effective Length (inch)	Burst Pressure (ksi)	Burst Effective Average Depth (%TW)	Burst Effective Length (inch)
TSP#1 180°	4.79	78.2	0.446	4.19	85.9	0.430
TSP#2 180°	6.94	53.7	0.403	6.62	57.2	0.416

a,b,c



Figure 9-1: Uncorroded Ligament Corrected Depths for the TSP#1 180° Crack



Figure 9-2: Uncorroded Ligament Corrected Depths for the TSP#2 180° Crack

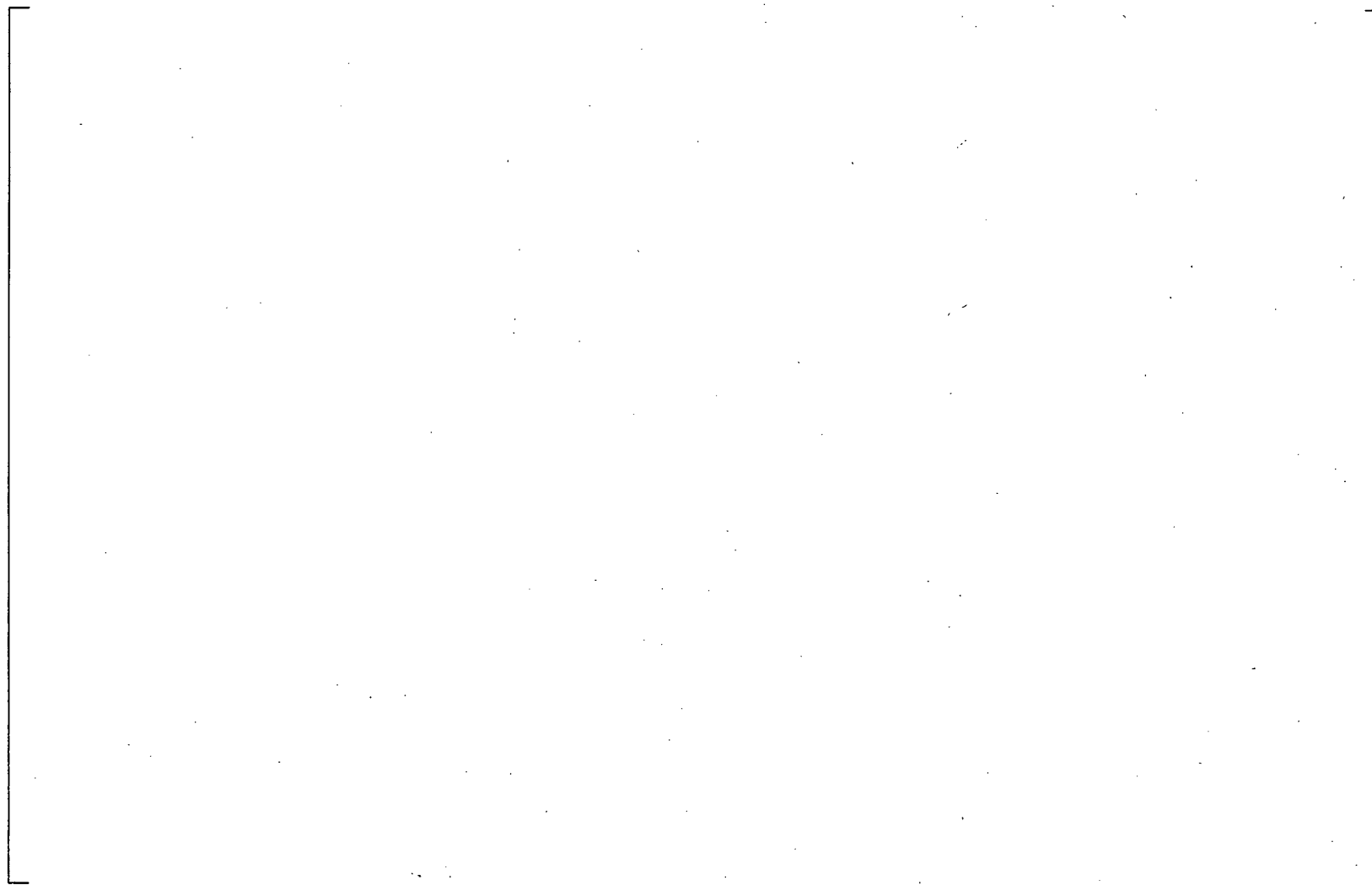


Figure 9-3: Uncorroded Ligament Corrected Depths for the TSP#1 110° Crack

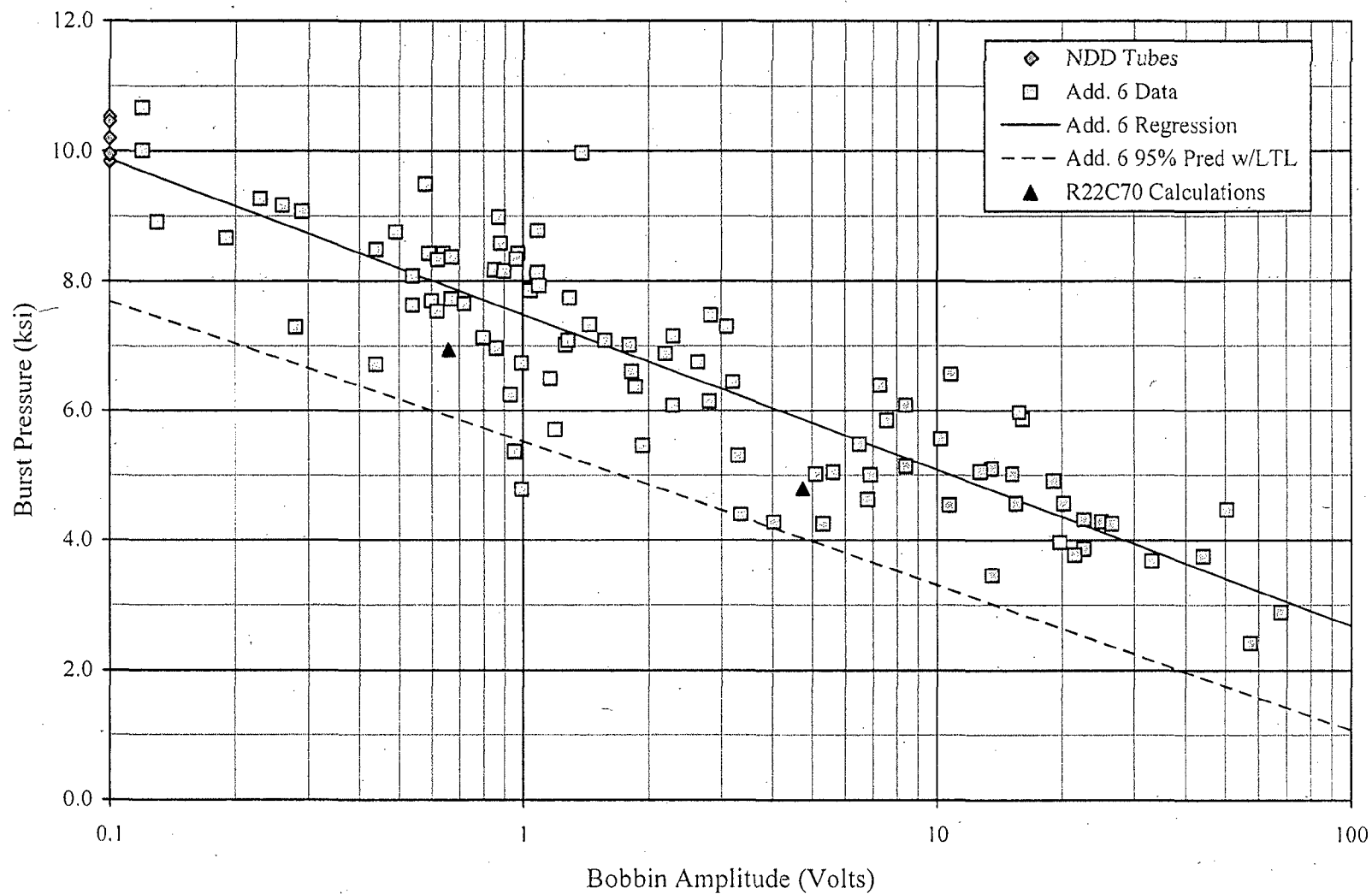


Figure 9-4: Addendum 6 Burst Pressure vs. Volts for 7/8" OD Alloy 600 SG Tubes

Reference Database, Reference $S_y + S_u = 137.56$ ksi



Figure 9-5: SLB Leak Rate (CRACKFLO) Versus Throughwall Axial Crack Length

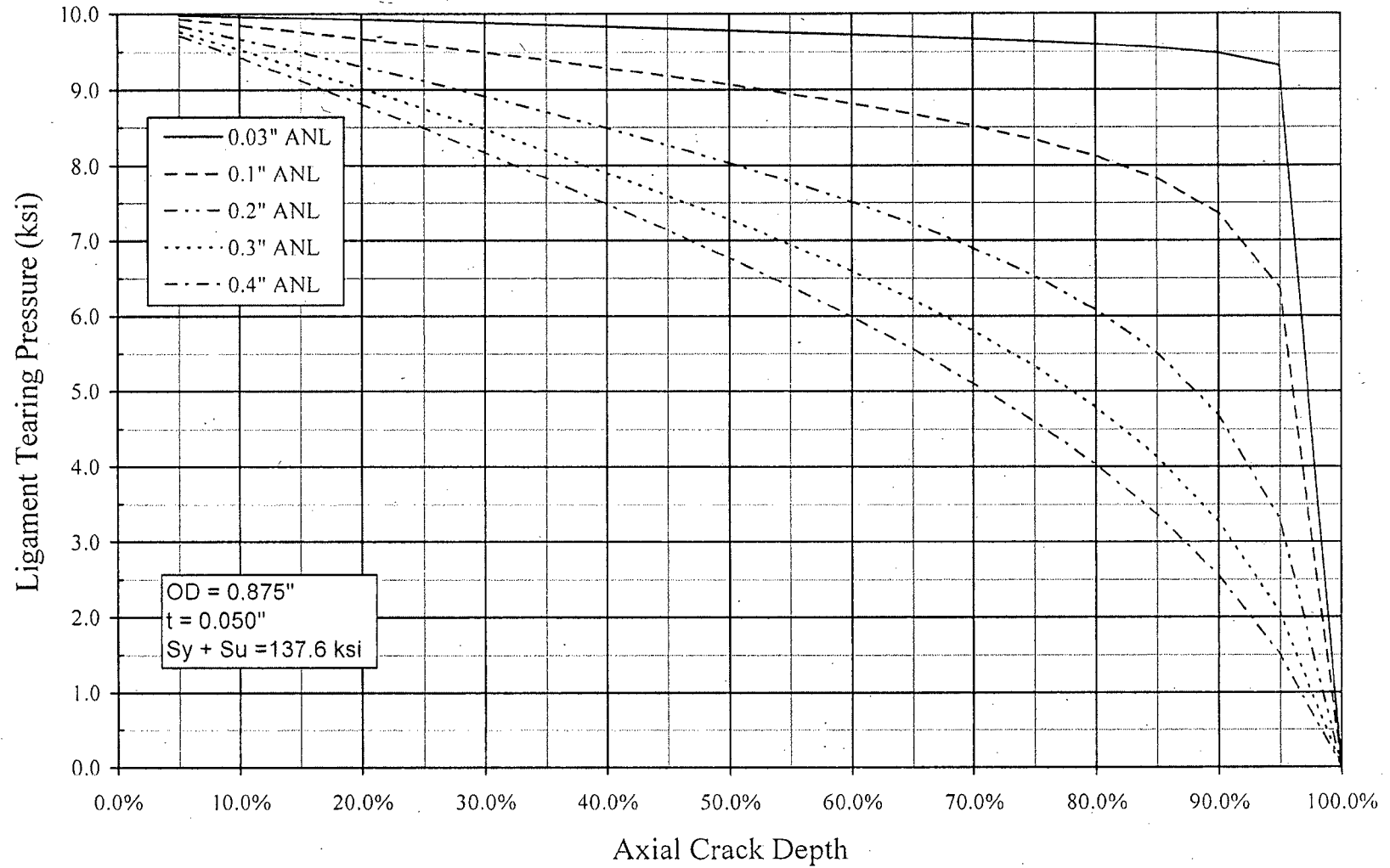


Figure 9-6: ANL Ligament Tearing Pressures vs. Crack Depth

Alloy 600 MA SG Tubes with Part-Throughwall Axial Cracks

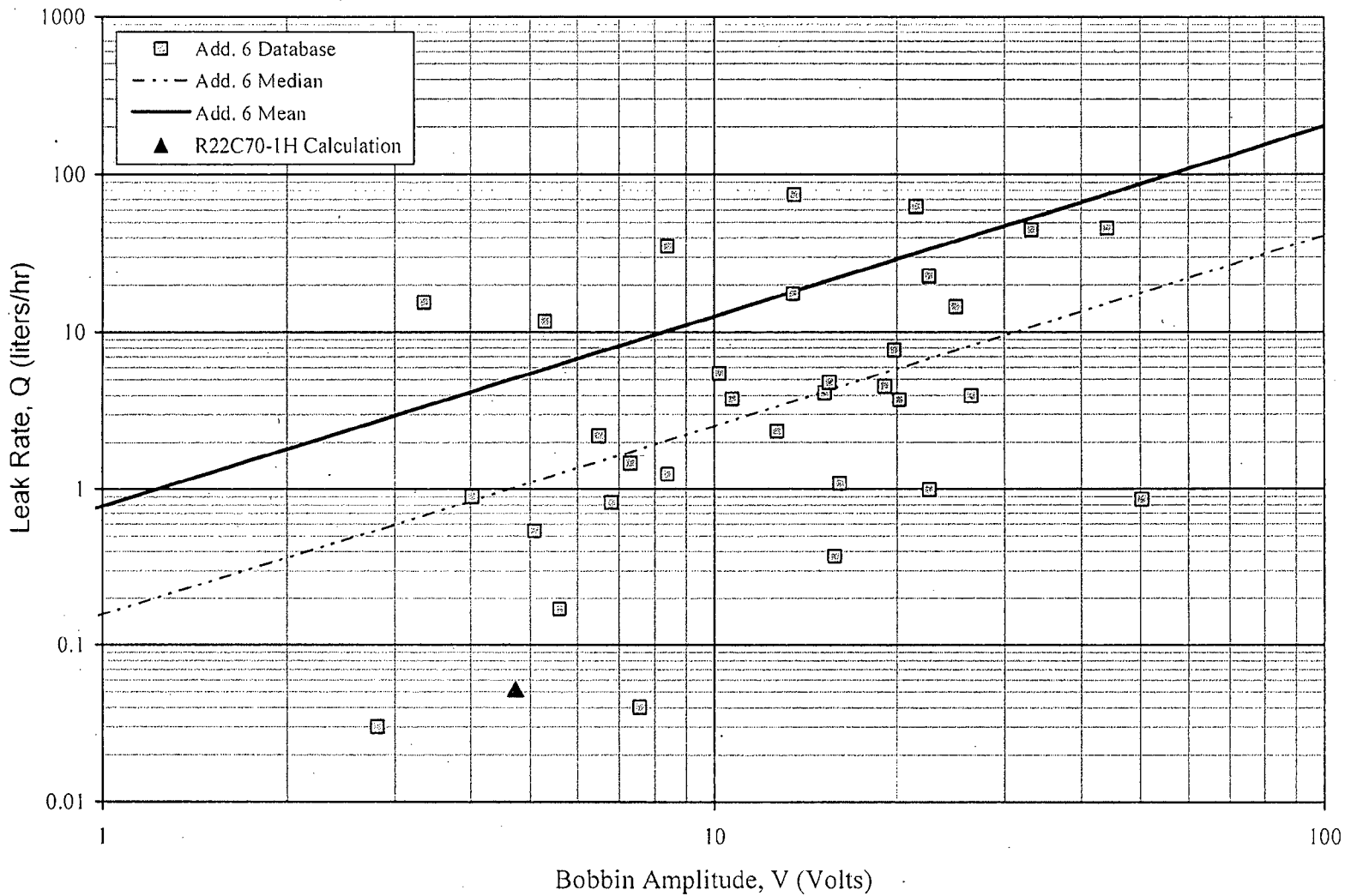


Figure 9-7: SLB Leak Rate (2405 psi) vs. Bobbin Amplitude

7/8" x 0.050" Alloy 600 MA Tubes Data



Figure 9-8: Comparison of DE and NDE Results with Pre-Pull and Post-Pull Depth and Volts for the TSP#1 180° Crack



Figure 9-9: Comparison of NDE and Ligament Corrected DE for the TSP#1 180° Crack



Figure 9-10: Comparison of NDE and Ligament Corrected DE for the TSP#2 180° Crack



Figure 9-11: Comparison of Field NDE and DE Depths for the TSP#1 110° Crack



Figure 9-12: +Point Volts for Field, Lab and Field Adjusted for Crack Separation

10.0 DISCUSSION / CONCLUSIONS

The non-destructive and destructive examinations of Sequoyah-2 steam generator tube R22C70 confirmed the presence of axial deep OD initiated intergranular stress corrosion cracking (ODSCC) within the both of support plate crevices that were pulled for examination. The corrosion was limited to the support plate crevices. Small patches of cellular corrosion, with short shallow circumferential elements, were identified in both TSP regions. Shallow (1-2 grain deep) intergranular attack (IGA) was also observed. The maximum depth of corrosion in TSP#1 was 100%TW. The maximum depth of corrosion in TSP#2 was 70.8%TW.

Tube Integrity

It was judged, based on the results of visual observations, dimensional measurements, laboratory eddy current signal increases and leak screening tests, that the cracks in the pulled sections of the tube were not representative of their in-generator condition.

Based on the evaluations of this report, it can be concluded the predictions of the burst pressures and SLB leak rates from the destructive examination depth profiles are consistent with the burst and leak rate correlations in the ODSCC ARC Database Addendum 6 (Reference 5). The TSP#1 180° crack leak rate analyses indicate that the wall thickness ligament between the two throughwall crack segments would not be expected to tear at SLB pressure differentials, which results in a low leak rate for the indication.

The criterion established in the NRC teleconference (see Section 2.3) has been met and a replacement tube does not need to be pulled.

It is further concluded that the tube pulling operations led to tearing of uncorroded ligaments including the shallow wall thickness ligament between the TSP#1 180° crack throughwall crack segments and also resulted in crack face separation. This conclusion is supported by the large increases in post-pull +Point amplitudes compared to the pre-pull field data and by calculations of the crack opening area needed to obtain the measured low pressure leak rate.

Given the changes to the cracks from the tube pull operations, post-pull measurements of burst pressures or SLB leak rates would not have yielded meaningful results.

The testing performed on tube R22C70, and the results of the tests, satisfy the Alternative Repair Criteria of Reference 2.

Cause

The cause of the cracking was not investigated in detail; however a limited examination of deposits and material characterization tests were performed that served to eliminate possible contributing factors to the corrosion that was observed. Stress corrosion cracking, of any type, requires the simultaneous presence of three elements; if any one is absent, SCC will not initiate or will not propagate, if already initiated. These elements are:

1. A susceptible metallurgical condition. Depending on the environment, Alloy 600 in different metallurgical conditions (i.e., mill annealed, high temperature mill annealed, sensitized, cold worked) is susceptible to stress corrosion cracking.
2. A significant tensile stress (dependent on the environment to which the material is exposed).
3. An aggressive environment. Alloy 600, depending on its metallurgical condition, is susceptible to SCC in a wide range of environments, including high temperature pure or relatively pure water, caustic environments, acidic environments and relatively neutral environments contaminated with certain chemical species.

Material Condition

Some of the examinations that were performed to assess the material condition were affected by the high forces encountered during the pulling operation. Both the tensile test and the microhardness test results reflected aspects of the tube pull. However, the assessment of the microstructure, the sensitization and the chemistry of the bulk material of the tube would almost entirely remain unaffected by the tube pull.

The Sequoyah-2 tube was not sensitized, the chemistry of the tube material was well within specifications and the micrographs showed a fine grain microstructure with few grain boundary carbides. These conditions were typical of low temperature mill annealed tubing that was part of most early Westinghouse supplied steam generators. Typically, material fabricated with a low temperature final mill anneal (with its resulting grain structure, high strength and few grain boundary carbides) has a relatively high susceptibility to SCC and IGA, as demonstrated by numerous laboratory tests and field experience (Reference 15).

Stress

The axial orientation of the cracks in R22C70 indicates that the major stresses were in the hoop direction. There were short shallow circumferentially oriented cracks within the cellular corrosion. The most likely source of tensile hoop stresses in the TSP crevices would be the primary water pressure. The final polishing of the tubes could conceivably produce residual stresses that could have been either compressive or tensile, but investigation of this was not part of the scope of this examination.

Because of significant tube ovalization, the presence of denting could not be confirmed or shown to be absent. However the field eddy current results did not indicate the presence of denting in either TSP region that was pulled for examination.

Chemistry

The crevice that is formed between the tube and the support plate hole may serve as a site for the formation of an aggressive environment. These crevices are quite capable of being fouled with corrosion products from the feedtrain and once fouled, the crevices can become effective

concentrators of contaminants such as chlorides, sulfates and similar aggressive species that are present in the feedwater as a result of condenser in-leakage. When concentrated solutions form, the crevice becomes a preferential site for the initiation of tube corrosion. This explains why the corrosion in the Sequoyah-2 tube was confined to the support plate regions, and why the major part of the OD surfaces, which are readily flushed by the secondary environment and thus exposed only to bulk water contaminant levels, were relatively free of any corrosion.

The concentrated solutions that form within the crevices may also result in the accelerated corrosion of the carbon steel support plate, especially if concentrations of chlorides are present in an acidic aqueous environment with copper or its ions present. The volumetric expansion accompanying the formation of magnetite (Fe_3O_4) or hematite (Fe_2O_3) may cause an inward denting of the Alloy 600 tube. In solid drilled plates, denting is typically initiated on one side of the tube leading to some ovalization (based on UT examinations of dented TSPs), however the field eddy current data did not indicate the presence of a dent in these TSP regions.

The deposit analysis did not yield any conclusive evidence about the nature of the environment within the TSP crevices. Copper was identified adjacent to the tube surface as distinct particles. Copper can be associated with an oxidizing environment; however the oxidation state of the copper could not be assessed from EDS testing. Lead was identified in both the deposits and on the crack surface in amounts above that found in the base metal. Lead has been associated with both IGSCC and transgranular SCC of Alloy 600 in secondary-side environments, although the level of lead required to initiate corrosion is undecided. The effect of the lead in the crevice environment could not be assessed from EDS testing, however its presence was confirmed.

11.0 REFERENCES

1. "Steam Generator Information Report," NSD-RMW-90-070 and SG-90-02-026, Revision 6, February 1990.
2. "Voltage-Based Repair Criteria for Westinghouse Steam Generator Tubes Affected by Outside Diameter Stress Corrosion Cracking," United States Regulatory Commission Generic Letter 95-05, August 3, 1995.
3. "Nuclear Services Policies & Procedures," Westinghouse Quality Management System - Level 2 Policies and Procedures, Revision 24, Effective 02/28/07.
4. TVA Contract Work Authorization No. N2007-004, Revision 01, April 19, 2007.
5. EPRI Report NP-7480-L, Addendum 6, 2004 Database Update, "Steam Generator Tubing Outside Diameter Stress Corrosion Cracking at Tube Support Plates Database for Alternate Repair Limits," October 2004.
6. "Acknowledgement of Pulled Tube R22C70 Receipt," LTR-CDME-07-7, January 14, 2007.
7. "Steam Generator Tube Sample Identification," Westinghouse Science and Technology Department Procedure MR 0201, Rev 0, June 18, 2002.
8. "Procedure for Laboratory Heat Tinting Fracture Surfaces of Steam Generator Tubes by High Temperature Oxidation," TP-SGDA-07-1, Revision 0, April 2007.
9. "Sequoyah Unit 2 Steam Generator Tube Examination," SG-SGDA-02-40, Revision 0, December 2002.
10. Dirats Laboratories, Report Number R465720, June 21, 2007.
11. Westinghouse Calculation Note CN-CDME-07-13, "Evaluation of Pulled Tubes and POPCD for EPRI Report NP 7480-L, Addendum 7," September 2007 (Westinghouse Proprietary Class 2).
12. EPRI Report TR-107197, "Depth Based Structural Analysis Methods for Steam Generator Circumferential Indications," November, 1997.
13. EPRI Report 1001191, Revision 0, "Steam Generator Degradation Specific Management Flaw Handbook," Final Report, January 2001.
14. WCAP-15128, Rev. 2, "Depth Based SG Tube Repair Criteria for Axial PWSCC at Dented TSP Intersections," February, 2003.
15. Z. Szkarska-Smialowska, "Factors Influencing IGSCC of Alloy 600 in Primary and Secondary Waters of PWR Steam Generators", Proceedings of the Fifth International Symposium on Environmental Degradation of Materials in Nuclear Power Systems - Water Reactors, NACE, 1995.

APPENDIX A - CRACK DEPTH PROFILE DATA

TSP#1 180° Crack (Sample 4C1)

Axial Position Above Bottom End of Crack (mils)	Crack Depth (%TW)	Ligament Orientation	Ligament Area (mils ²)	Ligament Depth (%TW)
0.0	0.0			
1.8	12.4			
5.3	14.2			
10.6	14.2			
15.0	19.5			
19.4	42.5			
24.6	47.8			
29.9	58.4			
35.2	61.9			
40.5	65.4			
45.8	61.9			
51.9	63.7			
57.2	63.7			
62.5	60.1			
67.8	49.5			
73.9	56.6	in-plane	134.5	19.5
79.2	67.2			
85.4	70.8			
91.6	72.5			
96.8	72.5			
102.1	74.3			
107.4	76.1			
112.7	81.4			
118.0	84.9			
122.4	88.4			
127.6	92.0			
132.9	93.8			
137.3	95.5			
141.7	95.5			
146.1	95.5			
151.4	93.8			
156.7	77.8	out-of-plane	243.5	61.9
162.9	81.4			
168.1	77.8			
172.5	72.5			
176.9	72.5	in-plane	121.3	33.6
182.2	76.1			
186.6	76.1			

TSP#1 180° Crack (Sample 4C1)

Axial Position Above Bottom End of Crack (mils)	Crack Depth (%TW)	Ligament Orientation	Ligament Area (mils ²)	Ligament Depth (%TW)
191.0	76.1			
195.4	74.3			
199.8	72.5			
205.1	67.2			
209.5	60.1			
214.8	54.8			
220.1	70.8	out-of-plane	513.3	88.4
225.4	74.3			
230.6	77.8			
235.0	44.2	out-of-plane	672.4	69.0
239.4	76.1			
243.8	84.9			
248.2	92.0			
252.7	100.0			
257.1	100.0			
261.5	100.0			
265.9	100.0			
270.3	100.0			
274.7	100.0			
279.1	100.0			
283.5	100.0			
288.7	97.3			
293.1	90.2			
298.4	90.2	out-of-plane	71.2	40.7
303.7	84.9			
309.0	86.7			
314.3	86.7			
319.6	99.1	out-of-plane	121.3	40.7
325.7	100.0			
331.0	100.0			
336.3	100.0			
340.7	100.0			
345.1	100.0			
349.5	100.0			
353.9	100.0			
358.3	100.0			
362.7	100.0			
367.1	100.0			
371.5	100.0			
375.9	100.0			

TSP#1 180° Crack (Sample 4C1)

Axial Position Above Bottom End of Crack (mils)	Crack Depth (%TW)	Ligament Orientation	Ligament Area (mils ²)	Ligament Depth (%TW)
381.2	100.0			
385.6	100.0			
390.0	97.3			
393.5	93.8			
397.0	83.1	out-of-plane	179.3	63.7
401.4	90.2			
405.8	90.2			
410.2	90.2	out-of-plane	114.3	31.8
414.6	84.9			
419.0	88.4			
422.6	88.4			
426.1	88.4			
430.5	86.7			
434.9	84.9			
439.3	84.9			
443.7	84.9	out-of-plane	341.0	100.0
448.1	84.9			
451.6	84.9			
456.0	86.7			
460.4	88.4			
464.8	86.7			
468.3	84.9			
472.7	83.1			
477.1	77.8			
481.5	79.6			
485.9	79.6			
490.3	77.8			
495.6	76.1			
500.0	76.1			
504.4	74.3			
507.9	74.3			
512.3	70.8			
516.7	67.2			
521.1	69.0			
525.5	65.4			
530.8	61.9			
535.2	61.9			
538.8	56.6			
542.3	61.9			
545.8	58.4			

TSP#1 180° Crack (Sample 4C1)

Axial Position Above Bottom End of Crack (mils)	Crack Depth (%TW)	Ligament Orientation	Ligament Area (mils ²)	Ligament Depth (%TW)
550.2	56.6			
554.6	46.0			
559.0	0.0			

TSP#1 110° Crack (Sample 4C5)

Axial Position Above Bottom End of Crack (mils)	Crack Depth (%TW)	Ligament Orientation	Ligament Area (mils ²)	Ligament Depth (%TW)
0.0	0.0			
1.8	29.4			
4.6	40.5			
7.6	44.1			
11.0	50.4			
14.6	54.4			
18.1	56.1			
21.3	57.0			
24.7	55.8			
28.2	61.9			
32.2	62.2			
36.2	63.4			
40.2	65.1			
44.2	65.6			
47.4	65.3			
50.5	66.5			
53.3	66.4	out-of-plane	149.4	69.0
56.0	67.0			
59.2	70.5			
62.9	72.0			
66.6	74.0			
70.7	76.9			
74.9	75.7			
78.8	76.6			
83.2	76.3			
87.7	75.8			
91.9	75.2			
95.9	75.2			
100.2	72.3			
104.6	71.1			

TSP#1 110° Crack (Sample 4C5)

Axial Position Above Bottom End of Crack (mils)	Crack Depth (%TW)	Ligament Orientation	Ligament Area (mils ²)	Ligament Depth (%TW)
108.9	67.9			
113.1	66.8	out-of-plane	630.2	61.9
117.6	89.1			
122.0	90.2			
126.7	91.4			
131.4	90.5			
136.4	88.8			
141.5	88.2			
145.7	89.7			
150.6	89.1			
156.6	89.1			
161.4	90.0			
166.1	88.5			
170.5	86.8	out-of-plane	294.4	83.1
174.6	88.5			
179.6	91.1			
183.5	90.5			
188.6	90.5			
192.7	88.5			
196.6	88.2			
199.9	85.9			
203.5	83.0			
207.3	77.8			
210.8	71.7			
214.1	56.2			
216.7	54.9			
219.5	57.2			
223.2	64.1			
226.5	68.2			
230.7	74.0			
234.7	80.1			
239.0	85.9			
244.1	89.4			
248.8	89.1			
253.4	89.7			
257.8	88.0			
262.4	84.9			
266.0	83.1			
269.3	80.7			
272.2	77.0			

TSP#1 110° Crack (Sample 4C5)

Axial Position Above Bottom End of Crack (mils)	Crack Depth (%TW)	Ligament Orientation	Ligament Area (mils ²)	Ligament Depth (%TW)
274.9	79.0			
277.6	79.3			
281.6	75.9			
284.1	76.7			
286.7	75.9			
290.7	72.7			
294.1	69.8			
297.1	68.4	out-of-plane	246.1	46.0
300.1	73.3			
303.3	75.4			
306.5	73.1			
309.2	70.6			
311.9	70.8			
314.8	69.6			
317.6	67.3			
320.1	67.2			
322.4	67.7			
325.4	60.4			
328.2	59.3			
331.0	55.9			
333.6	52.5			
336.5	53.1			
339.3	51.6			
342.1	52.7			
345.0	54.2			
348.3	55.1			
351.4	53.0			
354.5	56.1			
357.6	55.9			
361.2	56.2			
364.4	55.6			
367.0	54.0			
370.3	54.4			
373.9	50.8			
377.6	48.5			
380.8	48.6			
383.4	45.7			
386.9	41.3			
390.2	37.4			
395.0	0.0			

TSP#2 180° Crack (Sample 6B1)

Axial Position Above Bottom End of Crack (mils)	Crack Depth (%TW)	Ligament Orientation	Ligament Area (mils ²)	Ligament Depth (%TW)
0.0	0.0			
2.7	28.3			
7.1	33.6			
11.5	37.1			
16.0	44.2			
20.4	46.0	out-of-plane	51.0	44.2
24.8	46.0			
29.3	47.8			
33.7	49.5	out-of-plane	102.8	30.1
38.1	49.5			
42.6	49.5			
47.0	54.8			
51.4	53.1			
55.9	51.3			
60.3	54.8			
64.7	53.1			
69.2	51.3			
73.6	51.3			
78.0	51.3			
82.5	49.5			
86.9	51.3			
91.3	53.1			
95.8	56.6			
100.2	56.6			
104.6	58.4			
109.1	58.4			
113.5	54.8			
117.9	54.8			
122.4	53.1			
125.9	49.5			
130.3	47.8	out-of-plane	144.1	56.6
134.8	44.2			
139.2	47.8			
143.6	47.8			
148.1	60.1			
152.5	60.1			
156.9	54.8			
161.4	56.6			
165.8	56.6			

TSP#2 180° Crack (Sample 6B1)

Axial Position Above Bottom End of Crack (mils)	Crack Depth (%TW)	Ligament Orientation	Ligament Area (mils ²)	Ligament Depth (%TW)
170.2	54.8			
174.7	51.3			
179.1	53.1			
183.5	51.3			
188.0	54.8			
192.4	58.4			
196.8	56.6			
201.3	60.1			
205.7	60.1			
210.1	58.4			
213.7	56.6			
218.1	54.8			
222.6	58.4			
227.0	60.1			
231.4	60.1			
235.9	61.9			
240.3	58.4			
244.7	56.6			
249.2	47.8	in-plane	276.9	63.7
253.6	70.8			
258.0	70.8			
262.5	69.0			
266.9	70.8			
271.3	67.2			
275.8	61.9			
280.2	54.8	out-of-plane	39.6	21.2
284.6	56.6			
289.1	53.1			
293.5	56.6			
297.9	61.9			
302.4	60.1			
306.8	61.9			
311.2	61.9			
315.7	65.4			
320.1	63.7			
324.5	61.9	in-plane	290.9	70.8
329.0	46.0			
333.4	65.4			
337.8	58.4			
342.3	63.7			

TSP#2 180° Crack (Sample 6B1)

Axial Position Above Bottom End of Crack (mils)	Crack Depth (%TW)	Ligament Orientation	Ligament Area (mils ²)	Ligament Depth (%TW)
346.7	65.4			
351.1	67.2			
355.6	67.2			
360.0	67.2			
364.4	69.0			
368.9	61.9			
373.3	65.4			
377.7	65.4			
382.2	65.4			
386.6	63.7			
391.0	61.9			
395.5	58.4	out-of-plane	178.4	72.5
399.9	51.3			
404.3	58.4			
408.8	51.3			
413.2	54.8			
417.6	56.6			
422.1	54.8			
426.5	53.1			
430.9	51.3			
435.4	51.3			
439.8	51.3			
444.2	31.8	out-of-plane	89.6	40.7
448.7	24.8			
453.1	40.7	out-of-plane	348.9	46.0
456.7	40.7			
461.1	33.6			
465.5	35.4	out-of-plane	309.4	58.4
470.0	42.5			
474.4	46.0			
478.8	47.8			
483.3	47.8			
487.7	46.0			
492.1	42.5			
496.6	38.9	out-of-plane	260.2	42.5
501.0	40.7			
505.4	42.5			
509.9	40.7			
514.3	42.5			
518.7	44.2			

TSP#2 180° Crack (Sample 6B1)

Axial Position Above Bottom End of Crack (mils)	Crack Depth (%TW)	Ligament Orientation	Ligament Area (mils ²)	Ligament Depth (%TW)
523.2	37.1	out-of-plane	392.9	47.8
527.6	44.2			
532.0	47.8			
536.5	42.5			
540.9	49.5			
545.3	47.8			
549.8	47.8			
554.2	44.2			
558.6	26.5			
563.1	1.8			
567.5	1.8			
571.9	7.1			
576.4	3.5			
580.8	3.5			
585.2	5.3			
588.8	12.4			
594.1	0.0			
598.5	0.0	in-plane	250.5	23.0
603.0	1.8			
606.5	24.8			
610.9	23.0			
615.4	17.7			
619.8	15.9			
624.2	14.2	out-of-plane	77.3	17.7
628.7	19.5			
633.1	7.1			
636.7	10.6	out-of-plane	87.0	19.5
641.1	12.4			
645.5	1.8	out-of-plane	72.1	23.0
650.0	24.8			
654.4	21.2			
657.9	12.4			
662.4	1.8	in-plane	201.3	21.2
666.8	31.8			
671.2	37.1			
675.7	38.9			
680.1	40.7			
684.5	35.4			
689.9	12.4			
694.3	17.7			

TSP#2 180° Crack (Sample 6B1)

Axial Position Above Bottom End of Crack (mils)	Crack Depth (%TW)	Ligament Orientation	Ligament Area (mils ²)	Ligament Depth (%TW)
697.8	3.5	in-plane	460.5	31.8
702.3	10.6			
707.6	33.6			
711.1	30.1			
715.6	26.5			
720.0	0.0			